International
# WOCE
Newsletter

Number 38 ISSN 1029-1725 May 2000

## IN THIS ISSUE



## News from the WOCE IPO

*W. John Gould, Director, WOCE IPO and ICPO, Southampton Oceanography Centre, UK. john.gould@soc.soton.ac.uk*

### Research ships, tall ships and AUVs

Two recent events have reinforced in my mind a fact of which we should not lose sight – making observations at sea is still central to our understanding of the oceans but is at times very difficult.

In February Penny Holliday, known to many of you as the person in the WOCE IPO with responsibility for data issues, led her first cruise. She and her team set off to occupy a hydrographic section from the UK to Iceland including the often repeated "Ellett" Line from the UK to Rockall. February is never the best time of year to work in the N. Atlantic but one objective was to observe end-of-winter conditions. They endured winds of 30 m/s and waves approaching 30 m in height and despite their best efforts they were only able to occupy shelf stations and the Ellett Line.

In mid-April almost 20 large old sailing ships set off from Southampton on a Tall Ships race to Cadiz, Bermuda, Newport RI, Halifax NS, ending in Amsterdam. They were an impressive sight and attracted thousands of visitors. The Southampton Oceanography Centre mounted a series of exhibits (including one about what WOCE and CLIVAR are doing to better understand climate variability and change). The displays were both backward-looking (to the days of sail when HMS Challenger made the first global ocean survey) and forward-looking (to the use of AUVs and profiling floats). The day is not far away when these new techniques and satellite and maybe acoustic remote sensing will provide much of our information about the oceans. Even then, people like Penny and her team will still have to endure considerable discomfort to collect the complementary ship-board ocean observations.

## About WOCE

The World Ocean Circulation Experiment (WOCE) is a component of the World Climate Research Programme (WCRP), which was established by WMO and ICSU, and is carried out in association with IOC and SCOR.

WOCE is an unprecedented effort by scientists from more than 30 nations to study the large-scale circulation of the ocean. In addition to global observations furnished by satellites, conventional in-situ physical and chemical observations have been made in order to obtain a basic description of the physical properties and circulation of the global ocean during a limited period.

The field phase of the project lasted from 1990–1997 and is now being followed by Analysis, Interpretation, Modelling and Synthesis activities. This, the AIMS phase of WOCE, will continue to the year 2002.

The information gathered during WOCE will provide the data necessary to make major improvements in the accuracy of numerical models of ocean circulation. As these models improve, they will enhance coupled models of the ocean/atmosphere circulation to better simulate – and perhaps ultimately predict – how the ocean and the atmosphere together cause global climate change over long periods.

WOCE is supporting regional experiments, the knowledge from which should improve circulation models, and it is exploring design criteria for long-term ocean observing system.

The scientific planning and development of WOCE is under the guidance of the Scientific Steering Group for WOCE, assisted by the WOCE International Project Office (WOCE IPO):

- W. John Gould, *Director*
- Peter M. Saunders, *Staff Scientist*
- N. Penny Holliday, *Project Scientist*
- Roberta Boscolo, *Project Scientist*
- Sheelagh Collyer, *Publication Assistant*
- Jean C. Haynes, *Administrative Assistant*

For more information please visit:
http://www.soc.soton.ac.uk/OTHERS/woceipo/ipo.html

### This and future Newsletter issues

For this the first Newsletter of the new century we have a wide-ranging selection of papers. Several (some a legacy from last year's N. Atlantic workshop, the extensive report from which has now been published by the IPO) deal with Atlantic Ocean circulation using floats, models, remote sensing and hydrography. The overall content of this Newsletter is refreshingly global.

We announce here some important landmarks. The next of the series of WOCE AIMS workshops – the joint WOCE/CLIVAR Workshop on Variability will be held in Fukuoka, Japan. I would like to acknowledge the hard work that has been put in by the organising committee and especially by Shiro Imawaki as the local organiser. I encourage you to attend (see p.41). It promises to be an interesting and productive gathering. The following week PICES holds its annual science meeting in Hakodate Japan (http://pices.ios.bc.ca/annual/announce.htm).

There are a number of theme sessions relating to N. Pacific Circulation so some of you may want to make an extended stay in Japan and attend both meetings.

The second announcement is of the WOCE Book. You will see from the contents list (p. 42) that it will contain an important set of contributions describing the present status of science in a number of areas central to WOCE. A great deal of hard work has been and is being done. An announcement about price and exact publication date will be made later by Academic Press.

Inevitably effort is moving into publishing WOCE results in the refereed literature (approximately 200 new papers each year) and away from Newsletter articles. Therefore we plan only three Newsletter issues in 2000. We will continue to use the Newsletter to feature science stemming from the workshops (in 2001 we expect a focus on ocean heat and freshwater transports).

*Our WOCE and CLIVAR secretaries Jean (right) and Sandy (left) look very pleased when the last Newsletter was about to leave SOC.*

# Eddy variability from direct current measurements in the Antarctic Circumpolar Current south of Australia

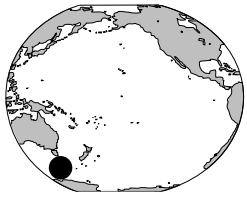

*Helen E. Phillips, IASOS, University of Tasmania, Australia; and Stephen R. Rintoul, Antarctic Cooperative Research Centre, CSIRO Division of Marine Research, Australia. h.e.phillips@utas.edu.au*

Prior to 1995, long-term, in situ measurements of velocity and temperature had been made at only two locations in the Antarctic Circumpolar Current (ACC): in the Drake Passage (Bryden, 1979; Sciremammano, 1980; Nowlin et al., 1985); and south-east of New Zealand (Bryden and Heath, 1985).

A third location in the ACC has been recently monitored with an array of current meter moorings south of Australia, the AUSSAF array (Fig. 1, page 23). The location is a choke point for the ACC, but not a tight one, and satellite altimeter maps of velocity variance have shown it to be a region of low but growing eddy energy (Morrow et al., 1994). The array was positioned so as to be centred on the strongest jet of the ACC which is the Subantarctic Front (SAF) south of Australia.

In this article we present some highlights of results from the AUSSAF current meter array, focusing on the role of eddies in the heat balance of the Southern Ocean. The eastward propagation of five SAF meanders through the array during the deployment also allowed a relationship between vertical motion and meander phase (Lindstrom and Watts, 1994) to be examined.

## Observations

The AUSSAF array, near 50°30′S, 143°E, consists of 4 tall current meter moorings deployed during March 1993 and recovered in January 1995 (Fig. 1). The array sits in approximately 3800 m of water on the northern flank of the Southeast Indian Ridge, downstream of the point where the ridge, and the ACC, turn south-eastward.

In total, 18 Aanderaa current meters were deployed at nominal depths of 300, 600, 1000, 2000 and 3200 m on the West, South and Central moorings, and at 1000, 2000 and 3200 m on North. Temperature and velocity at nominal depths of 1000 m and above were corrected for mooring motion, using the method of Hogg (1991), to constant pressure levels of 420, 780 and 1150 dbar, the mean pressures of these instruments averaged over the array.

## Temperature and velocity fields at AUSSAF

Fig. 2 is a vertical section of temperature from the SR3 hydrographic line during January 1994. The SAF is clearly visible near 51°S as the sharp shoaling of isotherms toward the south. A cold-core ring is visible north of the SAF near 48.5°S; these were frequently observed along SR3 and a nearby high-density XBT line (Rintoul et al., 1997).

Ten-day maps of sea surface height (anomalies from satellite altimeters TOPEX/POSEIDON, ERS-1 and ERS-2 (Le Traon et al., 1998) added to Olbers et al. (1992) climatology) show that during the array deployment 5 meanders of the SAF propagate slowly eastward through the array, occasionally stalling over the array for several months. Mean current vectors turn across the array, consistent with a meander crest to the west of the array. Instantaneous current flow at the array is energetic and highly variable. The maximum horizontal speed is 74 cm s$^{-1}$ at 420 dbar, with record length mean speeds up to 33 cm s$^{-1}$. Current directions vary from south-westward to north-westward through the eastern half of the compass.

There is no evidence of seasonality in either the temperature or velocity records, rather variability is dominated by the passage of the SAF through the array. Temperature and velocity fluctuations are highly coherent through the water column.

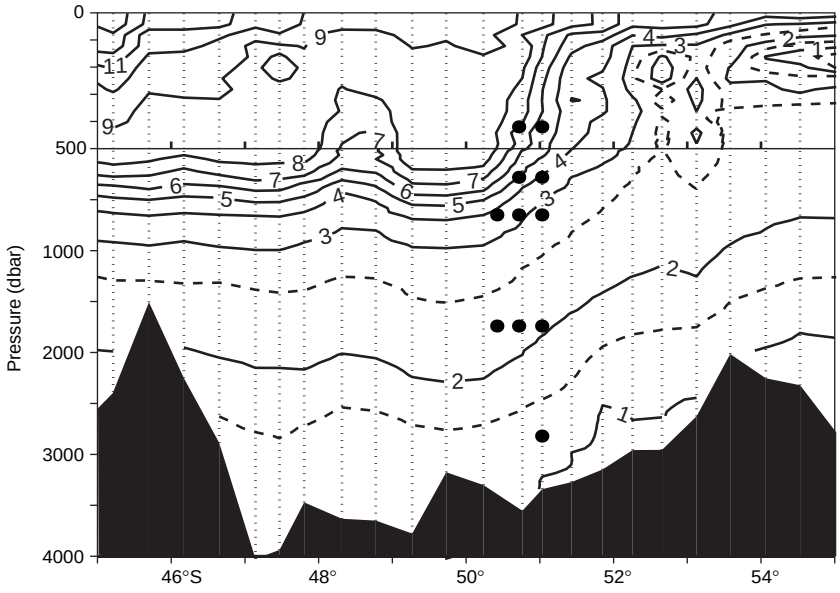


*Figure 2. CTD temperature (°C) section along part of WOCE SR3 during January 1994. Working current meters on the main line (solid circles) and CTD stations (dotted lines) are shown. The top 500 m is expanded.*

## Temperature, 3-D velocity and meander phase

Due to the meandering nature of the SAF we examine horizontal velocity in time-

varying shear coordinates (Hall, 1986; Phillips and Rintoul, 2000). Along-stream is defined as the daily direction of the vertical current shear between 420 and 2240 dbar, and cross-stream is 90° to the left of along-stream. The shear definition allows the changing front orientation to be isolated from the true mesoscale eddy field.

In Fig. 3, we illustrate the coupling between the temperature and 3-dimensional velocity field with time series from the south mooring. Vertical velocity is inferred from the current meter data (Bryden, 1980; Phillips and Rintoul, 2000). Temperature $T$ and along-stream velocity $\hat{u}$ (Fig. 3a,b) clearly show whether the SAF is north of (low $T$, low $\hat{u}$), south of (high $T$, low $\hat{u}$), or in (high $\hat{u}$) the array.

Cross-stream velocity $\hat{v}$ (Fig. 3c) is much weaker and more erratic than along-stream but is significantly anti-correlated with $T$ at 95% or higher for all levels at south and at 90% or higher for 5 of the 11 remaining instruments, suggesting strong poleward transport of heat by eddy fluxes.

When the rotation of the horizontal velocity vectors with decreasing depth (Fig. 3e) is anticyclonic (anticlockwise), known as veering, upwelling is present (Fig. 3d). For the opposite scenario, backing, downwelling is present. Note also that cross-stream velocity (Fig. 3c) is predominantly poleward (producing warm advection) during upwelling events and equatorward (cold advection) at times of downwelling. Cross-stream velocity is anti-correlated with vertical velocity at 95% significance.

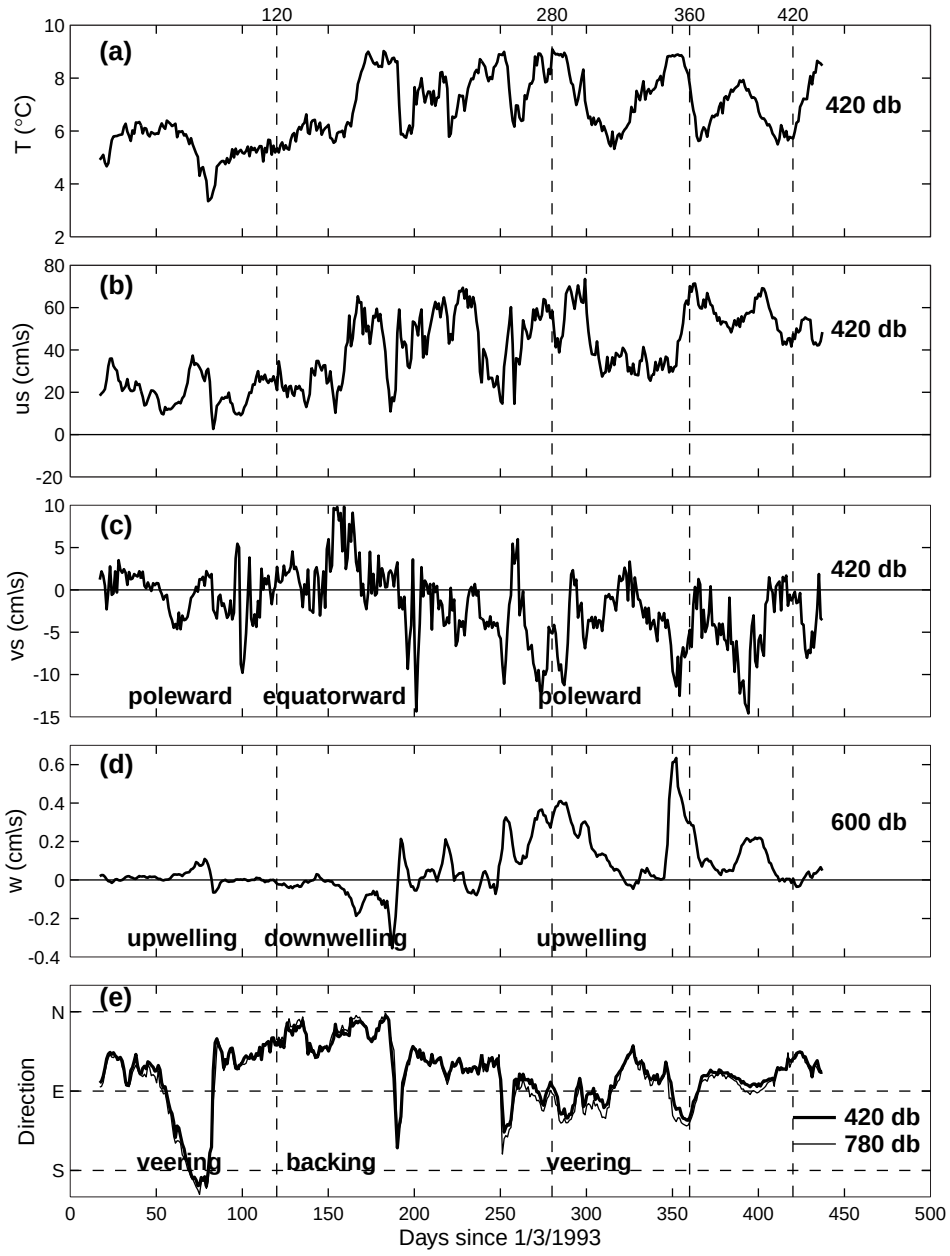


*Figure 3. Time series from South showing the link between rotation of current vectors with depth, cross-stream and vertical velocities: (a) temperature, (b) along-stream velocity and (c) cross-stream velocity, all at 420 dbar, (d) vertical velocity at 600 dbar and (e) current direction at both 420 and 780 dbar. Downwelling (upwelling) and cold (warm) advection occur when the current is backing (veering). The 4 days selected relate to Fig. 4.*

From the SSH maps, the location of meanders relative to the moorings can be clearly seen. Whenever the western edge of a meander crest was over the array, the moorings revealed veering, warm advection and upwelling (case A). The backing scenario was observed when an eastern edge was over the array (case B). Fig. 4a,b show SSH for 2 examples of case A (days 280 and 360) with current vectors from the 1150 dbar current meters overlaid (the level with fewest gaps). The current vectors are closely aligned with the surface height contours. In Fig. 3, we see that there is strong upwelling on both days ($2-3\,\mathrm{mm\,s^{-1}}$) at the south mooring, the current is veering, and cross-stream flow is poleward, producing warm advection. For case B (days 120 and 420, Fig. 4c,d), the current is backing, vertical motion is weakly downward and cross-stream flow is either weakly equatorward (cold advection) or zero.

Thus, the relationship between vertical motion and meander phase described by Lindstrom et al. (1997) for the Gulf Stream also holds for the SAF and probably the ACC in general. That is: backing, cold advection and downwelling, "bcd" to use Lindstrom et al.'s

mnemonic, occur entering a trough (exiting a crest); veering warm advection and upwelling, "uvw", occur exiting a trough (entering a crest).

## Heat balance of the Southern Ocean

Heat loss from the Southern Ocean south of the Polar Front has been estimated at $4.5 \times 10^{14}$ W (Nowlin and Klinck, 1986), which must be balanced by poleward eddy heat flux or heat transport via deep boundary currents. There are no measurements to date of the latter, but existing in-situ observations suggest eddies are able to transport all of the required heat.

In calculating cross-SAF heat fluxes, we isolate the "eddy" band, which is thought to play such a crucial role in the transfer of properties across the ACC fronts, from the "low-frequency" band composed of meanders, rings and large-scale shifts of the front which are dynamically very different. Based on examination of cospectra of temperature and cross-stream velocity, we define the eddy band as motions with periods between 40 hours and 90 days (as also done by Nowlin et al. 1985).

Fig. 5a shows the record length mean eddy heat flux at each instrument on the four moorings. Cross-stream eddy heat flux is defined as $\rho_0 C_p \hat{v}_i' T_i'$, where $\hat{v}_i'$ and $T_i'$ are fluctuation cross-stream velocity and temperature at time $t_i$, $\rho_0$ is a representative water density for the location ($= 1035\,\mathrm{kg\,m^{-3}}$), and $C_p$ is the specific heat at constant pressure ($\approx 4000\,\mathrm{J\,kg^{-1}\,°C^{-1}}$).

Eight of the 16 flux estimates are significantly different from zero at 95% and a further 2 estimates are significant at 90%. The average of these 4 profiles (Fig. 5b, solid circles) shows poleward eddy heat flux at all levels, with a depth-average of $11.3\,\mathrm{kW\,m^{-2}}$. The mean annual heat loss from the ocean south of the Polar Front corresponds to a point heat flux of approximately $5.6\,\mathrm{kW\,m^{-2}}$ (reckoning a path length of 20,000 km and a depth of 4 km). Thus, poleward eddy heat flux at the AUSSAF array is more than large enough to balance the observed loss.

In Fig. 5b we compare AUSSAF eddy heat flux with that from south-east of New Zealand and northern Drake Passage. The AUSSAF eddy heat flux profile (solid circles) may be compared directly with eddy band fluxes relative to the 90-day low-passed current in northern Drake Passage (solid squares). To compare with all-frequency geographic coordinate heat flux estimates south-east of New Zealand (open triangles, Bryden and Heath, 1985) and in northern Drake Passage (open squares, Bryden, 1979), we have also plotted AUSSAF all-frequency, shear coordinate fluxes (open circles).

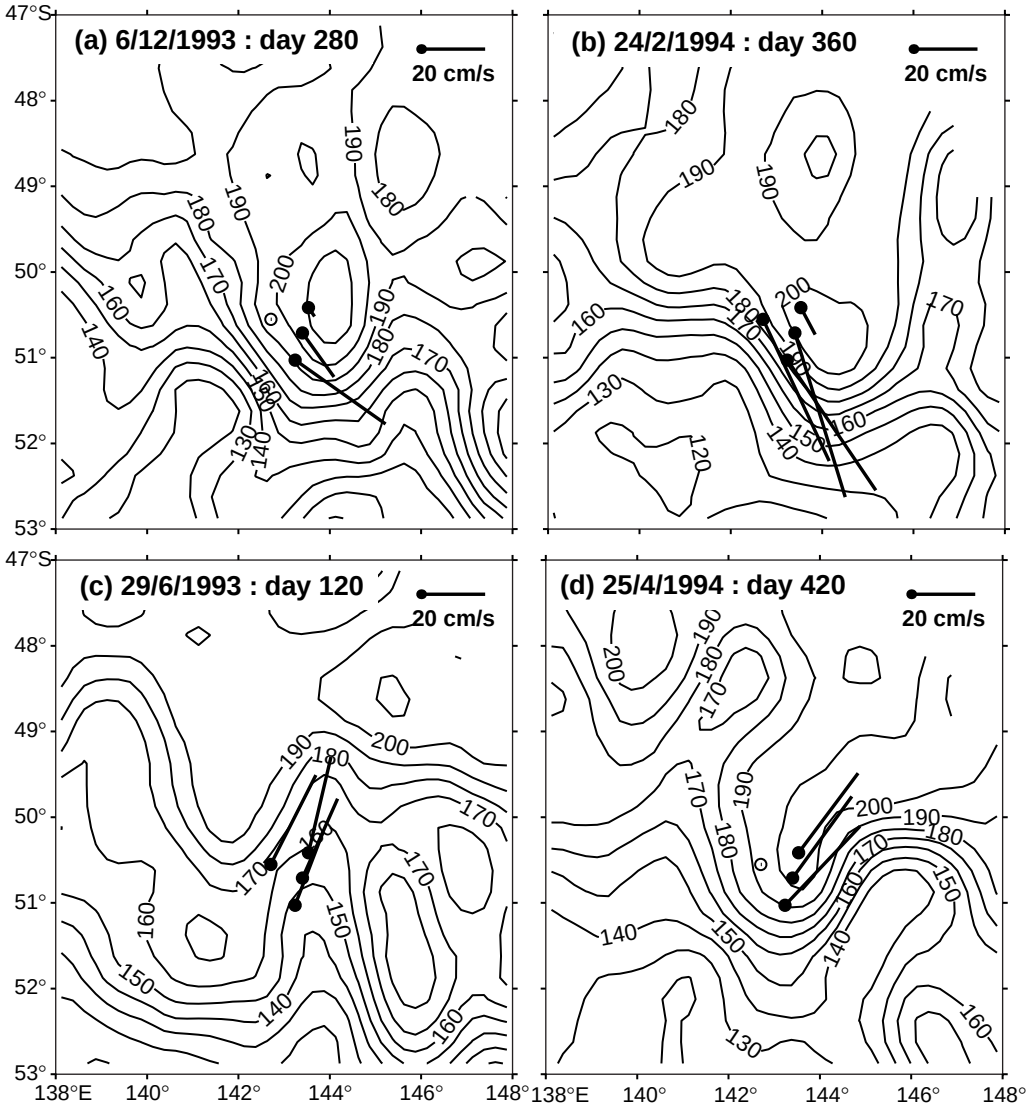


*Figure 4. Ten-day average current vectors at 1150 dbar on 4 days, and corresponding sea surface height. Sea surface height anomalies from the TOPEX/POSEIDON, ERS-1 and ERS-2 satellite altimeters, merged and mapped onto a 0.25° grid (the CLS "MSLA" data set (Le Traon et al., 1998)), have been added to the 0–2000 m dynamic height from the Olbers et al. (1992) climatology.*

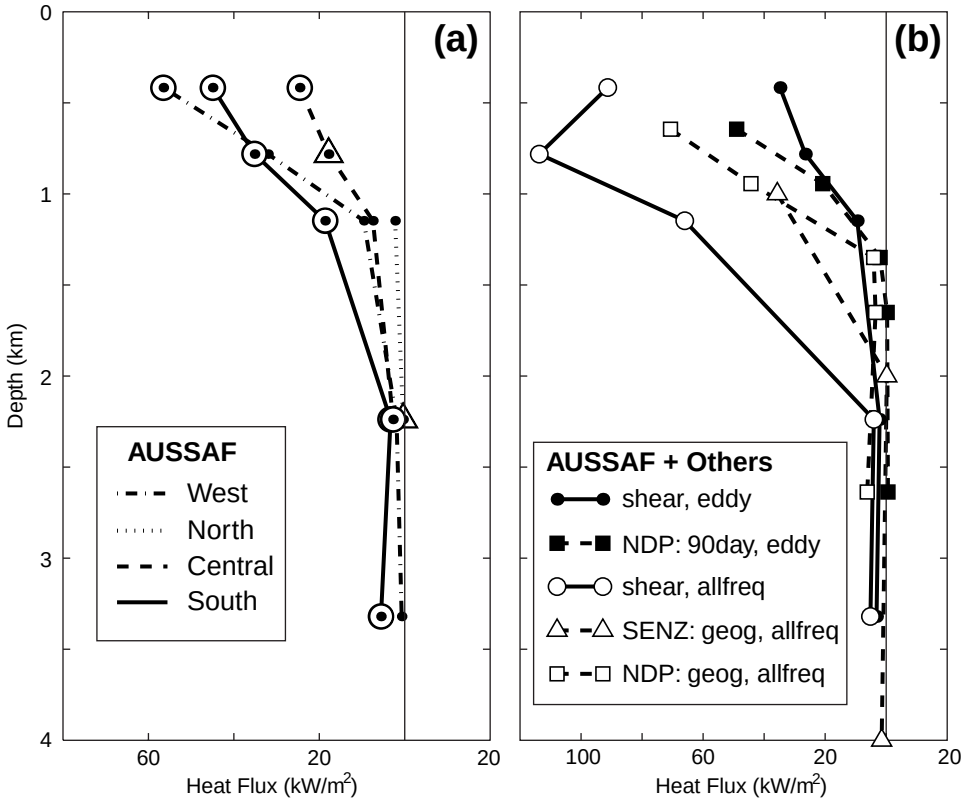


*Figure 5. Profiles of cross-stream eddy heat flux $\rho_0 C_p \overline{v' T'}$. (a) 4 AUSSAF moorings, shear coordinate, bandpassed data. Symbols over the data point indicate statistical significance: triangle = 90%, circle = 95%, (b) representative profiles from all available SAF sites: array-mean of AUSSAF shear-coordinate, bandpassed fluxes; array-mean of AUSSAF shear-coordinate, all-frequency fluxes; south-east of New Zealand (Bryden and Heath, 1985); and 2 northern Drake Passage estimates (Nowlin et al., 1985).*

All fluxes are poleward or not statistically significant. The comparison suggests that poleward eddy heat flux across the SAF is approximately the same size in Drake Passage and south of Australia, and that poleward heat flux by lower frequency motions is much stronger south of Australia. South-east of New Zealand, poleward heat flux is weaker than at the other two sites.

## Summary and conclusions

Current flow at the AUSSAF array is energetic, episodic and highly variable. Mean current vectors turn across the array, consistent with a meander crest to the west of the array. Sea surface height maps show that 5 meanders propagate slowly eastward during the deployment, occasionally stalling over the array for several months. Vertical motion at the array, inferred from the current meter data, is of order $1\,\mathrm{mm\,s^{-1}}$, similar to that found in the Gulf Stream and Kuroshio Extension. The relationship between vertical motion and meander phase identified by Lindstrom et al. (1997) for the Gulf Stream has been found to apply to the ACC.

The definition of a daily-varying coordinate frame which follows the direction of current flow allows the mesoscale variability of the SAF to be examined in isolation from the variability caused by the changing orienation of the front, and proved to be the best coordinate frame with which to assess cross-stream eddy fluxes of heat.

Poleward eddy heat flux at AUSSAF is large ($11.3\,\mathrm{kW\,m^{-2}}$ averaged over the array and vertically integrated) and significantly different from zero at 95%. Zonally integrating this point estimate leads to a circumpolar eddy heat flux of $9\times10^{14}\,\mathrm{W}$, more than enough to balance the estimated $4.5\times10^{14}\,\mathrm{W}$ lost south of the Polar Front.

The site of the AUSSAF array is a region of growing eddy energy in contrast to the mature eddy fields of Drake Passage and south-east of New Zealand. The strongest indication of this is the larger eddy heat flux at AUSSAF and the correspondingly large baroclinic conversion of available potential energy. While the ACC remains sparsely monitored, the AUSSAF array provides new estimates of eddy variability in a region dynamically different to the sites previously monitored.

## Acknowledgements

We thank the officers and crew of the RSV Aurora Australis for their contribution to this work; Fred Boland, Kevin Miller, Danny McLaughlin and Mark Rosenberg for the design, deployment and recovery of the moorings; and John Church, Richard Coleman and Nathan Bindoff for valuable comments on an earlier draft of this paper. The altimeter products were produced as part of the Environment and Climate EU projects AGORA and DUACS, and are made available on CD-ROM by AVISO. This work was supported in part by Environment Australia through the National Greenhouse Research Program, and by the Australian National Antarctic Research Expeditions (ANARE). This paper is a contribution to the World Ocean Circulation Experiment (WOCE).

## References

Bryden, H. L., 1979: Poleward heat flux and conversion of available potential energy in Drake Passage. J. Mar. Res., 37, 1–22.

Bryden, H. L., and R. A. Heath, 1985: Energetic eddies at the northern edge of the Antarctic Circumpolar Current. Prog. Oceanogr., 14, 65–87.
Bryden, H. L., 1980: Geostrophic vorticity balance in midocean. J. Geophys. Res., 85, 2825–2828.
Hall, M. M., 1986: Horizontal and vertical structure of the Gulf Stream velocity field at 68°W. J. Phys. Oceanogr., 16, 1814–1828.
Hogg, N. G., 1991: Mooring motion corrections revisited. J. Atmos. Oceanic Technol., 8, 289–295.
Le Traon, P. Y., F. Nadal, and N. Ducet, 1998: An improved mapping method of multi-satellite altimeter data. J. Atmos. Oceanic Technol., 25, 522–534.
Lindstrom, S. S., X. Qian and D. R. Watts, 1997: Vertical motion in the Gulf Stream and its relation to meanders. J. Geophys. Res., 102, 8485–8503.
Lindstrom, S. S., and D. R. Watts, 1994: Vertical motion in the Gulf Stream near 68°W. J. Phys. Oceanogr., 24, 2321–2333.
Morrow, R., R. Coleman, J. Church, and D. Chelton, 1994: Surface eddy momentum flux and velocity variances in the Southern Ocean from Geosat altimetry. J. Phys. Oceanogr., 24, 2050–2071.
Nowlin, Jr., W. D., and J. M. Klinck, 1986: The physics of the Antarctic Circumpolar Current. Rev. Geophys., 24, 469–491.
Nowlin, Jr., W. D., S. J. Worley, and T. Whitworth, III, 1985: Methods for making point estimates of eddy heat flux as applied to the Antarctic Circumpolar Current. J. Geophys. Res., 90, 3305–3324.
Olbers, D., V. Gouretski, G. Seiβ and J. Schröter, 1992: Hydrographic atlas of the Southern Ocean. Alfred-Wegener-Institut, Bremerhaven, Germany, 17pp.+82 plates.
Phillips, H. E., and S. R. Rintoul, 2000: Eddy variability and energetics from direct current measurements in the Antarctic Circumpolar Current south of Australia. J. Phys. Oceanogr., in press.
Rintoul, S. R., J. R. Donguy, and D. H. Roemmich, 1997: Seasonal evolution of upper ocean thermal structure between Tasmania and Antarctica. Deep-Sea Res., 44, 1185–1202.
Sciremammano, F. Jr., 1980: The nature of the poleward heat flux due to low-frequency current fluctuations in Drake Passage. J. Phys. Oceanogr., 10, 843–852.
Smith, W. H. F., and D. T. Sandwell, 1994: Bathymetric prediction from dense satellite altimetry and sparse shipboard bathymetry. J. Geophys. Res., 99, 21803–21824.

## The dynamics of ocean heat transport variability

*Steven R. Jayne*, National Center for Atmospheric Research, USA; and*
*Jochem Marotzke, Southampton Oceanography Centre, UK. surje@ncar.ucar.edu*

One of the principal goals of WOCE is to understand the global large-scale ocean heat transport and its variability over a broad range of time and length scales (World Climate Research Programme, 1986). The north–south heat transport is the prime manifestation of the ocean's role in global climate, but understanding of its variability has been fragmentary owing to uncertainties in observational analyses, limitations in models, and the lack of a convincing mechanism. With the completion of the observational phase of WOCE, more hydrographic sections are now available and better estimates of the global time-mean ocean heat transport are possible. In general, it can be said that the sign and magnitude of the ocean heat transport are known over the global ocean, and that quantifiable error estimates can be made. Hence, it is timely to consider the time-dependent nature of ocean heat transport, the nature and magnitude of which are not well known, with extant estimates differing not only in magnitude but in sign as well.

In this note we touch upon some of the questions concerning the ocean's role in climate, by addressing temporal variability in the ocean's transport of heat and, in particular, the global nature of the relevant ocean dynamics (this article summarises some results contained in a more detailed paper Jayne and Marotzke, 2000). An ocean general circulation model (the Parallel Ocean Climate Model, POCM, Semtner and Chervin, 1988, 1992; Stammer et al., 1996; McClean et al., 1997) is used to understand the ocean's response to the seasonally varying wind stress. The numerical simulation output from run 4_B of the POCM, is used to calculate ocean mass and heat transport at three day intervals. The POCM is a primitive-equation, level model configured for the global ocean between 75°S and 65°N, with realistic topography. The heat transport from the model was calculated at 3-day intervals and the time-mean heat transport was then removed. The results are presented in a Hovmöller diagram (Fig. 1, page 22) of the heat transport anomaly (from the time-mean) as a function of latitude and time for the World Ocean, and the annual cycle for the ocean basins is summarised in Fig. 2.

Globally, the cross-equatorial, seasonal heat transport fluctuations are close to $\pm 4.5 \times 10^{15}$ watts, the same amplitude as the seasonal, cross-equatorial atmospheric energy transport. The seasonal cycle of ocean heat transport is directed from the summer hemisphere to the winter hemisphere (i.e. northward in boreal winter and southward in austral winter), in phase with the annual cycle of total energy transport by the atmosphere's Hadley cell (Peixoto and Oort, 1992). At 7°N, the Atlantic and Pacific Oceans have their maximum amplitude in the seasonal cycle of 1 PW and 3 PW, respectively. The Indian Ocean has its

*Also at CIRES and Dept. of Physics, University of Colorado, USA.

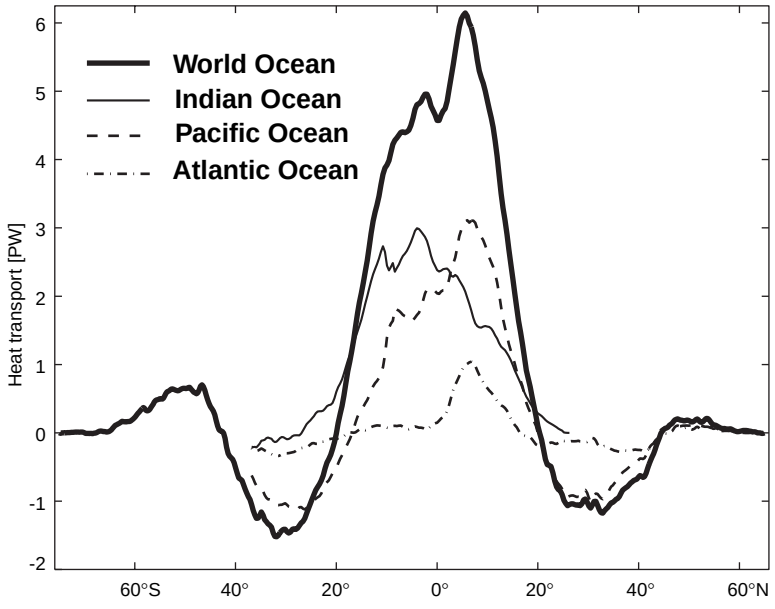


*Figure 2. Annual cycle of heat transport defined as the difference between averaged January and averaged July values for the World Ocean (heavy solid line), the Indian Ocean (thin solid line), the Pacific Ocean (dashed line) and the Atlantic Ocean (dashed–dotted line).*

maximum peak-to-peak seasonal cycle of 2.6 PW at 5°S. Globally, the variability is concentrated within 20° of the equator and dominated by the annual cycle, with higher-frequency variability superimposed on it.

To explain this large variability, we build upon the approach put forth by Bryan (1982) which we expand by linking it to the theoretical work of Willebrand et al. (1980) and Schopf (1980). In summary, the majority of the heat transport variability can be ascribed to the "Ekman heat transport". Introduced by Bryan (1962), it was expanded upon by Bryan (1982) in his analysis of early modelling work, and then used with observational data by Kraus and Levitus (1986) and later by Levitus (1987), Adamec et al. (1993) and Ghirardelli et al. (1995). The definition of the Ekman heat transport given by Kraus and Levitus (1986)in the following equation:

$$H(t) = -\int \rho_0 c_p \frac{\tau_\lambda}{f\rho_0}\{T_{Ek} - [\theta]\} a \cos\phi \, \mathrm{d}\lambda$$

where $c_p$ is the specific heat of seawater, $f$ is the Coriolis parameter, $T_{Ek}(x)$ is the temperature of the surface Ekman layer, $[\theta]$ is the zonal and depth-averaged potential temperature, $\tau_\lambda(x)$ is the zonal wind stress, and $a$ is the radius of the earth.

Simply put, this equation expresses the heat transport as the integral of the Ekman mass flux times the difference between the Ekman layer temperature and the section averaged potential temperature. It implies that for any given section the mass transport in the Ekman layer is compensated by a return flow distributed uniformly across the depth and zonal extent of the section. Indeed, Kraus and Levitus (1986) and succeeding writers, such as Levitus (1987), Adamec et al. (1993), and Ghirardelli et al. (1995), all assumed that this equation held over all timescales. Adamec et al. (1993) and Ghirardelli et al. (1995) also made the further assumption the local Ekman transport was returned locally at the same longitude, but this is not necessary. In these previous works both the time-varying and the time-mean flows have been lumped together. The assumption that the return flow for the time-varying Ekman transport is deep and barotropic is supported by theory (Willebrand et al., 1980; Schopf, 1980; Jayne and Marotzke, 2000) and modelling studies (Bryan, 1982; Böning and Herrmann, 1994; Lee and Marotzke, 1998). However, Klinger and Marotzke (2000) have shown that the time-mean Ekman mass transport is returned at shallow depths, and relatively warm temperatures, within the main thermocline. Therefore, the heat transport by the time-mean Ekman flow would not be well represented by the assumption that its return flow was barotropic.

To compare the heat transport variability in the full model to the Ekman heat transport, a simple estimate from data can be made of the annual cycle based on the climatology of ocean temperature (Levitus et al., 1994) and monthly-averaged wind stress fields derived from the same fields used to force the POCM simulation. The results are shown in Fig. 3. Overall, the agreement between the heat transport variability in POCM and this simple calculation are excellent, and supports our conclusion that the time-dependent ocean heat transport is essentially given by the time-varying part of the Ekman heat transport.

In summary, the temporal variability in the ocean heat transport is dominated by the Ekman heat transport. The deep compensating return flows have little shear associated with them and therefore would not affect estimates of the heat transport from hydrographic surveys in any of the ocean basins, in agreement with the findings for the Atlantic Ocean of Böning and Herrmann (1994). As for other sources of variability, away from the tropics, the heat transport variability associated with the barotropic gyre and baroclinic circulations, are much weaker than the Ekman variability, and can amount to a 0.2–0.4 PW variance in the heat transport measured by a one-time hydrographic survey. Hence estimates of the time-mean heat transport made from one-time hydrographic surveys using the method of Hall and Bryden (1982) are fundamentally sound. One of the goals of future observations and modelling efforts should be to understand smaller, but perhaps locally significant, baroclinic heat transport variations, as well as longer time scale variability.

## Acknowledgements

Special thanks are due to Robin Tokmakian and Bert Semtner from the Naval Postgraduate School, who generously provided their numerical model output. Funding

for this research came from the Department of Defence under a National Defence Science and Engineering Graduate Fellowship (SRJ), from the National Science Foundation (NSF), the American Automobile Manufacturers Association, and the Tokyo Electric Power Company through the TEPCO/MIT Environmental Research Program. The computational resources for this work were provided by the National Center for Atmospheric Research, which is supported by the National Science Foundation.

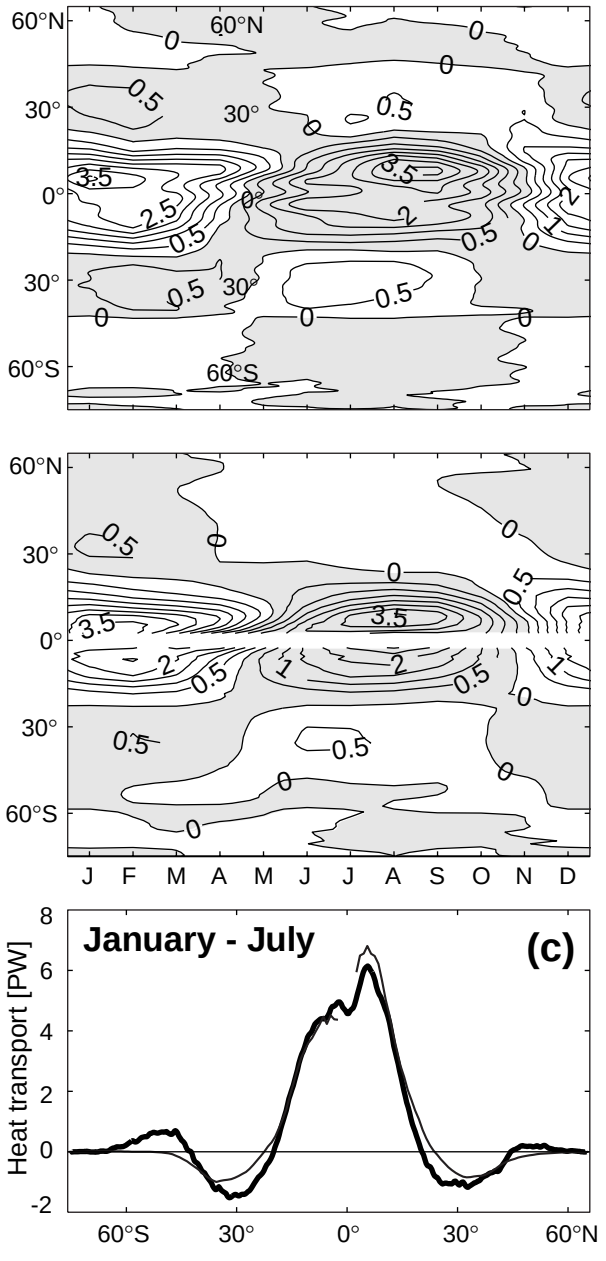


*Figure 3. (a) Annual cycle of heat transport from POCM. (b) Annual cycle of Ekman heat transport from wind stress and temperature anomalies for the World Ocean using the Levitus et al. (1994) climatology and (1). (c) The annual cycle (January–July) from the POCM (heavy line) versus climatology (thin line) for the World Ocean. Contour interval for (a) and (b) is 0.5 PW.*

## References

Adamec, D., M. M. Rienecker, and J. M. Vukovich, 1993: The time-varying characteristics of the meridional Ekman heat transport for the world ocean. J. Phys. Oceanogr., 23, 2704–2716.

Böning, C. W., and P. Herrmann, 1994: Annual cycle of poleward heat transport in the ocean: Results from high-resolution modeling of the North and Equatorial Atlantic. J. Phys. Oceanogr., 24, 91–107.

Bryan, K., 1962: Measurements of meridional heat transport by ocean currents. J. Geophys. Res., 67, 3403–3414.

Bryan, K., 1982: Seasonal variation in meridional overturning and poleward heat transport in the Atlantic and Pacific Oceans: a model study. J. Mar. Res., 40, Suppl., 39–53.

Ghirardelli, J. E., M. M. Rienecker, and D. Adamec, 1995: Meridional Ekman heat transport: Estimates from satellite data. J. Phys. Oceanogr., 25, 2741–2755.

Hall, M. M., and H. L. Bryden, 1982: Direct estimates and mechanisms of ocean heat transport. Deep-Sea Res., 29, 339–359.

Jayne, S. R., and J. Marotzke, 2000: The dynamics of wind-induced ocean heat transport variability. Rev. Geophys., submitted.

Klinger, B. A., and J. Marotzke, 2000: Meridional heat transport by the subtropical cell. J. Phys. Oceanogr., in press.

Kraus, E. B., and S. Levitus, 1986: Annual heat flux variations across the tropic circles. J. Phys. Oceanogr., 16, 1479–1486.

Lee, T., and J. Marotzke, 1998: Seasonal cycles of meridional overturning and heat transport of the Indian Ocean. J. Phys. Oceanogr., 28, 923–943.

Levitus, S., 1987: Meridional Ekman heat fluxes for the World Ocean and individual ocean basins. J. Phys. Oceanogr., 17, 1484–1492.

Levitus, S., R. Burgett, and T. Boyer, 1994: World Ocean Atlas 1994, Vol. 3, Salinity, and Vol. 4, Temperature. NOAA Atlas NESDIS 3 & 4, US Department of Commerce, Washington, DC.

McClean, J. L., A. J. Semtner, and V. Zlotnicki, 1997: Comparisons of mesoscale variability in the Semtner-Chervin $\frac{1}{4}°$ model, the Los Alamos Parallel Ocean Program $\frac{1}{6}°$ model, and TOPEX/POSEIDON data. J. Geophys. Res., 102, 25203–25226.

Peixoto, J. P., and A. H. Oort, 1992: Physics of Climate. American Institute of Physics.

Schopf, P. S., 1980: The role of Ekman flow and planetary waves in the oceanic cross-equatorial heat transport. J. Phys. Oceanogr., 10, 330–341.

Semtner, A. J., and R. M. Chervin, 1988: A simulation of the global ocean circulation with resolved eddies. J. Geophys. Res., 93, 15502–15522, plates 15767–15775.

Semtner, A. J., and R. M. Chervin, 1992: Ocean general circulation from a global eddy-resolving model. J. Geophys. Res., 97, 5493–5550.

Stammer, D., R. Tokmakian, A. J. Semtner, and C. Wunsch, 1996: How well does a $\frac{1}{4}°$ global circulation model simulate large-scale oceanic observations? J. Geophys. Res., 101, 25779–25811.

Willebrand, J., S. G. H. Philander, and R. C. Pacanowski, 1980: The oceanic response to large-scale atmospheric disturbances. J. Phys. Oceanogr., 10, 411–429.

World Climate Research Programme, 1986: Scientific Plan for the World Ocean Circulation Experiment. WCRP Publication Series No. 6, WMO/TD-No. 122.

# US JGOFS team examines Pacific Ocean $CO_2$ data quality

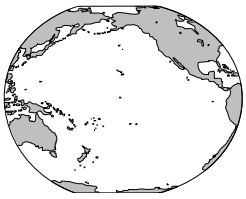

*C. L. Sabine, M. F. Lamb, J. L. Bullister, R. A.Feely, and G. C. Johnson, Pacific Marine Environmental Laboratory, NOAA, USA; R. M. Key, Department of Geosciences, Princeton University, USA; A. Kozyr, CDIAC, Oak Ridge National Laboratory, USA; and K. Lee, F. J. Millero, T.-H. Peng, and R. Wanninkhof, Atlantic Oceanographic and Meteorological Laboratory, NOAA, USA. sabine@pmel.noaa.gov*

The recently completed WOCE/JGOFS global carbon survey produced over an order of magnitude more high-quality carbon measurements than previous global survey efforts. These data provide an important asset to the scientific community investigating biogeochemical cycling in the oceans. Most of the data have been reported to national archive facilities, but have not been synthesised into a unified, internally consistent global data set. As a part of the US JGOFS synthesis and modelling project several groups of investigators have been working to synthesise the global survey data to better understand carbon cycling in the ocean. Investigators compiling global data on the spatial and temporal patterns in inorganic carbon are working closely with groups compiling the inorganic nutrients, chlorofluorocarbons (CFC), carbon-14, carbon-13 and carbonate saturation states from the JGOFS/WOCE cruises as part of the Global Data Analysis Project (GLODAP). We are also working through the Ocean Carbon Model Intercomparison Project (OCMIP) to directly compare these global datasets with 13 global ocean carbon models. By working together, observationalists and modellers hope to achieve a better understanding of the ocean carbon cycle than any one group might be able to accomplish on their own.

The carbon synthesis effort is currently focusing on the Pacific data set. Between 1991 and 1996, carbon measurements were made by 16 different groups on 24 survey cruises in the Pacific Ocean (Tables 1 and 2; Fig. 1, page 22). At least two carbon parameters were run on every leg, but the techniques and even the carbon pair measured varied depending on which group ran the individual leg. Total carbon dioxide ($TCO_2$) was measured on all 24 legs but additional carbon parameters depended on the analysis group. Two of the lines had $TCO_2$ and pH as the primary carbon pair. Six lines were analysed for $TCO_2$ and $CO_2$ partial pressure ($pCO_2$). $TCO_2$ and total alkalinity (TA) were measured on the remaining lines. Nearly half of the cruises with TA measurements also had $pCO_2$ and/or pH measured as well.

## Approach

Given the diversity of carbon measurements in the Pacific, we have made a special effort to evaluate the quality and internal consistency of these data by examining the following information:

(1) A comparison of calibration techniques for the various measurements as well as the frequency and consistency of these calibrations help provide some information on the reliability of the results.

(2) Many of the analysis teams frequently collected and analysed replicate samples at sea. While these replicates do not provide information on accuracy, they do provide information on the precision and overall quality of the measurements.

(3) Certified Reference Materials (CRM) are preserved seawater samples that have been certified at Scripps Institution of Oceanography (SIO) to have given $TCO_2$ and TA concentrations (UNESCO, 1991; Dickson, 1992; Dickson and Anderson, submitted; Dickson et al., submitted). Analyses of these samples provide a secondary standard by which the at-sea calibrations can be evaluated. These CRMs were just coming on line as the Pacific survey was beginning, so they were not consistently run until the latter cruises.

(4) Most of the US carbon teams collected a limited number of replicate samples to be returned to C. D. Keeling at SIO for manometric $TCO_2$ analysis. These results provide an independent assessment of the shipboard measurements.

(5) Where three or more carbon parameters were measured, the internal consistency of all of the carbon measurements on that leg can be examined by comparing measured values with values calculated from different carbon pairs.

(6) A comparison of deep water (P>2000 dbar) values in locations where two or more cruises cross or overlap provides a powerful test of the internal consistency of different cruises. Sixty-four crossover locations were analysed for $TCO_2$. Fewer crossovers were available for other parameters that were not measured on every leg.

(7) A basic assumption of the crossover comparison is that the waters did not change in the time between cruises. As a double check on the validity of this assumption, the crossovers that were more than one standard deviation from the mean difference were also examined using a multiparameter linear regression (MLR) approach. With the MLR technique, the carbon data from one of the crossover stations were fit as a function of other hydrographic parameters measured at that station (e.g. temperature, salinity). This fit was then used to estimate the carbon data for the second crossover station using the hydrographic data on that cruise. Differences between the cruise two estimated carbon values and the measured carbon values should be the same as the differences observed

in approach #6 if there were no significant water mass differences. This approach has the advantage that it should account for any real changes in the water between cruises, but has the disadvantage that it will fold in any errors in the hydrographic measurements. This technique was primarily used to confirm any large differences observed in approach #6.

(8) The number of crossovers in the North Pacific was limited by the fact that only one zonal line (P2) had reported carbon values. To evaluate the internal consistency of the cruises in this region, all of the deep water (P>2500 dbar) values in the North Pacific were combined and used to generate MLR functions for $TCO_2$ and TA. These fits captured the average carbon distribution in the North Pacific. Deviations in the residuals of the individual cruises indicate which cruises do not follow the general distribution patterns described by the overall data set. The limitations with this approach are that the cruises with significant offsets may bias the overall fits. We attempted to minimise this potential bias by repeating the fit without the cruises that fell outside the two-sigma interval of the initial fit.

## Results

The Pacific $TCO_2$ values were all analysed using coulometric techniques outlined in the Handbook of Methods for the Analysis of the Various Parameters of the Carbon Dioxide System in Sea Water (DOE, 1994). No obvious problems were noted with the slight variations in the basic techniques used by the differing groups. Many of the groups used the Single Operator Multiparameter Metabolic Analyzer (SOMMA) described by Johnson et al. (1985, 1987), which has proven to be a very reliable instrument. The results of 64 crossover comparisons and the other approaches described above suggest that the reported $TCO_2$ values for the Pacific are generally accurate to $\sim \pm 3\,\mu mol\,kg^{-1}$.

TA values were analysed by closed cell (50–210 ml) potentiometric titration using the methods described by Millero et al. (1993) and the DOE Handbook (DOE, 1994). These data were generally found to be less precise than the $TCO_2$ values. The accuracy also varied depending on the analytical group. Twenty-two crossover locations were compared for TA where discrete measurements were made in the deep water; an additional 23 locations were compared by calculating TA, by using the combination of pH / $TCO_2$ or $pCO_2$ / $TCO_2$. These results together with the other approaches described above suggest that, in general, the accuracy of the reported Pacific TA values was approximately $\pm 6\,\mu mol\,kg^{-1}$.

Only four crossover points were examined for pH with an average difference of 0.004 ±0.001. Almost all of the measurements were based on the spectrophotometric techniques described by Clayton and Byrne (1993). The spectrophotometric technique appears to have very high precision, but there are some questions about the accuracy of these measurements. The revised "tris" buffer characterisation of DelValls and Dickson (1998) indicates that the reported pH data should be adjusted upward by 0.0047 pH units. This adjustment is also supported by our internal consistency checks as reported by Lee et al. (2000). Further laboratory tests are underway that will hopefully resolve this issue.

Discrete $pCO_2$ samples were analysed using three basic approaches: 500 ml sample with a 50 ml headspace analysed on a gas chromatograph (large volume-GC method described by Chipman et al., 1993), 500 ml sample with an 80 ml headspace analysed by non-dispersive infrared analyser (large volume-IR method described by Wanninkhof and Thoning, 1993), and 120 ml sample with 10 ml headspace analysed on a gas chromatograph (small volume-GC method described by Neill et al., 1997). Fifteen crossover comparisons were made for $pCO_2$. The $pCO_2$ crossover comparisons were complicated by the fact that $pCO_2$ measurements were performed at two different temperatures. $pCO_2$ is not a state variable like TA and $TCO_2$, but rather is a function of pressure and temperature. For this analysis, all samples analysed at 4°C were normalised to 20°C using the carbonate dissociation constants of Mehrbach et al. (1973) as refit by Dickson and Millero (1987). Based on this analysis it appears that the $pCO_2$ measurements in the Pacific are accurate to approximately ±24 µatm, which is roughly comparable to an accuracy of $\pm 3 - 4\,\mu mol\,kg^{-1}$ in $TCO_2$ or TA. However, we have found that the deep-water data measured with the large volume-IR system may give low results at $pCO_2$ values >700 µatm. This is in accordance with recent findings based on careful analyses of the internal consistency of the data (McElligott et al., 1998; Lee et al., 2000). We are investigating this matter further.

## Conclusions

Given the long timeframe over which the Pacific survey was conducted and the number of analytical groups and systems used to measure carbon in the Pacific, a thorough investigation into the quality and internal consistency of the data was a difficult but important task. The best data coverage was for $TCO_2$. These data were generally of very high quality with accuracy and precision that was close to an order of magnitude better than GEOSECS. Although the other carbon parameters were not sampled as frequently and generally had more analytical problems, they also represent the state-of-the-art at the time the measurements were made. The synthesis team is working to resolve the few outstanding issues. We are working to develop a set of recommendations for making these data as accurate and internally consistent as possible. We will also generate basin-wide gridded carbon distributions based on the optimised dataset and make these products available to the community. For further information on this and related projects see the GLODAP web page at:

http://cdiac.esd.ornl.gov/oceans/glodap.

*Table 1. Standardisation techniques, Pipet volume, CRM analyses, replicate analyses, and shorebased analyses for DIC during the Pacific Ocean Survey cruises.*

| *Cruise Name* | *$TCO_2$ Analysis Technique* | *$PI/TCO_2$* | *Standardisation Technique* | *Pipet Vol. (~ml)* | *CRM correction (SIO -cruise)* | *Field Replicate Analyses Average Difference µmol/kg* | *Shorebased Replicate Analyses Average Difference µmol/kg* | *Shore-based SD µmol/kg* | *n* |
|---|---|---|---|---|---|---|---|---|---|
| P8 | Coulometer | Shitashima | Liquid Stds. | 30 | 2.0±2.8 | 1.8 | N/A | N/A | |
| P9 | Coulometer | Ishii | Liquid Stds. | | 1.1±1.3 | 2.0 | N/A | N/A | |
| P10 | Coulometer/ SOMMA | Sabine | Gas Loops | 22 | ±1.9 | 1.7 | 0.6 | 1.8 | 9 |
| P13N | Coulometer/ SOMMA | Dickson | Gas Loops | | ±2.4 | 0.9 | -1.4 | 3.1 | 138 |
| P14N | Coulometer/ SOMMA | Winn | Gas Loops | | N/A | N/A | 0.7 | 2.3 | 27 |
| P14S/15S | Coulometer/ SOMMA | Feely | Gas Loops | 26 | -1.1±0.9 | 1.9 | N/A | N/A | N/A |
| P15N | Coulometer/ SOMMA | Wong | Liquid Stds. | 29 | -0.1±2.7 | N/A | N/A | N/A | N/A |
| EQS92 | Coulometer/ SOMMA | Feely | Gas Loops | 26 | -0.8±1.2 | N/A | N/A | N/A | N/A |
| P16C | Coulometer/ SOMMA | Goyet | N/A | 30 | (a) | N/A | -2.1 | 2.4 | 66 |
| P16N | Coulometer | Feely | Liquid Stds. | 50 | 3.0±2.5 | 2.8 | N/A | N/A | N/A |
| P16S/17S | Coulometer | Takahashi | Gas Loops | 20 | 1.3±1.5 | 0.03% | -3.5 | 2.0 | 11 |
| P16A/17A | Coulometer | Takahashi | Gas Loops | 20 | 1.0±1.7 | 0.03% | -3.4 | 1.8 | 14 |
| P17C | Coulometer/ SOMMA | Goyet | N/A | 30 | (a) | N/A | -3.4 | -4.0 | 40 |
| P17N | Coulometer/ SOMMA | Goyet | Liquid Stds. | 30 | (b) | N/A | -1.0 | 4.1 | 9 |
| CGC-91/1 | Coulometer | Feely | Liquid Stds. | 50 | 3.0±2.5 | 2.8 | N/A | N/A | N/A |
| P17E/19S | Coulometer | Takahashi | Gas Loops | 20 | 1.4±2.1 | 0.03% | N/A | N/A | N/A |
| P18 | Coulometer/ SOMMA | Feely | Gas Loops | 26 | -1.3±1.4 | 2.0 | -0.4 | 2.0 | 28 |
| P19C | Coulometer | Takahashi | Gas Loops | 20 | -0.2±2.1 | 0.03% | -1.0 | 1.9 | 15 |
| P2 | Coulometer | Ono | Gas Loops | 32 | 6.8±3.1 | N/A | N/A | N/A | N/A |
| P21 | Coulometer/ SOMMA | Millero | Gas Loops | | 0.9±1.1 | N/A | -2.3 | 1.5 | 15 |
| P31 | Coulometer/ SOMMA | Winn | Gas Loops | | -0.9±2.7 | N/A | 0.2 | 3.4 | 8 |
| P6 | Coulometer/ SOMMA | Wallace | Gas Loops | | -0.6±1.9 | N/A | -2.6 | N/A | 21 |
| S4P | Coulometer | Takahashi | Gas Loops | 20 | -0.9±1.8 | 0.03% | N/A | N/A | N/A |
| SR3/S4 | Coulometer/ SOMMA | Tilbrook | Gas Loops | 22 | 10.0±0.95 | 2.0 | N/A | N/A | N/A |

(a) CRM used as a primary standard
(b) CRMs not available

*Table 2. Summary of analytical techniques and PIs for TA, $pCO_2$ and pH during the Pacific Ocean Survey.*

| *Cruise Name* | *TA Analysis Technique* | *PI/TA* | *TA Cell Vol (~ml)* | *(c) $pCO_2$ Analysis Technique* | *PI/$pCO_2$* | *(d) Analysis Temperature (° C)* | *pH Analysis Technique* | *PI/pH* | *pH Cell Vol (~ml)* |
|---|---|---|---|---|---|---|---|---|---|
| P8 | Potentiometric | Shitashima | 50 | N/A | N/A | N/A | Spec. | Shitashima | 30 |
| P9 | N/A | N/A | N/A | N/A | N/A | N/A | N/A | N/A | N/A |
| P10 | Potentiometric | Sabine | 100 | N/A | N/A | N/A | N/A | N/A | N/A |
| P13N | Potentiometric | Guenther/ Keeling | | N/A | N/A | N/A | N/A | N/A | N/A |
| P14N | Potentiometric | Millero | 200 | N/A | N/A | N/A | Spec. | Winn | 30 |
| P14S/15S | Potentiometric | N/A | N/A | GC/Small | Wanninkhof | 20 | Spec. | Byrne | 10 |
| P15N | Potentiometric | Wong | 203 | N/A | N/A | N/A | N/A | N/A | N/A |
| EQS92 | Potentiometric | Millero | 200 | IR | Wanninkhof | 20 | Spec. | Byrne | 10 |
| P16C | Potentiometric | Guenther/ Keeling | 90 | N/A | N/A | N/A | N/A | N/A | N/A |
| P16N | N/A | N/A | N/A | N/A | N/A | N/A | Spec. | Byrne | 10 |
| P16S/17S | N/A | N/A | N/A | GC/Large | Takahashi | 20 | N/A | N/A | N/A |
| P16A/17A | N/A | N/A | N/A | GC/Large | Takahashi | >54° S=4/ <37° S=20c | N/A | N/A | N/A |
| P17C | Potentiometric | Goyet | 100 | N/A | N/A | N/A | N/A | N/A | N/A |
| P17N | (a) Potentiometric | Goyet | 100 | N/A | N/A | N/A | N/A | N/A | N/A |
| CGC-91/1 | N/A | N/A | N/A | N/A | N/A | N/A | Spec. | Byrne | 10 |
| P17E/19S | N/A | N/A | N/A | GC/Large | Takahashi | 4 | N/A | N/A | N/A |
| P18 | Potentiometric | Millero | 200 | IR | Wanninkhof | 20 | Spec. | Byrne | 10 |
| P19C | N/A | N/A | N/A | GC/Large | Takahashi | >54° S=4/ <37° S=20c | N/A | N/A | N/A |
| P2 | (a) Potentiometric | Ono | 150 | N/A | N/A | N/A | Potentio-metric | Ono | 150 |
| P21 | Potentiometric | Millero | 200 | N/A | N/A | N/A | Spec. | Millero | 30 |
| P31 | Potentiometric | Winn | 200 | N/A | N/A | N/A | Spec. | Winn | 30 |
| P6 | N/A | N/A | N/A | GC | N/A | N/A | N/A | N/A | N/A |
| S4P | N/A | N/A | N/A | GC/Large | Takahashi | 4 | N/A | N/A | N/A |
| SR3/S4 | Potentiometric | Tilbrook | 210 | N/A | N/A | N/A | N/A | N/A | N/A |

(a) CRMs not analysed
(c) IR=infrared analyser with samples in 500ml volumetric flasks (Wanninkhof and Thoning, 1993);
GC/small=GC with 120ml bottles (Neill et al., 1996);
GC/large=GC with samples in 500ml volumetric flasks (Chipman et al., 1993)
(d) Temperature varied according to surface water temperature
(f) Suspected to have anomalously low values at high $pCO_2$ (≈ >700 µatm)

## References


Chipman, D. W., J. Marra, and T. Takahashi, 1993: Primary production at 47°N and 20°W in the North Atlantic Ocean: A comparison between the $^{14}C$ incubation method and mixed layer carbon budget observations. Deep-Sea Res., II(40), 151-169.

Clayton, T., and R. H. Byrne, 1993: Spectrophotometric seawater pH measurements: total hydrogen ion concentration scale calibration of m-cresol purple and at-sea results. Deep-Sea Res., 40, 2115-2129.

DelValls, T. A., and A. G. Dickson, 1998: The pH of buffers based on 2-amino-2-hydroxymethyl-1,3-propanediol ("tris") in synthetic seawater. Deep-Sea Res., 45, 1541-1554.

Dickson, A. G., 1992: The determination of total dissolved inorganic carbon in sea water using extraction/coulometry: the first stage of a collaborative study. US Department of Energy Report No. DOE/RL/01830T-H14.

Dickson, A. G., and G. C. Anderson, 2000: Sea water based reference materials for $CO_2$ analysis: 1. Preparation, distribution and use. Mar. Chem., submitted.

Dickson, A. G., and F. J. Millero, 1987: A comparison of the equilibrium constants for the dissociation of carbonic acid in seawater media. Deep-Sea Res., 34, 1733–1743.

Dickson, A. G., J. D. Afghan, and G. C. Anderson, 2000: Sea water reference materials for $CO_2$ analysis: 2. A method for the certification of total alkalinity. Mar. Chem., submitted.

DOE, 1994: Handbook of methods for the analysis of the various parameters of the carbon dioxide system in sea water, version 2.0, A. Dickson and C. Goyet (eds.).

Johnson, K. M., A. E. King, and J. McN. Sieburth, 1985: Coulometric DIC analyses for marine studies: An introduction. Mar. Chem., 16, 61–82.

Johnson, K. M., P. J. Williams, L. Brandstrom, and J. McN. Sieburth, 1987: Coulometric total carbon analysis for marine studies: Automation and calibration. Mar. Chem., 21, 117–133.

Lee, K., F. J. Millero, R. H. Byrne, R. A. Feely and R. Wanninkhof, 2000: The recommended dissociation constants for carbonic acid in seawater. Geophys. Res. Lett., 27, 22–232.

McElligott, S., R. H. Byrne, K. Lee, R. Wanninkhof, F .J. Millero and R. A. Feely, 1998: Discrete water column measurements of $CO_2$ fugacity and pHT in seawater: A comparison of direct measurements and thermodynamic calculations. Mar. Chem., 60, 63–73.

Merhbach, C., C. H. Culberson, J. E. Hawley, and R. M. Pytkowicz, 1973: Measurement of the apparent dissociation constants of carbonic acid in seawater at atmospheric pressure. Limnol. Oceanogr., 18, 897–907.

Millero, F. J., J. Z. Zhang, K. Lee, and D. M. Campbell, 1993: Titration alkalinity of seawater. Mar. Chem., 44, 153–165.

Neill, C, K. M. Johnson, E. Lewis, and D. W. R. Wallace, 1997: Accurate headspace analysis of $fCO_2$ in discrete water samples using batch equilibration. Limnol. Oceanogr., 42(8), 1774–1783.

UNESCO, 1991: Reference materials for oceanic carbon dioxide measurements. Technical Papers in Marine Science No. 60, 41 pp.

Wanninkhof, R., and Thoning, K., 1993: Measurement of fugacity of $CO_2$ in surface water using continuous and discrete sampling methods. Mar. Chem., 44, 189–204.

# Warm-water pathways in the Subpolar North Atlantic: An overview of the ACCE RAFOS float programme

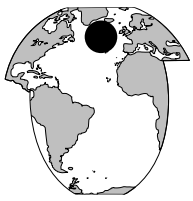

*A. S. Bower, P. L. Richardson, and H. D. Hunt, Woods Hole Oceanographic Institution, USA; and T. Rossby, M. D. Prater, H.-M. Zhang, S. Anderson-Fontana, P. Perez-Brunius, and P. Lazarevich, University of Rhode Island, USA.*
*abower@whoi.edu*

The flow of warm, subtropical waters into the subpolar gyre and Nordic Seas in the northern North Atlantic is an important part of the meridional overturning circulation. These waters lose large amounts of heat to the atmosphere (moderating the climate of northern Europe), and are transformed into the intermediate and deep water masses that spread southward and fill the deep North Atlantic and other basins. A major source of warm, saline water is the Gulf Stream, and its northern extension, the North Atlantic Current (NAC). At about 50°N, the NAC turns sharply toward the east (at the "Northwest Corner"), and what was a narrow, well-defined western boundary current becomes a weaker, more diffuse eastward flow along the Subpolar Front (SPF). It is along and across this front that the warm subtropical waters make their way into the subpolar region. A second source of warm water for the subpolar region has been proposed – the Mediterranean Water via the poleward eastern boundary current. Still unknown are the relative importance of these two sources, their pathways, and the processes (e.g., eddy mixing versus large-scale advection) that flux warm water into the subpolar region.

As part of the WOCE Atlantic Circulation and Climate Experiment (ACCE), a total of 115 RAFOS floats were deployed across the SPF and in the Mediterranean Water along the eastern boundary to investigate the above issues. RAFOS floats are acoustically-tracked, and therefore provide high-resolution trajectories (daily position fixes) that are valuable for resolving eddy processes and narrow boundary currents. The last floats surfaced in January 2000, and data processing is still underway. In this note, we provide an overview of the RAFOS float programme, and highlight some preliminary findings. A companion note in this issue discusses some particularly interesting case studies.

Floats were deployed on various CTD cruises between November 1996 and July 1998, at the sites indicated in Fig. 1a. The floats were isopycnal-following, and ballasted for a specific volume anomaly surface that corresponds closely to the $27.5\sigma_t$ surface, which reaches nearly 900 dbars at the eastern boundary, and shoals to less than 100 dbars (and even outcrops in winter) in the Irminger and Labrador Basins. Climatological mean properties on this surface are also shown in Fig. 1 for reference. All floats measured temperature and pressure daily, and in addition, about half were equipped with dissolved oxygen sensors (URI). Float missions were generally 18–24 months long.

Fig. 2 shows the vector displacements for all floats: those that were launched across the SPF west of the Mid-Atlantic Ridge (MAR) (thin arrows), and those deployed along the eastern boundary (thick arrows). The most striking feature in the SPF group is that a majority of the floats ended up in the Iceland Basin. This is consistent with

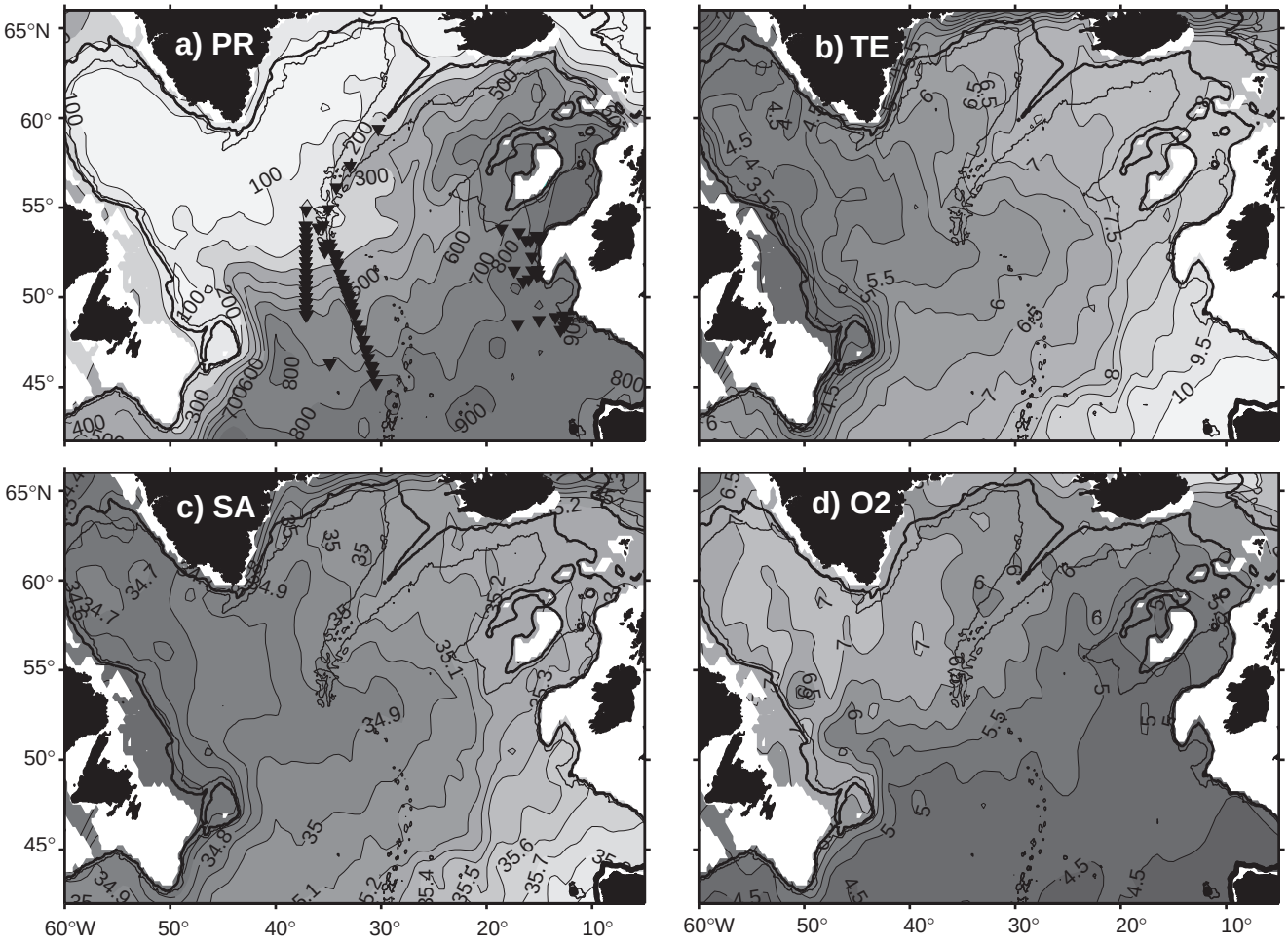


*(above) Figure 1. Mean properties on the 27.5 $\sigma_t$ density surface from the North Atlantic climatology (HydroBase). (a) pressure (db), and the float launch sites; (b) in-situ temperature (°C); (c) salinity; and (d) dissolved oxygen (ml/l). Properties were gridded onto a $1° \times 1°$ grid and smoothed with a 2° boxcar filter.*

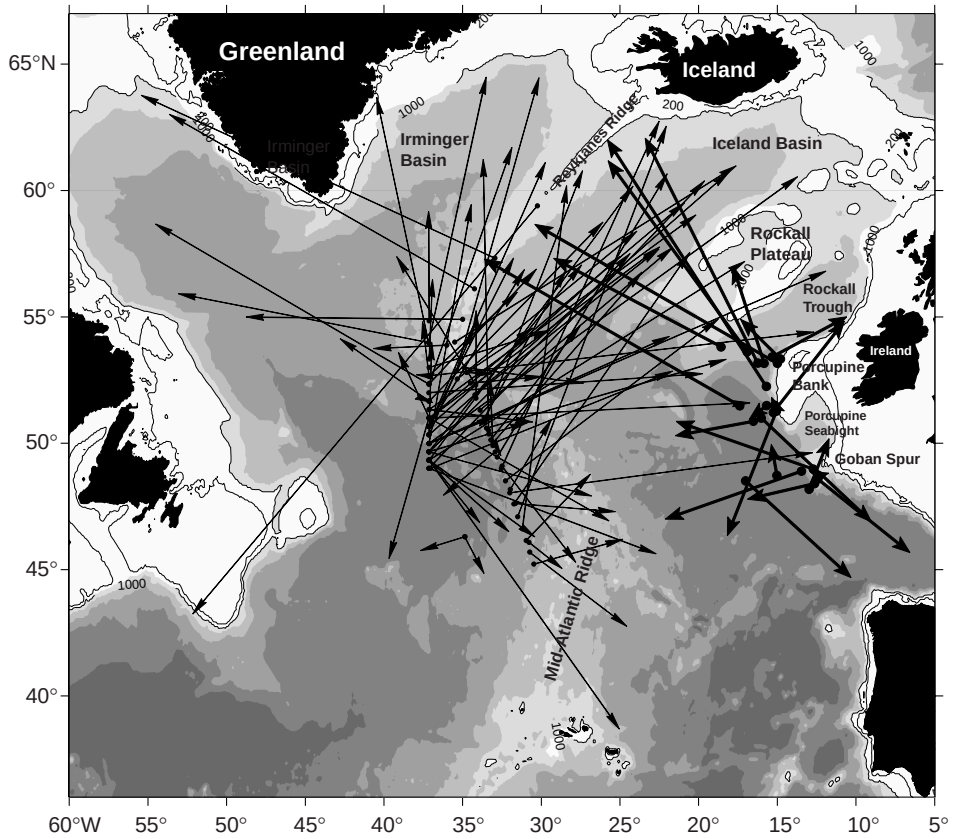


*(left) Figure 2. Vector displacements for all 115 RAFOS floats deployed as part of the ACCE Subpolar Experiment. Thin arrows indicate floats launched across the Subpolar Front, and thick arrows show floats deployed near the eastern boundary. Float missions generally were 18–24 months long.*

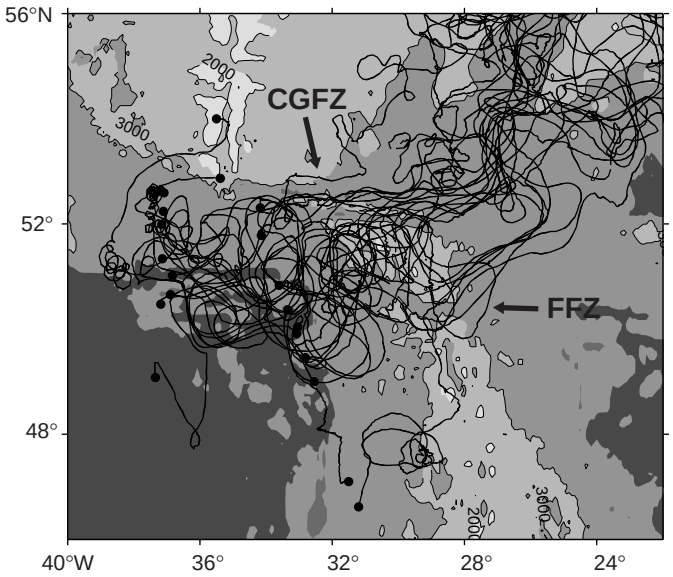


*Figure 4. Expanded view of the 21 floats that crossed the Mid-Atlantic Ridge and entered the Iceland Basin, showing two distinct pathways downstream (east) of the ridge.*

Fig. 1a, which shows that the pathway with the highest baroclinic shear (indicated here by the strongest slope of the density surface), extends east-north-eastward from the MAR to about 27°W, then turns sharply northward into the Iceland Basin. Relatively fewer floats in the SPF group ended up near the eastern boundary or in Rockall Trough. Considering the floats launched close to the eastern boundary, those deployed on the north-western side of Porcupine Bank mostly ended up in the Iceland Basin (except for one that wound up in Rockall Trough). Those floats launched near Goban Spur, south of the Porcupine Seabight generally drifted shorter distances over two years, and mostly to the west or south. Some of the floats starting west of the Bank, between the two other groups, went north, while others went west or south. There was very little evidence of a coherent poleward slope current carrying Mediterranean Water northward into Rockall Trough as has been suggested previously based on hydrographic observations: only two out of the 23 eastern boundary floats ended up there, and one of these was deployed at the entrance.

About ¾ of the floats have been tracked to date, and their trajectories are all superimposed in Fig. 3a (page 23), where the line thickness identifies floats launched in the SPF versus the eastern boundary. Straight dashed lines indicate segments where acoustic tracking was temporarily lost, mainly in the northern Irminger Basin which was not well-ensonified. The dominant pathway from the MAR first north-eastward, then northward into the Iceland Basin is clearly apparent. A fairly well-defined retroflection takes some of the floats following this main pathway back toward the west at about 57°N, and some of these wrap around the Reykjanes Ridge and enter the Irminger Basin. This pathway encloses a region that relatively few floats entered, centred at about 54°N, 32°W. The remainder of floats that entered the Iceland Basin generally continued northward farther into the basin, then along its northern rim in a cyclonic circulation. There is evidence for both of these pathways in the map of mean pressure, Fig. 1a: for example, the 300-dbar contour tends to turn back toward the west in the Iceland Basin near 57°N, 27°W, while the 500-dbar contour continues northward to the head of the basin. Curiously, none of the floats tracked so far approached the Iceland–Faroes Ridge, over which water shallower than about 600 m can enter the Nordic Seas. While eddy motion is apparent throughout the region is particularly elevated in the Iceland Basin.

From the north-western flank of Porcupine Bank, there is a relatively clear pathway across the entrance to Rockall Trough and around the southern and western flanks of the Rockall Plateau, and in a few cases, all the way to the continental slope south of Iceland. Near the western and southern flanks of Porcupine Bank, there is strong eddy variability, as well as several examples of persistent anticyclonic looping, characteristic of meddies (see accompanying Case Studies article). A preliminary summary of the main pathways observed with the floats is provided in Fig. 3b (page 23).

One particularly interesting feature of the SPF floats is illustrated in Fig. 4. Here we show an expanded view of the 21 floats that crossed the MAR and entered the Iceland Basin, just where they crossed the ridge. West of the ridge axis, there is significant eddy motion, but east of the ridge axis the floats cluster into two fairly well-defined branches – one aligned with the Charlie-Gibbs Fracture Zone (CGFZ) at about 52°N, and the other with the Faraday Fracture Zone (FFZ) at about 50°N. In a few cases, floats passed through one fracture zone then turned sharply north or south and followed the ridge axis to the other fracture zone before turning eastward into the eastern basin. A clear example of this is illustrated by float #530 in Fig. 1 of the accompanying article. Note also how the float launched at the most southerly position in Fig. 4 drifts northward along the ridge axis until it reaches the FFZ, where it crosses into the eastern basin. This "funnelling" of floats through the fracture zones illustrates the influence of these gaps on the thermocline-level flow field. We have also noticed that almost all the floats tracked so far that pass through the FFZ end up following the pathway far into the Iceland Basin, as depicted in the schematic diagram in Fig. 3b. As noted above, this is consistent with the climatology (Fig. 1a), which shows the southern part of the SPF extending far into the Iceland Basin. The influence of topography on the warm water pathways in the subpolar region will be one of many topics addressed in the continuing analysis of this unique data set.

## Acknowledgements

We thank the WHOI Float Operations Group for the preparation and ballasting of the floats. This work was supported under NSF Grant Number OCE-9531877.

# Warm-water pathways in the Subpolar North Atlantic: Some case studies

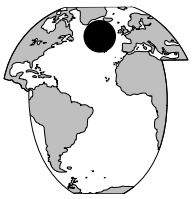

*T. Rossby, M. D. Prater, H.-M. Zhang, S. Anderson-Fontana, P. Perez-Brunius, and P. Lazarevich, University of Rhode Island, USA; and A. S. Bower, P. L. Richardson, and H. D. Hunt, Woods Hole Oceanographic Institution, USA. trossby@gso.uri.edu*

In this note we look more closely at a few floats representative of the pathways of spreading and eddy motion in the northern North Atlantic. The spaghetti diagram in the Bower et al. note (Fig. 3, page 23, this issue) indicates considerable structure to the northward transport and distribution of subtropical waters; and, more specifically, to the principal pathways of northward spreading. After entering the Iceland Basin, the main pathways were (1) north-east along the axis of the Iceland Basin and (2) retroflecting back westward across the Reykjanes Ridge and continuing into the Irminger Sea or north along the western slope of the ridge. To illustrate these pathways, we highlight trajectories from three isopycnal RAFOS floats deployed across the Subpolar Front at 37°W in July 1998. The spaghetti diagram also revealed persistent anticyclonic looping near the eastern boundary, characteristic of meddies observed farther south. To illustrate the features of these eddies, we highlight one float launched near the eastern boundary in November 1996.

## Principal pathways

Floats #563 and #530 illustrate the two different pathways into the subpolar region (Fig. 1). They were deployed in the northern and southern parts of the Subpolar Front, respectively. Ballasted for a specific volume anomaly surface corresponding closely to the 27.5 $\sigma_t$ surface, they were very close to Lagrangian in the horizontal and vertical. Their initial temperatures are virtually the same, about 6°C. Both floats cross into the southern Iceland Basin through the Charlie-Gibbs Fracture Zone (CGFZ) about 10 days apart, with float #530 moving faster and more eastwards than float #563 during the first 7 months. As float #530 reaches Rockall Plateau near 54°N, 23°W, it slows down and completes several loops for nearly half a year. This behaviour ends rather abruptly at day 360, when the float starts moving northwards just west of Rockall Plateau. Like many other floats entering this region, its eddy activity increases. Its temperature starts to increase towards 7°C while it deepens in a step-like pattern from 300 to 800 dbars. The steps suggest the presence of mixed layers with sharp density interfaces and enhanced temperature gradients (to which the point measurement of temperature at the float will be sensitive). When at its deepest, the float makes several anticyclonic loops before shoaling somewhat as it continues towards the north-east corner of the Iceland Basin, increasing its temperature further to 8°C. These depth and temperature patterns accord remarkably well with climatology (Fig. 1, Bower et al., this issue).

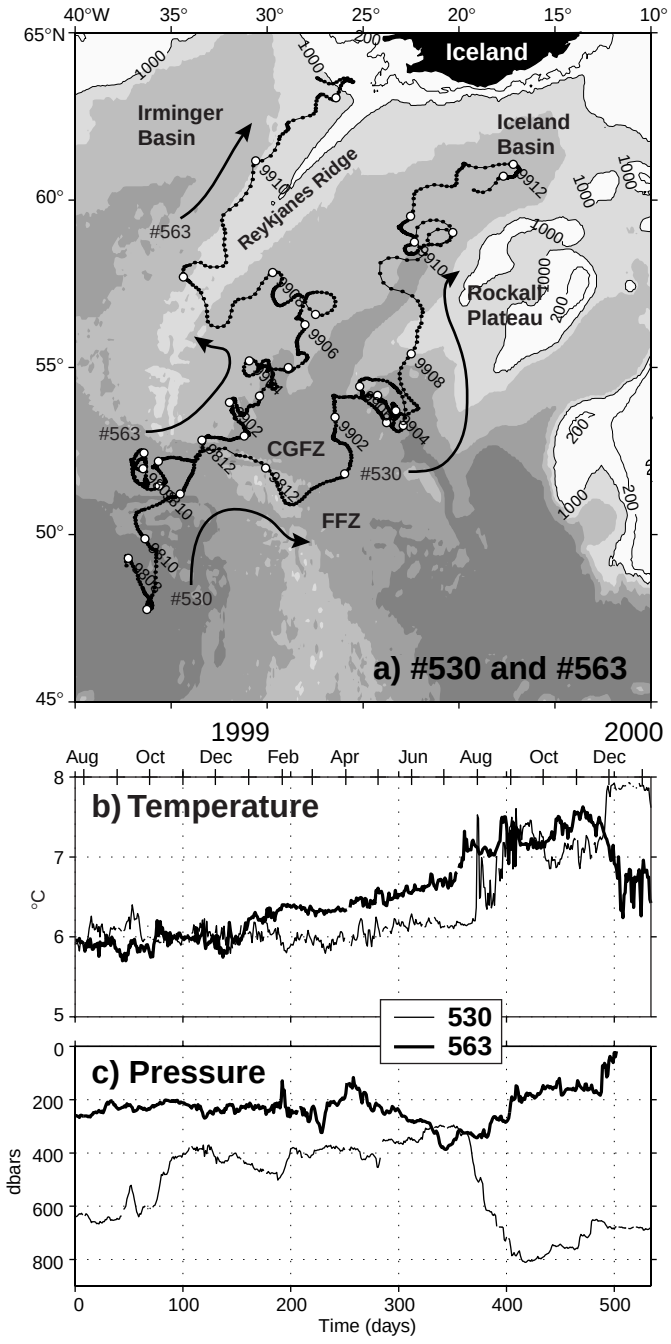


*Figure 1. Summary plot of RAFOS floats #530 and #563 (URI). Dots on track indicate daily positions, and open circles are plotted monthly and labelled bi-monthly.*

Float #563 enters the Iceland Basin farther to the west, following a more sinuous and northward path than does float #530. Characteristic of other floats in this region, it turns sharply to the west at 57°W, towards the Reykjanes Ridge. It then turns northwards along the western slope as its temperature increases. This increase in temperature may reflect a mixture of North Atlantic Current waters with warmer, saltier waters of Mediterranean origin (as suggested by the isopycnal climatology (Fig. 1, Bower et al., this issue). The rapid motion along the ridge has been observed in other float tracks, indicating a significant baroclinic transport towards Iceland.

Both floats indicate rapid motion west of steep topographic features. They also show an increase in temperature as they drift towards the north and north-east, in agreement with climatology. However, the temperature drop after day 490 (December 1999) for float #563 reveals that the density surface is outcropping. Unfortunately, this float dropped its ballast weight on day 500 and the acoustic tracking was lost, thereafter.

## Outcropping

Float #550 (Fig. 2), which was deployed north of the Subpolar Front, immediately entered the southern Irminger Sea, drifting first west and then east towards the Reykjanes Ridge, which it then followed northward. In these waters the 27.5 $\sigma_t$ surface is quite shallow and outcrops in winter. The float outcrops in the winter of 1998–1999, subducts at the end of spring 1999, and outcrops the following winter. The pressure record between the outcroppings suggests a gradual, seasonal deepening of the isopycnal. This continues up to the point where the deepening mixed layer reaches the isopycnal. After the float outcrops in the first winter, continued convective cooling causes the float to exhibit considerable vertical motion. The temperature levels-off and then, during days 200–220 (February 1999), begins to increase noticeably despite the continued convective activity. Since this is early February, this cannot be due to surface heating. On the other hand, the float is drifting east towards the Reykjanes Ridge so we assume the increase results from lateral mixing with warmer, saltier waters in that region. Vernal heating eventually warms the surface to the point where the float begins to subduct, but, curiously, some event causes it to resurface briefly in May before subducting for the summer. The outcropping the next winter, much farther north in the Irminger Sea, is accompanied by a more rapid rate of decrease in surface temperature.

The oxygen record for this float suggests that the sensor remained quite stable for the entire record. This assertion rests upon the fact that at all three times when the float outcrops, the oxygen saturation level is at 104±2% using the laboratory calibration and in situ temperature record to determine its solubility. However, at the end of the first winter the oxygen shows momentary drops as large as 2 ml $l^{-1}$. We speculate that

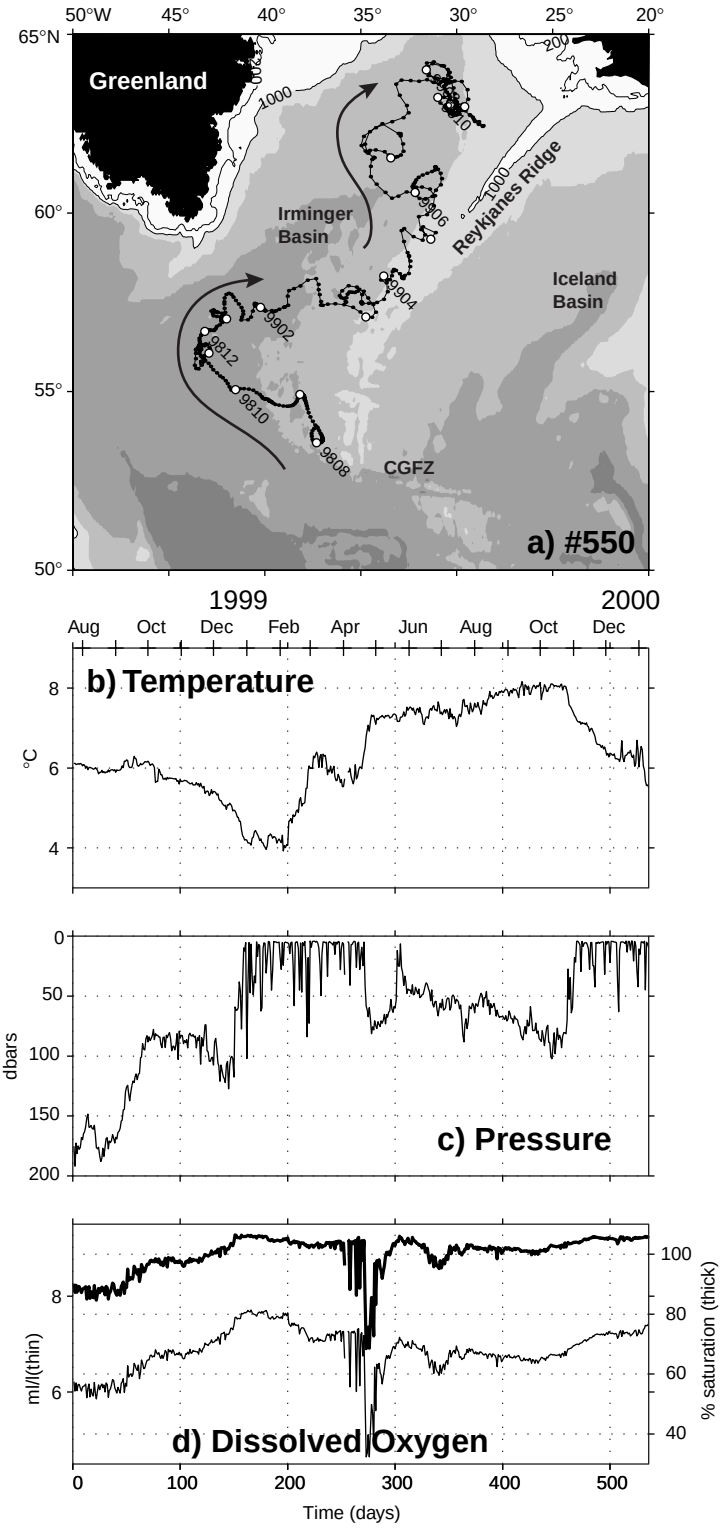


*Figure 2. Summary plot of RAFOS float #550 (URI).*

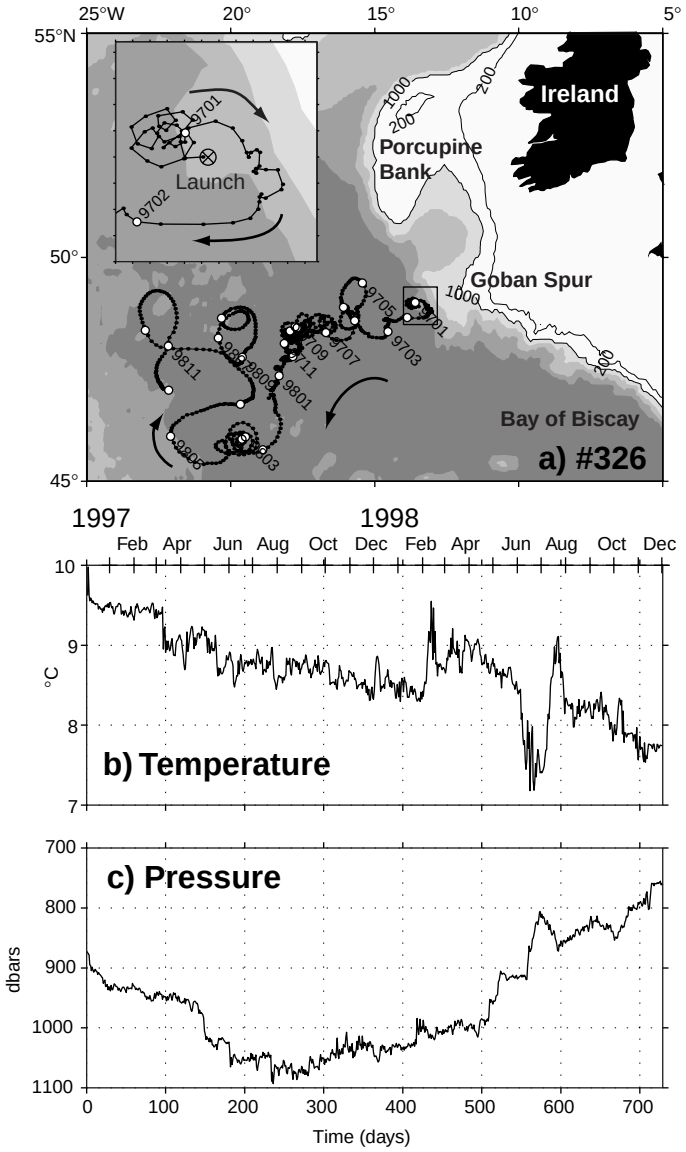


*Figure 3. (a) Two-year track of float #362, launched over the outer continental slope west of Goban Spur in December 1996 (WHOI). Inset shows first two months of track, during which the float looped in a meddy.*

these indicate a highly localised uptake of oxygen due to bacterial decay of detritus from the surface, possibly at the end of a spring bloom. See the September 1998 International WOCE Newsletter n.32 (pp. 32–35) for a detailed discussion of the oxygen sensor and its operation.

## The 'meddy' float

Finally, we shift attention to the eastern boundary, where about 23 floats were launched to directly observe the pathways of Mediterranean Water into the subpolar region. Several of these floats exhibited persistent anti-cyclonic looping typical of meddies farther south. One such float is #326 (Fig. 3), which was launched over the 4000 m isobath just west of Goban Spur for a two-year mission. Immediately after launch, the float made a series of about 5 small, closed anticyclonic loops, with an average period of 6 days at a radius of about 5–10 km (see inset). Temperatures were warm, >9.5°C, and CTD measurements at the same time indicate a detached blob of warm saline water next to the slope. We speculate that this meddy may have formed from northward flow of Mediterranean Water along the slope as it tried to negotiate Goban Spur.

After about a month, float #326 moved off to the south, then west, making a cusped path suggestive of a more rapidly translating meddy (inset). About 1–2 months later, the float began another, longer series of anticyclonic loops, making about 22 loops in 250 days for an average period of about 11 days, at a radius of 15–20 km. Looping stopped around January 1998, but two more periods of looping followed, both accompanied by abrupt temperature increases, one in February and the other in July 1998. While we cannot be certain that this float was in the same meddy for its entire two-year mission, this track and others confirm that meddies are formed well north of the Iberian Peninsula. This is the most northerly meddy (~49°N) that has been directly observed with floats.

## Concluding remarks

Despite the eddy motion we see in these and other trajectories, a rather robust pattern of float pathways emerges. The temperature and pressure properties of these three-dimensional trajectories do not merely corroborate the hydrography; they give us explicit information on advection and mixing along the isopycnal. Upcoming analyses include a quantitative description of mean flows and eddy kinetic energy (EKE) on this surface, a synthesis of Lagrangian pathways, and estimates of Lagrangian absolute dispersion and relative dispersion (since many of the floats were deployed in triplets). Many of the analysis tools for this have been developed during earlier float studies, including the series of studies emanating from the North Atlantic Current RAFOS float programme. A particularly challenging topic that will be addressed with these new float observations concerns the estimation of cross-frontal isopycnal eddy fluxes of heat and oxygen, i.e. $< v'T' >$ and $< v'O_2' >$.

## Acknowledgements

The authors would like to thank Mr Jim Fontaine (URI) for his technical expertise, float construction, and ballasting. We also thank Dr Chris Langdon (LDEO) for his assistance with the dissolved oxygen sensor. This research is supported by NSF OCE-9906775 and CONACYT.

# The contribution of Iceland–Scotland Overflow Water to the formation of North East Atlantic Deep Water in the Iceland Basin and the West-European Basin

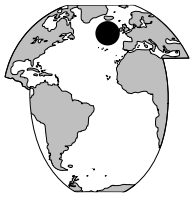

*Uli Fleischmann, University of Bremen, Germany; and Monika Rhein, Institüt für Ostseeforschung Warnemünde, Germany. ufleisch@physik.uni-bremen.de*

It is commonly thought, that the water masses overflowing the sills between Iceland and Scotland sink down and entrain ambient water masses. ISOW (Iceland–Scotland Overflow Water) then flows south along the eastern flank of the Reykjanes Ridge and crosses through the Gibbs Fracture Zone into the western Atlantic. The tracer and hydrographic measurements in 1991, 1994, and 1997 along the WOCE lines A1 and A2 (Fig. 1) in the north-eastern Atlantic show clearly, that part of the ISOW is found outside the core region at the Reykjanes Ridge and does not enter the western Atlantic, but remains in the eastern Atlantic and flows further south along the eastern flank of the Mid-Atlantic Ridge. The horizontal and vertical extent of the ISOW core varied strongly between 1994 and the other two cruises in 1991 and 1997.

## Introduction

The Iceland–Scotland Overflow Water (ISOW) is characterised by a core of high salinity, high oxygen and high CFC water flowing at the bottom along the eastern flank of the Reykjanes Ridge (e.g. Swift, 1984). It is commonly believed, that it leaves the eastern Atlantic through the Gibbs Fracture Zone (GFZ) at 53°N (e.g. McCartney, 1992; and Schmitz and McCartney, 1993).

Contour plots of CFC-11 on the deep eastern parts of A1 in 1991 and A2 in 1997 are shown in Fig. 2 (page 22) as examples for the CFC-11 distributions. The ISOW influence on A1 is obvious as a bottom maximum at the Reykjanes Ridge. Additionally the water between 2500 m and 4000 m has much higher CFC-11 concentrations west of 21.5°W than the water further east. On A2 the ISOW influence can be recognised from the inclination of the CFC-11 isolines. They are rising from west to east especially below 2500 m.

## Results

Θ-CFC-11 diagrams for all cruises are shown in Fig. 3. There are two groups of profiles that can be distinguished on all cruises by their CFC-11 values for 2.2°C<Θ<3.2°C. Profiles of group 1 (solid lines) have low values compared to profiles of group 2 (dotted lines) in this Θ range even though the profiles of both groups are very similar for Θ>3.2°C. The latter indicates that the increased CFC-11 values are not due to downward transport of CFC-11 by vertical mixing but caused by CFC-11 that originates in the corresponding density range. The only possible source for the increased tracer values is therefore ISOW. For the A1 diagrams a third group (dashed-dotted lines) is defined by having a bottom maximum indicating the flow of an ISOW core. 1–3 stations forming the transition between group 1 and group 2 have been omitted in the diagrams.

The increased tracer values of groups 2 and 3 on A1 compared to group 1 (Fig. 3a–3c) indicate a considerable ISOW influence outside the ISOW core at the Reykjanes Ridge. The spatial extent of the different groups is variable (white bars on the bottom of Fig. 2). On the A1 section, group 2 and 3 reached farthest to the east in 1991 and 1997. In those two years, the ISOW cores are also thicker (extending along the bottom of the RR to depth of 3450 m and 3600 m respectively) than in 1994, where the deepest bottom maximum was located in 2800 m.

The increased tracer values of the group 2 profiles on A2 prove the arrival of newly ventilated deep water in the

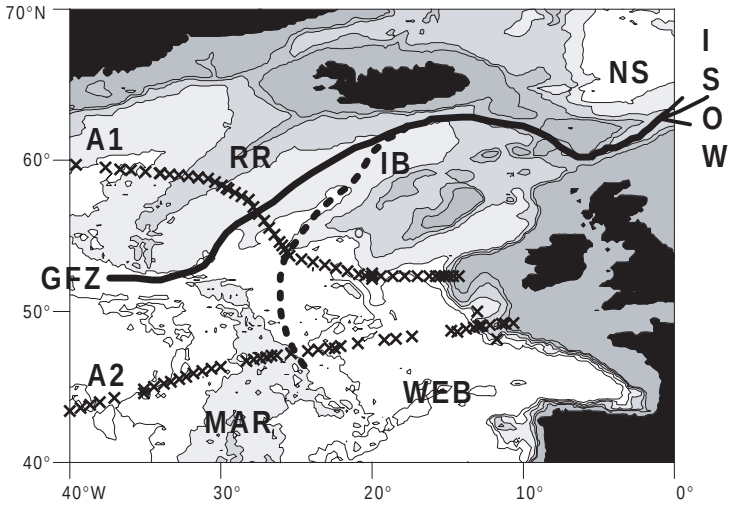


*Figure 1. Area of investigation with sections used in this study. NS: Norwegian Sea; IB: Iceland Basin; GFZ: Gibbs Fracture Zone; WEB West European Basin; RR: Reykjanes Ridge; MAR: Mid Atlantic Ridge. The flow path of the ISOW core (solid line) is shown as well as the suggested flow into the WEB (dotted line). The data used for this study are hydrographic and CFC-11 measurements from cruises with the German research vessel Meteor in 1991 (No. 18), 1994 (No. 30) and 1997 (No. 39). WHP A1 was occupied thrice (No. 18, 30/3 and 39/5), the WHP A2 section twice (No. 30/2 and 39/3).*

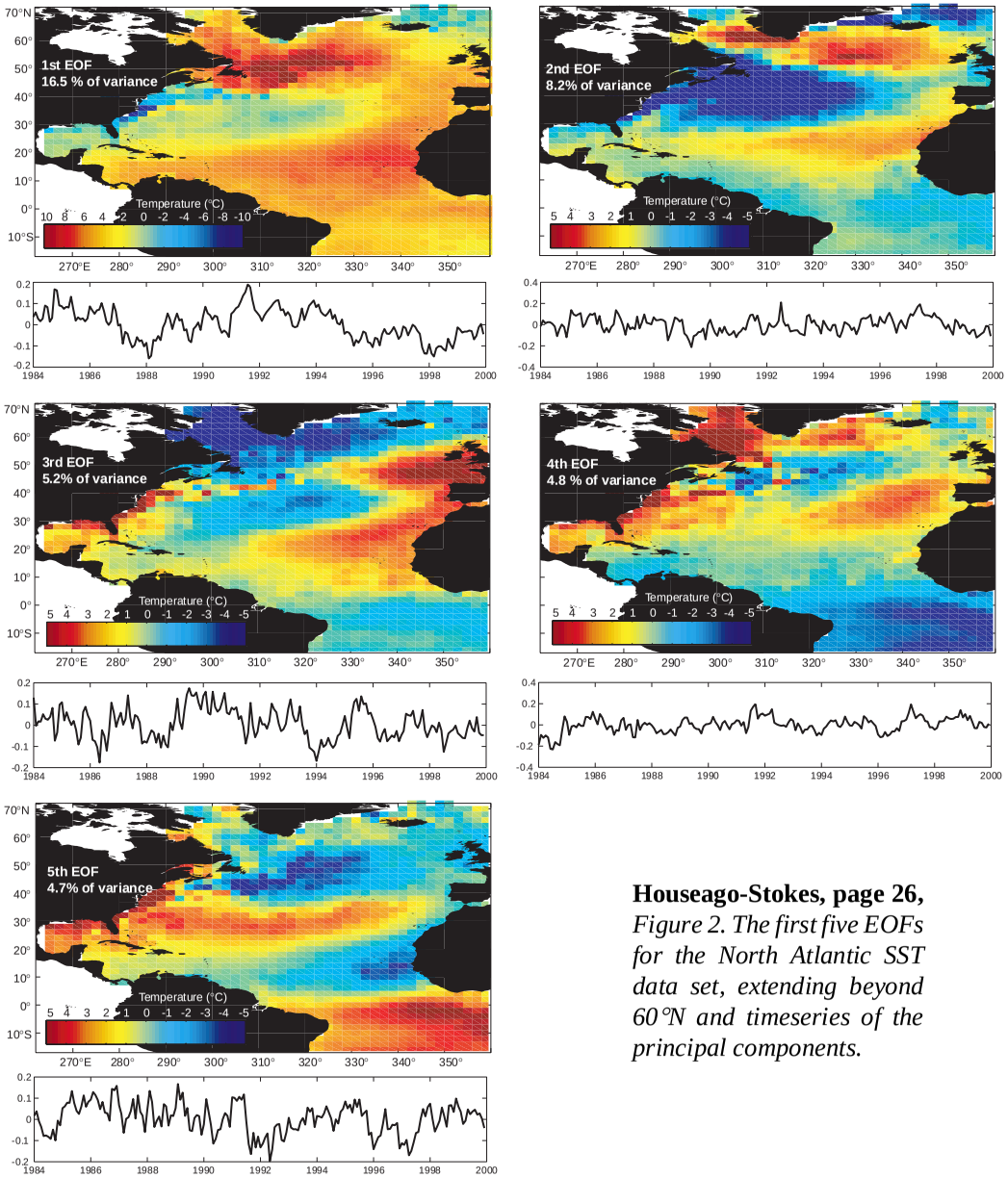


**Houseago-Stokes, page 26,** *Figure 2. The first five EOFs for the North Atlantic SST data set, extending beyond 60°N and timeseries of the principal components.*

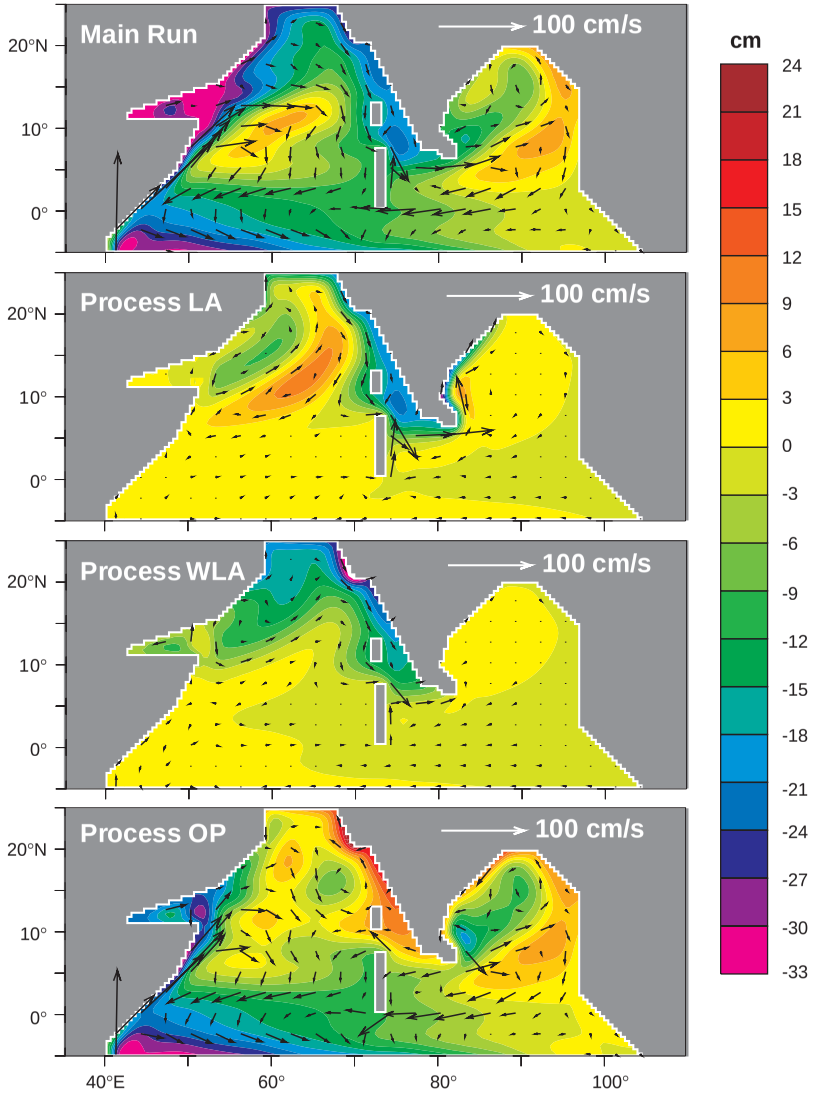


**Shankar, page 35,** *Figure 1. Sea-level deviation (cm) from the undisturbed sea surface and velocity (cm/s) for the main run and processes LA, WLA, and OP. All results are plotted for July.*

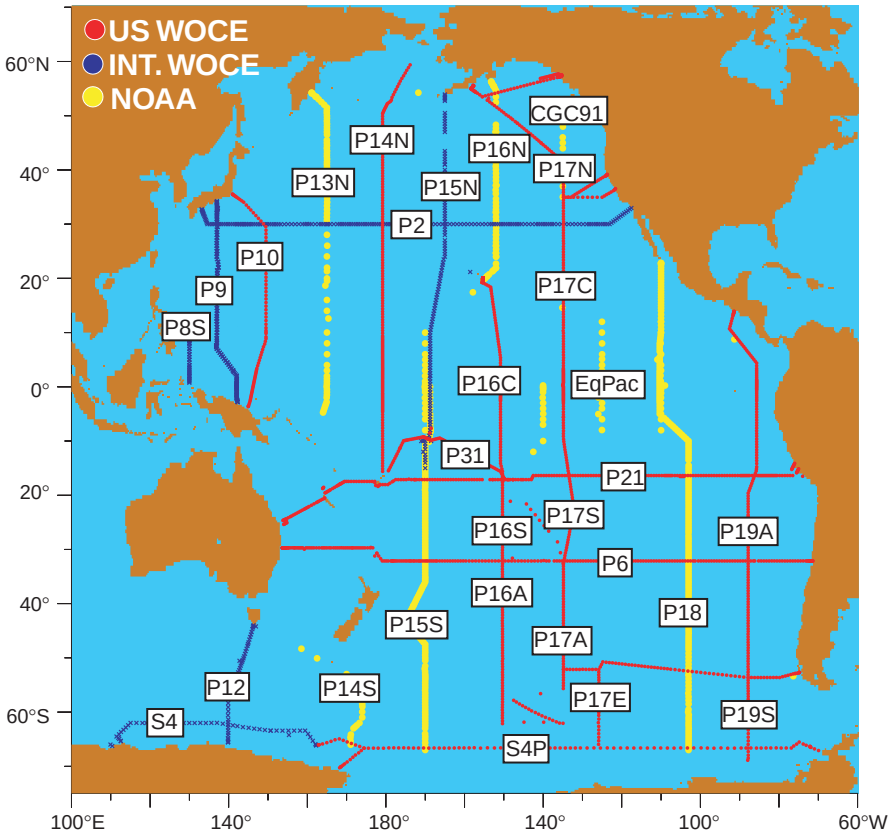


**Sabine et al., page 10,** *Figure 1. Pacific carbon survey.*

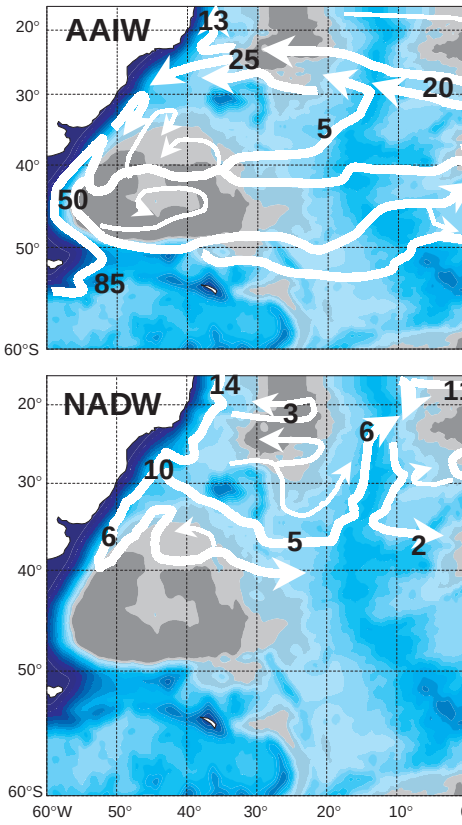


**de Miranda and Barnier, page 28,** *Figure 4 (arrows) and transports (in Sv) for AAIW (to the mean circulation and water mass pr integration of the MOCA model. Colours ind*

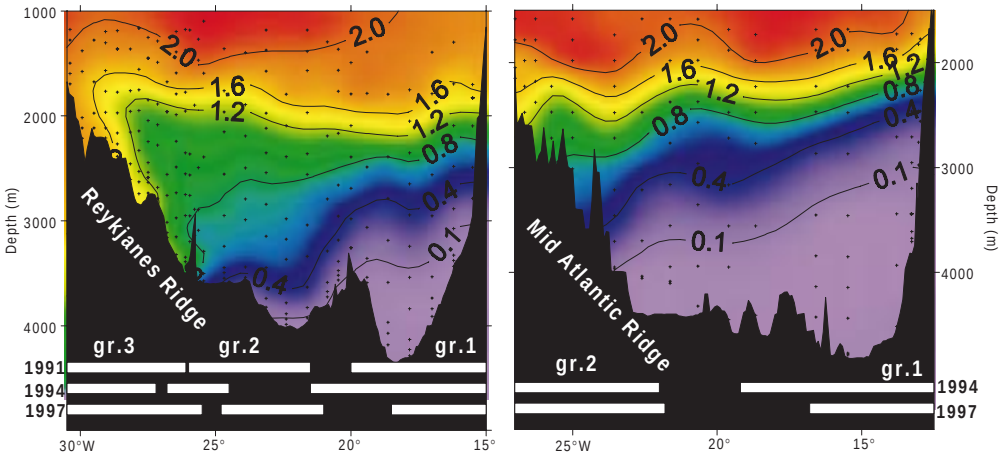


**Fleischmann and Rhein, page 20,** *Figure 2. CFC-11 (pmol/kg) on the deep eastern part of A1 in 1991 (left) and of A2 in 1997 (right). ISOW is seen as a bottom maximum layer on A1 at the eastern flank of the Reykjanes Ridge. Its influence shows up as well by increased CFC-11 values below 2500 m west of about 20° W on A1 and by the inclination of the CFC-11 below 2500 m on A2. The white bars at the bottom of the contour diagrams give the distribution of the groups of profiles (see text) on the sections in the different years.*

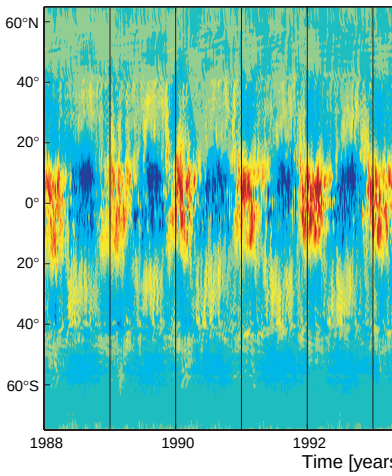


**Jayne and Marotzke, page 7,** *Figure anomaly for the World Ocean. The ti removed to highlight the variability.*

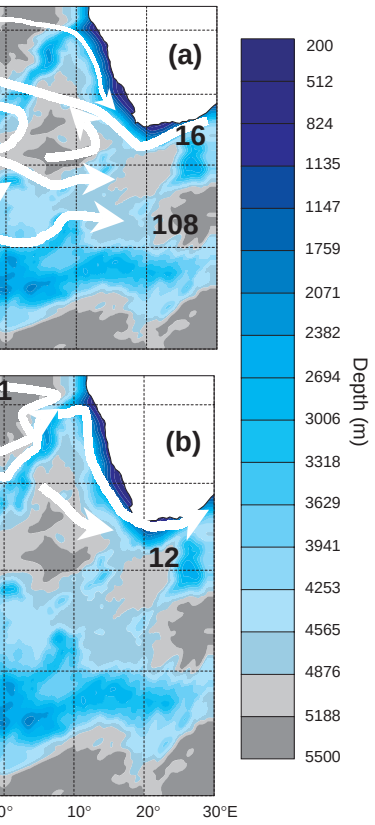


*4. Schematics of the mean circulation*
*op) and NADW (bottom), drawn after*
*operties simulated by 35 years of*
*dicate the model bottom topography.*

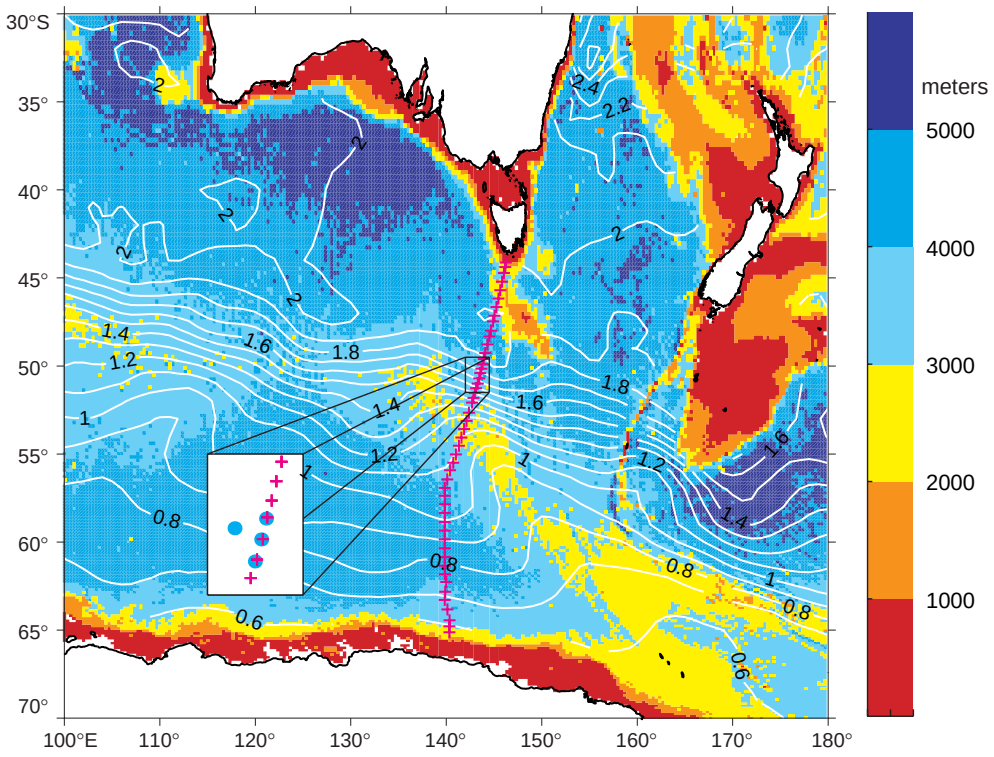


**Phillips and Rintoul, page 3,** *Figure 1. Location of the AUSSAF current meter array (blue circles) and the WOCE SR3 hydrographic section (magenta crosses), overlaid on shading of Smith and Sandwell (1994) bathymetry in metres and contours of 0–2000 dbar dynamic height (dyn. m.) from Olbers et al. (1992).*

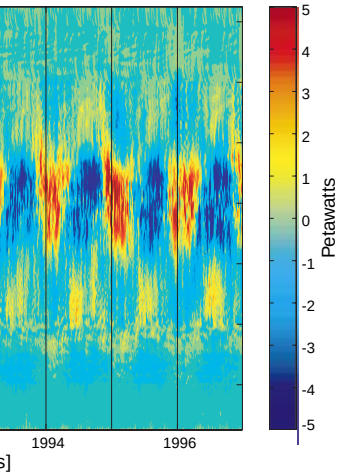


*s]*

*1. Time-dependent heat transport*
*me mean heat transport has been*
*Vertical lines mark 1 January.*

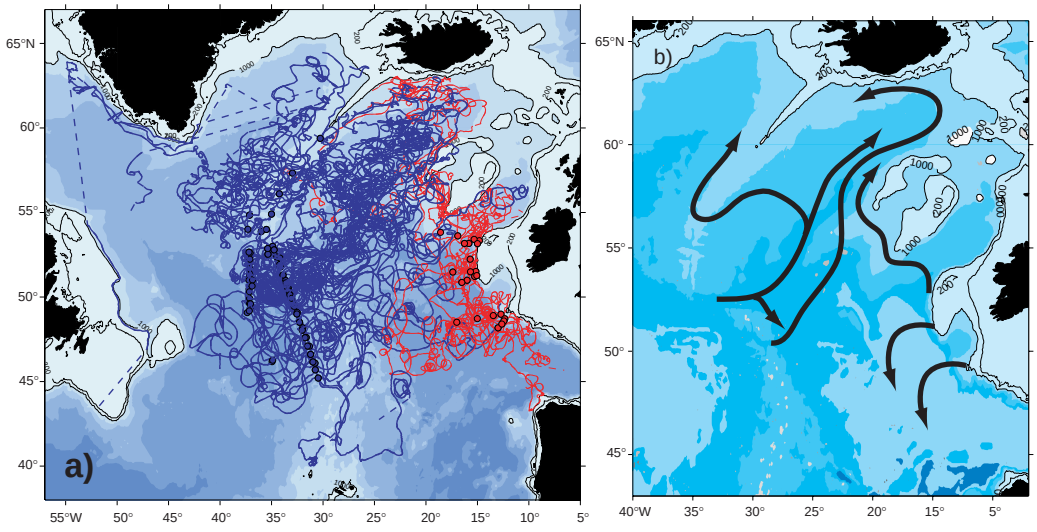


**Bower et al., page 14,** *Figure 3. (a) Preliminary spaghetti diagram of the 88 floats tracked to date, blue lines for floats deployed across and adjacent to the Subpolar Front, red lines for floats launched near the eastern boundary, (b) Schematic diagram summarising main float pathways.*

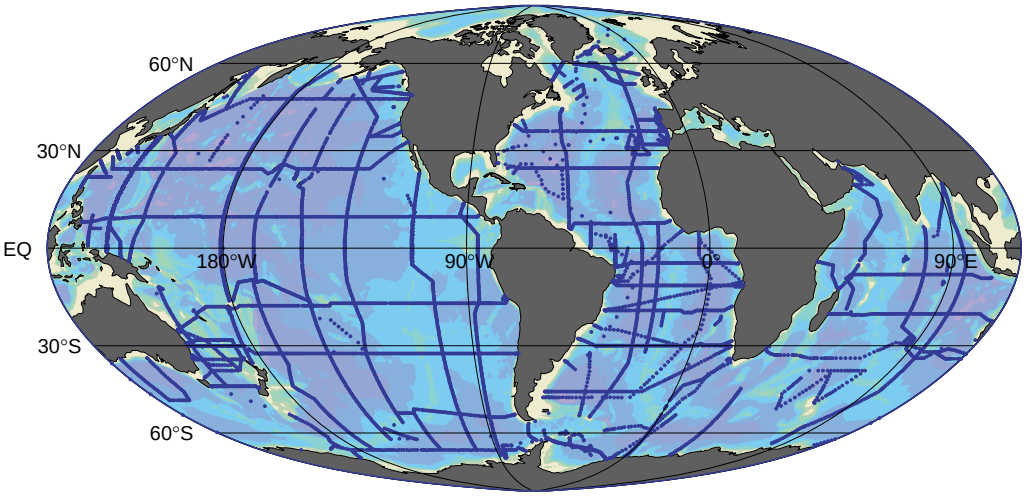


**Schlitzer, page 36,** *Figure 1. Map of eWOCE stations.*

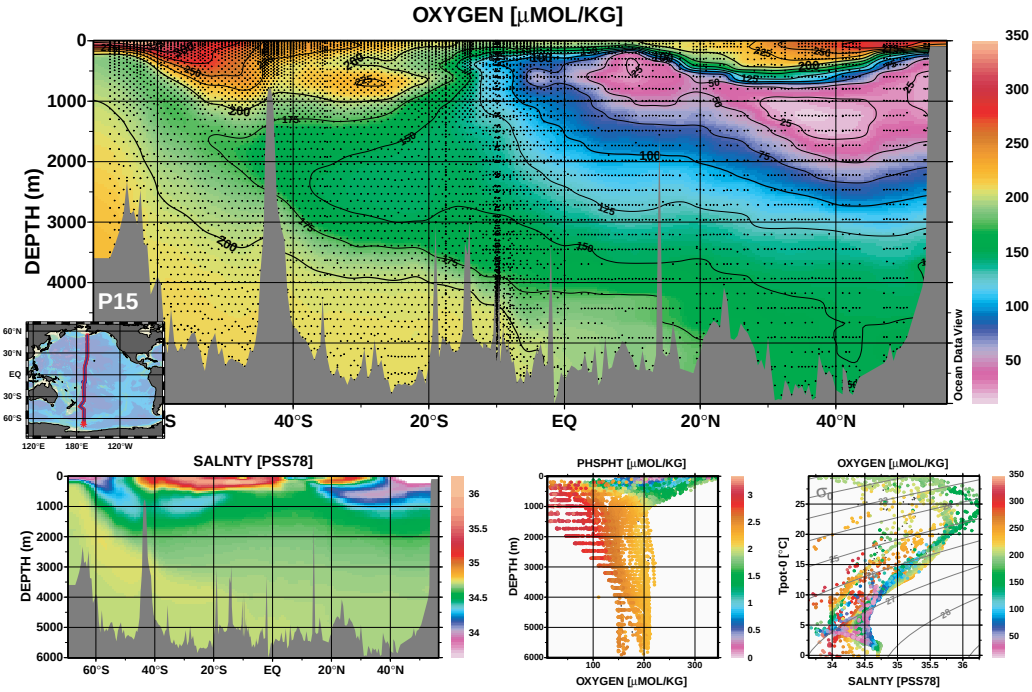


**Schlitzer, page 36,** *Figure 2. Example ODV section plot showing property distributions along WHP line P15 in the Pacific.*

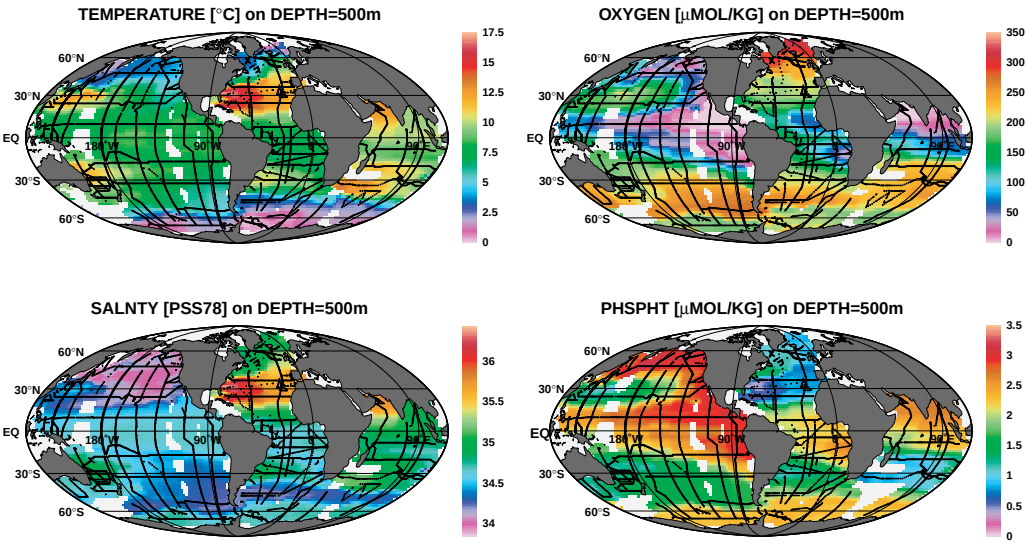


**Schlitzer, page 36,** *Figure 3. Example ODV surface plot showing property distributions at 500 m depth.*

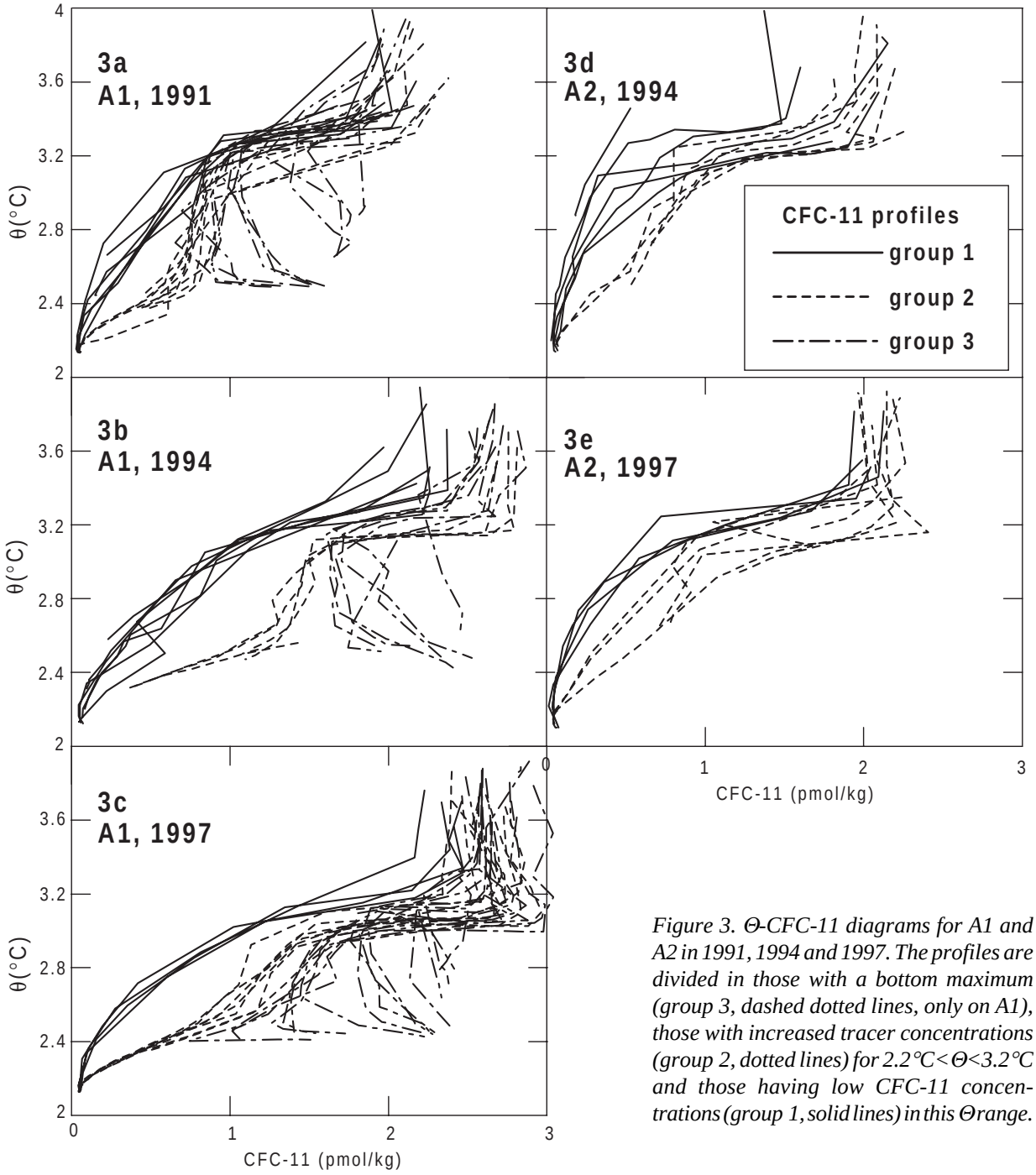


*Figure 3. Θ-CFC-11 diagrams for A1 and A2 in 1991, 1994 and 1997. The profiles are divided in those with a bottom maximum (group 3, dashed dotted lines, only on A1), those with increased tracer concentrations (group 2, dotted lines) for 2.2°C< Θ<3.2°C and those having low CFC-11 concentrations (group 1, solid lines) in this Θ range.*

WEB for both realisations. The 1991 and 1994 CFC-11 data have been used together with tritium and $^{3}$He data to calculate a transport of 1.55–2.45 Sv NEADW from A1 to A2 (Fleischmann et al., 2000). On the A2 section, the horizontal range of the transition zone between group 1 and group 2 (black space between the white bars on the bottom of Fig. 2b) showed the highest variability.

## Discussion

The tracer data show clearly, that the influence of ISOW in the Iceland Basin is not confined to the core layer that is found at the Reykjanes Ridge. Part of the DNBC flows southward along the eastern flank of the Mid-Atlantic Ridge (MAR). This is in contrast to the general believe, that the DNBC (including all ISOW) crosses the GFZ into the western Atlantic, although Lee and Ellett (1965) came to a similar conclusion from the analysis of salinity data. The southward flow of the DNBC in the NE Atlantic south of the GFZ might explain some of the discrepancies between the transport of ISOW through the GFZ of 2.4 Sv (Saunders, 1994) and the transport estimate of the waters forming the DNBC of 7 Sv (Schmitz and McCartney, 1993).

The reasons for the variability in the vertical and horizontal extent of the DNBC at the A1 and A2 section are unknown as is the temporal scale of the variability. The current meter moorings at the eastern flank of the MAR at about 51.5°N show that the variability in the intensity of the flow are dominated by advected eddies on a time scale of 4–6 weeks (W. Zenk, IfM Kiel, pers. comm.). However, it is possible as well that the intensity of ISOW formation was different in 1994 than in 1991 and 1997.


## Acknowledgement

We wish to thank captains, crews, scientists and chief scientists of the RV Meteor cruises M 18, M 30/2, M 30/3, M 39/3 and M 39/5. The work was supported by various grants of the BMBF and the DFG.


## References


Fleischmann, U., H. Hildebrandt, A. Putzka, and R. Bayer, 2000: Transport of newly ventilated deep water from the Iceland Basin to the West European Basin. Deep-Sea Res., submitted.

Lee, A., and D. Ellett, 1965: On the contribution of overflow water from the Norwegian Sea to the hydrographic structure of the North Atlantic Ocean. Deep-Sea Res., 12, 129–142.

McCartney, M. S., 1992: Recirculating components to the deep boundary current of the northern North Atlantic. Prog. Oceanogr., 29, 283–383.

Saunders, P. M., 1994: The flux of overflow water through the Charlie-Gibbs Fracture Zone. J. Geophys. Res., 99(C6), 12343–12355.

Schmitz, W. J. J., and M. S. McCartney, 1993: On the North Atlantic circulation. Rev. Geophys., 31(1), 29–49.

Swift, J. H., 1984: The circulation of the Denmark Strait and Iceland–Scotland overflow waters in the North Atlantic. Deep-Sea Res., 31, 1339–1355.


# Using optimal interpolation and EOF analysis on North Atlantic satellite data

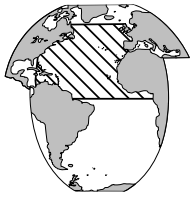


*Richenda Houseago-Stokes, James Rennell Division for Ocean Circulation and Climate, Southampton Oceanography Centre, UK. ryh@soc.soton.ac.uk*


The nature and mechanisms of the interannual and interdecadal ocean and climate variability in the North Atlantic region have received a lot of attention recently. The atmospheric variability of the North Atlantic has been found to be dominated by a combination of the North Atlantic Oscillation (NAO) and the tropical Atlantic, on both interannual and interdecadal timescales (Deser and Blackmon, 1993; Kushnir, 1994; McCartney, 1996; 1997; Bojaru, 1997; Sutton and Allen, 1997).

This study uses the Multi-Channel Sea-Surface Temperature (MCSST) data derived from the NOAA (National Oceanic and Atmospheric Administration) Advanced Very High Resolution Radiometer (AVHRR) data to examine the variability of the North Atlantic sea surface temperature (SST) and, in particular, to identify the NAO SST signal. This is carried out by using empirical orthogonal function (EOF) analysis on an interpolated data set.

## Method

In order to obtain a long record of sea surface temperature, and therefore be able to pick up the NAO signal, the MCSST data was used. The MCSST data set was chosen in preference to the Pathfinder data set, as the MCSST data set is available for a longer period. Satellite data are ideal for such a study of large-scale variability as they overcome the problems associated with the spread of time and space sampling associated with the ship based measurement system. The data resolution is approximately 5.689 pixels per degree of longitude and latitude, binned and averaged, at the University of Miami, into 8-day averages, overlapping the previous average by one day. The accuracy of the SST retrieval is approximately 0.3°C,

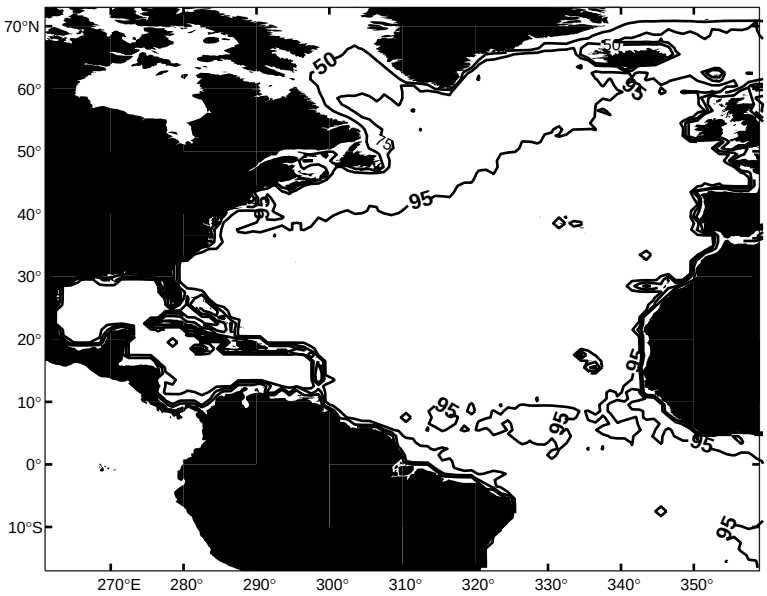


*Figure 1. The percentage of missing monthly MCSST data for the North Atlantic.*

as observed by McClain et al. (1985), after comparison with a-priori temperatures measured at the surface. The descending pass (night-time) data was used in this study, as it has fewer missing values. Data from 1982 to the present are available, but the timescale used in the study was restricted due to the number of missing values resulting from the aerosols produced after the eruption of El Chichon. Thus, the data for the period January 1984 to December 1999 was selected. One of the problems with the MCSST, as with other infra-red methods, is the lack of retrieval of data in areas of persistent cloud cover, such as the region surrounding the Intertropical Convergence Zone (ITCZ). Also, certain areas, particularly those north of 60°N, have very few values due to extensive periods of cloud cover, as well as sea-ice. In order to use EOF analysis on the North Atlantic SST, to identify large-scale variability, it is necessary to have a data set without missing values. The MCSST data set has been interpolated, by the University of Miami, by filling the missing vales with a weighted average of the surrounding eight pixels, until the data set is complete. However, in the regions, particularly north of 60°N, where there are few values, the interpolated data needs to be treated with caution (PO.DAAC Guide Document Page: http://podaac.jpl.nasa.gov:2031/DATASET_DOCS/avhrr_wkly_mcsst.html). As an alternative interpolation technique, this paper considers the use of optimal interpolation. It is hoped that optimal interpolation will provide a better approximation above all in the high latitudes as it uses all available data rather than a few surrounding pixels.

The weekly 18 km MCSST data were first converted to monthly 2° grids, in order to ease processing. This conversion also helped to reduce the number of missing values in the data set. The percentage of missing values for the North Atlantic is shown in Fig. 1. In the Labrador Sea, over 50% of the values are missing, with the same to the north of Iceland. Following conversion to a 2° grid, the annual and semi-annual cycles were removed, using a combination of sine and cosine curves. This enabled the lower frequency patterns to be identified. Optimal interpolation was then used to fill the remaining missing values. The Kalman filter is an optimal recursive data processing algorithm (Maybeck, 1979). It is a set of mathematical equations that provide an efficient computational solution to the least squares method. It estimates a process by means of feedback. The equations fall into 2 groups, 'time update' and 'measurement update' equations. The time update equations project forward in time the current state and the error covariance estimate to give an a priori estimate for the next time step. The measurement update equations are responsible for the feedback, by incorporating a new measurement into the a priori estimate. More information on the Kalman filter technique is given in Rodgers (2000). The basic Kalman filter is used in this study as it is able to use a combination of the previous time step, as well as the surrounding data to make up the interpolated value. The optimal interpolation was carried out, on a spatial scale, using the formula:

$$\underline{\hat{x}} = \underline{x}_a + \left[\left(H^T R^{-1} H + S_a^{-1}\right)^{-1} H^T R^{-1}\right]\left(\underline{y} - H\underline{x}_a\right) \quad (1)$$

The a priori, $\underline{x}_a$, was initially taken as zero, as these are anomalies, and then $\underline{x}_{t-1}$, for every following timestep. $S_a$, the 'priori covariance', was taken as:

$$\left[S_a\right]_{ij} = a_0{}^2 a_1^{|\theta_i - \theta_j|} a_2^{|\phi_1 - \phi_2|} \quad (2)$$

to add latitude and longitude components to the interpolation, with each '*a*' value given a high weighting of 0.9, to increase their relative importance in the interpolation scheme. *H* is the measurement model, taken to be the identity matrix, *I*. *R* is the noise term, where $R = \sigma^2 I$, with $\sigma$ given a relatively low value, of 0.05, in order to add a greater weighting to the other components. The observed values are represented by the term $\underline{y}$. Following calculation of the interpolated data set, EOF analysis was carried out.

The whole process was repeated with a cut-off at 60°N. This was to determine whether data interpolated above this latitude caused any biasing on the EOF analysis.

## Results and discussion

Fig. 2 (page 21) shows the North Atlantic SST EOF maps from the entire interpolated data set. The first five EOFs account for 39.4% of the variance. The first EOF, which accounts for 16.5% of the SST variance, resembles the North Atlantic Oscillation (NAO) (Wallace and Gutzler, 1981; Wallace et al., 1990). The second EOF accounts for 8.2% of the variance and appears to be related to the Gulf Stream variability. The third EOF mode has the strongest signal in the eastern basin, with a contrasting signal in the Labrador Sea. The fourth EOF has strongest signals in the Labrador Sea as well as in the equatorial Atlantic, whilst the fifth EOF, accounting for 4.7% of the variance, has strong tropical Atlantic signals. Very similar EOF patterns were found when the same analysis was carried out on the data set without interpolation at high latitudes. It therefore appears that the interpolation of the high latitudes is not biasing the EOF results. When EOF analysis was carried out on the data with the Miami interpolation, the first EOF identified large variability in the Labrador Sea region north of 60°N. Therefore, it appears that the optimal interpolation method used here is capable of extending the data into the high latitudes of the North Atlantic.

## Conclusions

The EOF analysis of the interpolated anomalies reveals that the NAO is the most dominant feature in the variability of the North Atlantic, with the Gulf Stream variability as the second most dominant component. Overall, it appears that optimal interpolation is a useful tool for extending the northward boundary of the North Atlantic data set.

## Acknowledgements

The MCSST data were obtained from the NASA Physical Oceanography Distributed Active Archive Center at the Jet Propulsion Laboratory, California Institute of Technology.

## References

Bojaru, R., 1997: Climate variability modes due to ocean-atmosphere interaction in the central Atlantic. Tellus, Series A-Dynamic Meteorology and Oceanography, 49(3), 362–370.

Deser, C., and M. L. Blackmon, 1993: Surface climate variations over the North Atlantic during winter: 1900–1989. J. Clim., 6, 1743–1753.

Kushnir, Y., 1994: Interdecadal variations in North-Atlantic sea-surface temperature and associated atmospheric conditions. J. Clim., 7(1), 141–157.

Maybeck, P. S., 1979: Stochastic models, estimation, and control, Volume 1. Academic Press.

McCartney, M., 1996: North Atlantic Oscillation. Oceanus, 39, 13.

McCartney, M., 1997: Climate change: is the ocean at the helm? Nature, 388, 521–522.

McClain, E. P., W. G. Pichel, and C. C. Walton, 1985: Comparative performance of AVHRR-based multichannel sea surface temperatures. J. Geophys. Res., 90, 11587–11601.

Rodgers, C. D., 2000: Inverse methods for atmospheric sounding: theory and practice. Series on Atmospheric, Oceanic and Planetary Physics, Vol. 2, 256 pp., World Scientific.

Sutton, R. T., and M. R. Allen, 1997: Decadal predictability of North Atlantic sea surface temperature and climate. Nature, 188, 563–567.

Wallace, J. M., and D. S. Gutzler, 1981: Teleconnections in the geopotential height field during the Northern Hemisphere winter. Mon. Weather Rev., 109, 784–812.

Wallace, J. M., C. Smith, and Q. R. Jiang, 1990: Spatial patterns of atmosphere ocean interaction in the Northern winter. J. Clim., 3, 990–998.

# Circulation schemes of AAIW and NADW in the South Atlantic as deduced from an eddy-resolving sigma-coordinate model simulation

*Anne P. de Miranda and Bernard Barnier, Laboratoire des Ecoulements Géophysiques et Indusriels, MEOM, France. Miranda@hmg.inpg.fr*

Oceanographers now recognise the key role played by bottom topography in setting up the oceanic general circulation. To represent correctly the complexity of interactions between currents and topography is a challenge that Ocean GCMs have to face. Sigma-coordinate models which use a terrain-following vertical coordinate were designed to better represent these interactions. This variety of model was originally designed for coastal oceanography, and its use to represent the general circulation at basin scale is still not very much widespread. The MOCA project (Modelling the Ocean Circulation in the south-Atlantic) was one of the very first eddy resolving application of a σ-coordinate model to simulate the circulation of an ocean basin, and we present here circulation schemes deduced from a 35 year integration of the MOCA model. An atlas of the WOCE sections has been produced from this simulation and is available through the WOCE IPO Web site.

## Model configuration and experiment

The model is the σ-coordinate primitive equation model (SPEM) developed by Haidvogel et al. (1991). A description of the South Atlantic model configuration is given in de Miranda et al. (1999a), but we recall here its most original features. The model domain, which covers the South Atlantic from the tropics to the Weddell Sea (Fig. 1), has three open boundaries which are treated by active radiation conditions; at the Drake Passage (68°W), at 16°S between Brazil and Angola, and at 30°E from the Cape of Good Hope to Antarctica. The smoothing of the bottom topography (a key issue for circulation models) takes into account the limits imposed by numerical constraints, but with the concern to be as close as possible to the real conditions (Fig. 1). The model isotropic horizontal-grid resolution is $\frac{1}{3}°$, and 20 σ-levels are used in the vertical.

The model has been integrated for 35 years forced by a monthly mean wind stress and heat flux climatology from ECMWF analyses (Barnier et al., 1995). The salinity forcing is a relaxation to the seasonal climatology of Levitus (1982). Biharmonic viscosity and diffusivity are used ($2.5 \times 10^{11}$ m$^4$ s$^{-1}$ with a dependency upon grid size), which allowed the generation of intense eddies in the confluence region (Fig. 2) and Agulhas Rings (de Miranda, 1999a).

The simulation started from an ocean at rest in which initial temperature and salinity fields (T,S) are derived from the mean annual climatology of Levitus (1982). The barotropic transport of the Antarctic Circumpolar Current (ACC) at Drake Passage is set by the open boundary condition to 140 Sv. A simple sea-ice parameterisation was used in the Weddell Sea. Results presented here have been obtained from the 5 year average of year 31 to 35 of the simulation.

## Mean surface circulation

The 5 year mean velocity field at 200 metres is shown in Fig. 3 for the western South Atlantic. The present discussion focuses on the circulation in the Argentine basin where quite interesting features are simulated by the σ-coordinate model. The branch of the Antarctic Circumpolar Current (ACC) which follows the northern continental slope of the Scotia Sea enters the Argentine Basin to form the Malvinas Current (a small part of the flow turns east at 50°S in the Polar Front). The Malvinas Current (75 Sv at 45°S) encounters the Brazil Current between 40°S and 30°S. The model circulation in the confluence region is significantly different from that simulated by z-coordinate models (the 0.28° POP5 model, Maltrud et al., 1998; the ⅓° CLIPPER model, Tréguier et al., 1999). These latter models usually present a Brazil Current which remains confined along the coast and overshoots to the south, and the region of confluence is a few degrees south of its observed location. In MOCA, it is the Malvinas Current which remains trapped along the coast, whereas the Brazil Current remains offshore on the 1000 m isobath. Between 40° and 35°S in the confluence region, the major part of the Malvinas Current retroflects offshore and joins the Brazil Current in a flow to the south. Despite a very high mesoscale eddy activity in the region (the eke is above $1500\,cm^2\,s^{-1}$, de Miranda et al., 1999a), both currents remain somewhat distinct (i.e. the properties of their waters do not mix rapidly), and a strong thermohaline front persists (Fig. 2). The part of the Malvinas Current which does not retroflect at the confluence continues northward, confined to the coast as far as 30°S. it is significant by its mean transport (nearly 20 Sv). Note that this mean flow is the results of cold eddies shed by the retroflection and moving northward along the coast, rather than a steady mean current (Fig. 2).

The 5 year mean shows a clear and realistic mean current pattern in the Argentine basin. The flow made by the confluence of the Malvinas and Brazil Currents follows the 1000 m isobath in the south-westward direction. The transport intensifies, and the direction of the currents shifts straight south at 40°S. At 42°S the Brazil Current turns off shore to the north, and at 40°S it splits in two branches, one which flows east, forming the Subtropical Front (STF), and the other branch continues to the north to form a tight inertial re-circulation, both features being in good agreement with observations (Stramma and England, 1999).

The colder vein of the current continues to flow south until it bifurcates eastward at 48°S to form the Sub-Antarctic Front, again quite a realistic behaviour. Thus at 50°W, the STF and SAF are distant by almost 800 km, and in the middle, centred at [45°S, 45°W] lies a strong anticyclonic eddy which extends to the bottom, the Zapiola Anticyclone. This feature was observed during the WOCE A11 hydrographic section (Saunders and King, 1995), and by other types of observations including Lagrangian floats. As shown by de Miranda et al. (1999b), this circulation feature results from an interaction between the eddies generated in the confluence region with the Zapiola Drift, a closed f/h topographic feature. The σ-coordinate MOCA model reproduces this feature quite well (de Miranda et al., 1999b), and the model circulation scheme suggests that this peculiar circulation feature plays a major role in the separation of the STF and SAF in the Argentine basin.

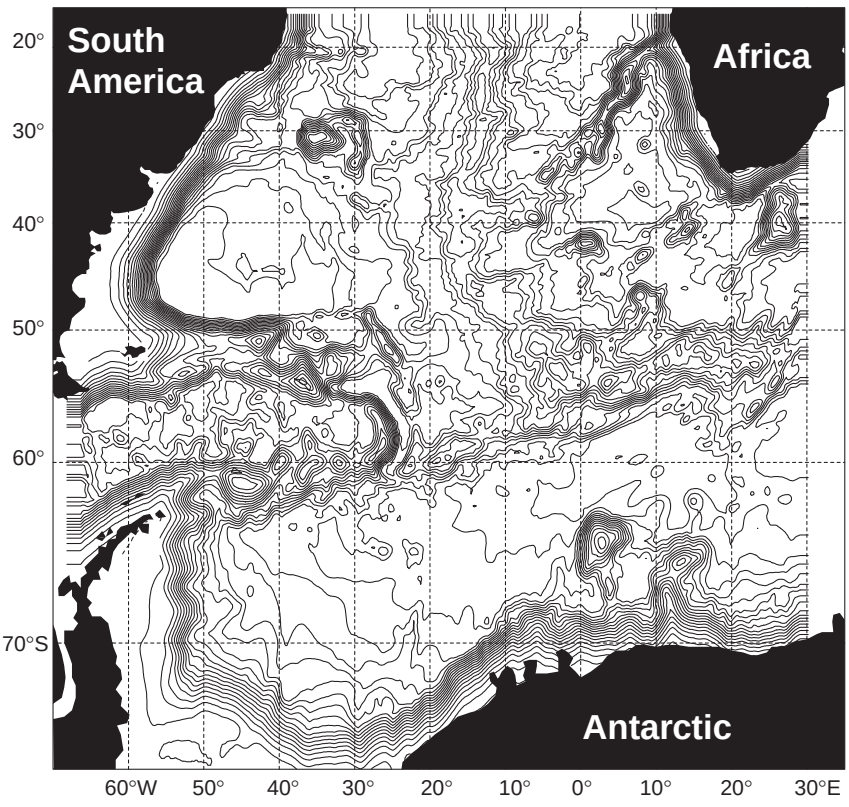


*Figure 1. Smoothed bottom topography used in the σ-coordinate MOCA model. Minimum depth is 250 m. Contour interval is 250 m.*

## Antarctic Intermediate Waters

Fig. 4a (page 22) shows a schematic view of the circulation of the AAIW. This scheme is deduced from mean velocities and transports in a layer defined by a minimum in salinity around isopycnal $\sigma_0 = 27.30$ which is representative of AAIW in the model.

The circulation pattern of the AAIW presents many similarities with the circulation of surface waters. Fresh intermediate waters coming from the Pacific Ocean flow northward within

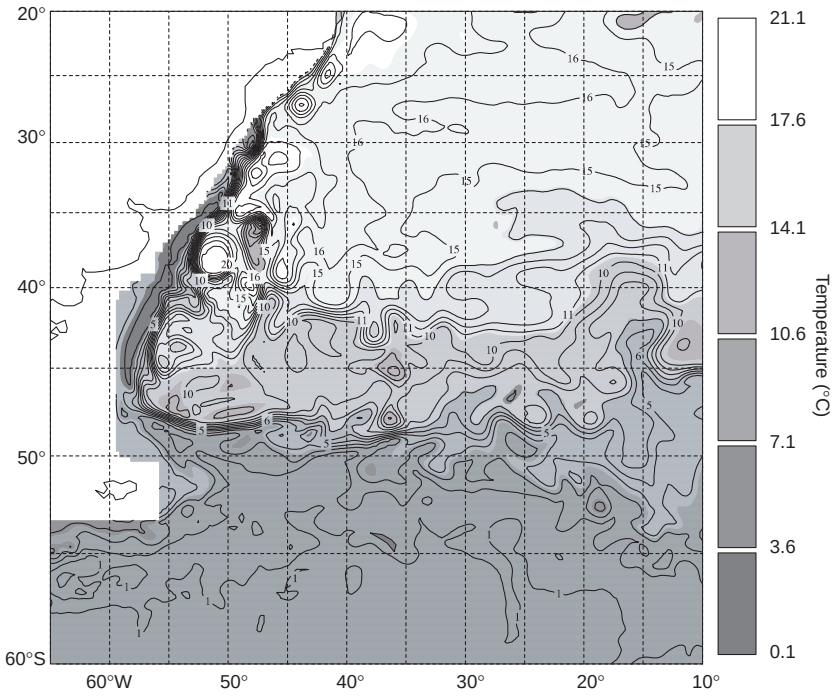


*Figure 2. A snapshot of the MOCA model temperature at 200 m depth in the western South Atlantic. Contour interval is 1°C.*

the Malvinas Current, and retroflect to the south-west between 40°S and 30°S. Very strong mixing occurs in the confluence region with more saline waters from the subtropical gyre. Mesoscale eddies have a dominant role in this mixing. The AAIW escape the confluence region and if most of it leaves the Atlantic toward the Indian Ocean within the ACC, about 10 Sv re-circulate to the north beneath the subtropical gyre. This re-circulation partly occurs in the western basin where 5 Sv flows on the western flank of the Mid-Atlantic Ridge (MAR), and in the eastern basin where 5 Sv joins the AAIW from Indian Ocean origin flowing to the north-west beneath the Benguela Current.

At 10°W, a total of 20 Sv of AAIW flows westward, three quarters of it (almost 15 Sv) being warmer and saltier intermediate waters which entered the Atlantic with the deep part of the Agulhas Current.

When the flow of AAIW reaches the western boundary near 25°S, it equally divides in two branches, 13 Sv continuing toward the equator along the western boundary, and 12 Sv re-circulating in the subtropical gyre. This separation is clearly seen in the trajectories of the MARVOR floats (Ollitrault, 1999).

## North Atlantic Deep Waters

The circulation of NADW has been studied as a layer of maximum in salinity around the $\sigma_0 = 36.90$ isopycnal, and a comprehensive scheme of this circulation according to model velocities and transports is given in Fig. 4b.

The open boundary condition at 16°S relaxes the model barotropic transport at the western boundary to a value 20 Sv southward. This certainly has a great influence on the amount of NADW which enters the Brazil basin. At 20°S, this transport is 14 Sv within the western boundary current (at depths between 2000 and 3000 metres). There, the zonal extent of the Victoria Ridge forces these waters to invade the Brazil basin, where we notice the presence of zonal jets which favours the spreading of deep waters in the basin interior.

Nevertheless, most of the deep western boundary current passes the Victoria Ridge and enters the Argentine basin; at 30°S the transport of the deep western boundary current is 10 Sv. The flow in the Argentine basin is characterised by two major branches. One flows east along the southern side of the Rio Grande topographic rise. The second branch (6 Sv) continues to the south along the slope of the shelf as a deep boundary current. When it reaches 33°S, NADW encounters fresher circumpolar waters coming from the south, and its characteristics begin to change and are significantly

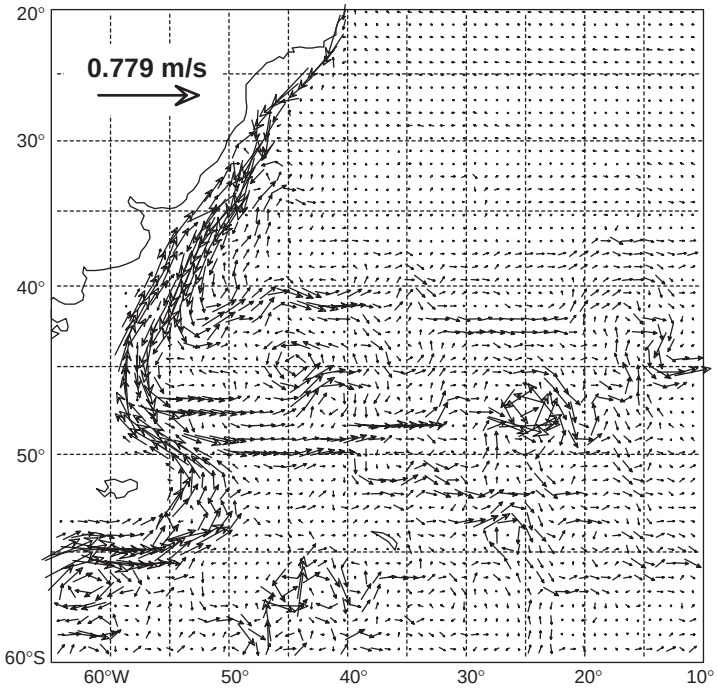


*Figure 3. Five-year mean current vectors from the MOCA model at 200 m depth in the western South Atlantic. The largest current vector is 80 cm/s.*

diluted south of 35°S. The NADW which passed 40°S is mixed with circumpolar waters in the confluence region where mesoscale eddy activity is very large, and the mixed waters join the circumpolar circulation. The branch of NADW which flows along the Rio Grande Rise is also partly diluted by mixing (fresher), but these deep waters flow northward along the flank of the MAR, go back into the Brazil basin, and 6 Sv of NADW cross the ridge at 22°S and enter the eastern basin.

The model suggests that NADW found in the eastern basin has two origins; that which come from the Brazil basin and crossed the mid-ocean ridge at 22°S, and that which enters the model at the open boundary. Although the open boundary condition does not specify any flow of NADW, the model simulates an inflow of 11 Sv mainly along the eastern flank of the MAR. This flow rapidly turns eastward, crosses the basin, and follows the Walvis Ridge to the south-east. 12 Sv of NADW cross this ridge, partly at the Namib Col and partly at another gap more to the south near 28°S. In the Cape Basin, NADW flow southward along the continental slope of Africa and escape the South Atlantic in an eastward undercurrent below the Agulhas Current. Evidence of this undercurrent has been shown by Beal and Bryden (1997). In the model, this counter current is also fed by waters coming directly from the Walvis Ridge across the Cape Basin and by fresher water coming from the south west with the Antarctic Circumpolar Current.

## Conclusion

The $\frac{1}{3}°$ $\sigma$-coordinate model of the South Atlantic provides circulation schemes which agree in many aspects with those deduced from recent WOCE observations, and illustrates again the role of the bottom topography in setting the details of the large scale circulation. The most striking example is the role of the eddy-driven Zapiola Anticyclone which determines the location of the subtropical and sub-Antarctic fronts in the Argentine basin. The influence of the topography on the circulation of AAIW appears to be of secondary importance compared to the influence of the subtropical gyre above. On the contrary, the circulation of NADW is largely influenced by topography, even by local features such as the Victoria Ridge, or the narrow passage in the MAR at 22°S.

Our model solution present similarities, but also differences, with other model simulations in several aspects which have not been discussed here. Considering the insights brought to our understanding of ocean modelling in the North Atlantic by the model comparison experiment DYNAMO (Willebrand et al., 2000), it seems appealing to pursue similar inter-comparison work with existing model simulations in the South Atlantic, and WOCE AIMS is an ideal framework for such studies.

## References


Barnier, B., L. Siefridt, and P. Marchesiello, 1995: Thermal forcing for a global ocean circulation model using a three-year climatology of ECMWF analyses. J. Mar. Sys., 6, 363–380.

Beal, M. L., and H. L. Bryden, 1997: Observation of an Agulhas undercurrent. Deep-Sea Res., 44, 1715–1724.

de Miranda, A. P., B. Barnier, and W. K. Dewar, 1999a: Mode Waters and subduction rates in a high resolution South Atlantic simulation. J. Mar. Res., 57, 213–244.

de Miranda, A. P., B. Barnier, and W. K. Dewar, 1999b: On the dynamics of the Zapiola Anticyclone. J. Geophys. Res., 104, 21137–21149.

Haidvogel, D. B., J. L. Wilkin, and R. Young, 1991: A semi-spectral primitive equation ocean circulation model using vertical sigma and orthogonal curvilinear horizontal coordinates. J. Comp. Physics, 94, 151–185.

Levitus, S., 1982: Climatological Atlas of the World Ocean. Professional Paper 12, NOAA, USA.

Maltrud, M. E., R. D. Smith, A. J. Semtner, and R. C. Malone, 1998: Global eddy-resolving ocean simulations driven by 1985–1995 atmospheric winds. J. Geophys. Res., 103, 30825–30853.

Ollitrault, M., 1999: MARVOR floats reveal intermediate circulation in the western equatorial and tropical South Atlantic. Int. WOCE Newsl., 34, 7–10.

Saunders, P. M., and B. A. King, 1995: Bottom currents derived from a shipborne ADCP on the WOCE Cruise A11 in the South Atlantic. J. Phys. Oceanogr., 25, 329–347.

Stramma, L., and M. England, 1999: On the water masses and mean circulation of the South Atlantic Ocean. J. Geophys. Res., 104, 20863–20883.

Tréguier, A. M., et al., 1999: The CLIPPER project, High resolution modelling of the Atlantic. Int. WOCE Newsl., 36, 3–5.

Willebrand, J., B. Barnier, C. Böning, C. Dieterich, P. D. Killworth, C. Le Provost, Y. Jia, J.-M. Molines, and A. L. New, 2000: Circulation characteristics in three eddy-permitting models of the North Atlantic. Prog. Oceanogr., in press.

# Observations of the Mozambique Current and East Madagascar Current in ACSEX, the Agulhas Current Sources Experiment

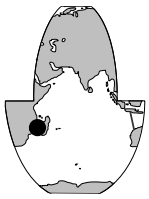

*W. P. M. de Ruijter, IMAU, Utrecht University, The Netherlands; J. R. E. Lutjeharms, University of Cape Town, South Africa; and H. Ridderinkhof, NIOZ, The Netherlands.*
*w.p.m.deruijter@phys.uu.nl*

The climatologically important inter-ocean leakage of Indian Ocean water into the South Atlantic is largely controlled by the strength and dynamical structure of the inflows into the Agulhas Current from the Indian Ocean far field (de Ruijter et al., 1999). In spite of their global significance surprisingly little observations have been made in these source regions. As part of the "Pelagia around Africa" programme the Dutch research vessel Pelagia is in the area in March 2000 and February 2001, to carry out the Agulhas Current Sources Experiment (ACSEX).

ACSEX is carried out jointly by a team of Dutch and South African oceanographers. Its main observational aim is to determine the strength, variability and hydrographic structure of the two sources of the Agulhas, the Mozambique Current and the East Madagascar Current, given the logistic limitations. Both branches exhibit a high variability, as observed by satellite altimetry, with eddies regularly drifting into the Agulhas thereby influencing its stability.

The ACSEX I cruise is presently underway and involves a detailed hydrographic survey to determine whether the Mozambique Current is a continuous current or whether it exists merely of a train of eddies, as the altimetric data suggest. An array of current meter moorings will be placed across the narrows of the Mozambique Channel to monitor the transport and its variability over the subsequent year.

In the Austral Summer of 2001 the ACSEX II cruise will investigate the characteristics of the East Madagascar Current and its contribution to the Agulhas Current. The few observations, mostly from satellites, indicate that the East Madagascar Current retroflects south of Madagascar, with attendant spawning of rings. These rings probably influence the behaviour and stability of the Agulhas and the associated variability and size of the Indian–Atlantic inter-ocean leakage.

Given the observed structure of the wind field over the Indian Ocean one would to first order expect a wind driven subtropical gyre bounded to the north by the South Equatorial Current (SEC). A unique feature of this gyre system is the positioning of Madagascar obstructing the SEC and causing it to bifurcate in a northward and southward branch. These two branches then form the western boundary currents of the anticyclonic and cyclonic wind-driven gyres. At the northern and southern tip of the island both branches would separate, proceed zonally as free jets until hitting the African continent, where they would proceed northward and southward, respectively, as part of the gyres. As a consequence of this (linear) scenario the Mozambique Channel would be shielded from the wind-driven gyres and no significant current is to be expected there.

Intermittently or seasonally the wind pattern shifts meridionally, such that the bifurcation of the SEC migrates northward of Madagascar. That would result in a significant inflow into the Mozambique Channel on its northern edge (Biastoch and Krauss, 1999). Moreover, global models (Maltrud et al., 1998) suggest a significant transport through the Channel that is probably thermohaline driven and connected to the Pacific-Indian Ocean throughflow as part of the global ocean conveyor (Gordon, 1986). The grid resolution of these models is still too large to expect a realistic representation of the complicated region around Madagascar, but the inferred global connection of the currents around Madagascar remains.

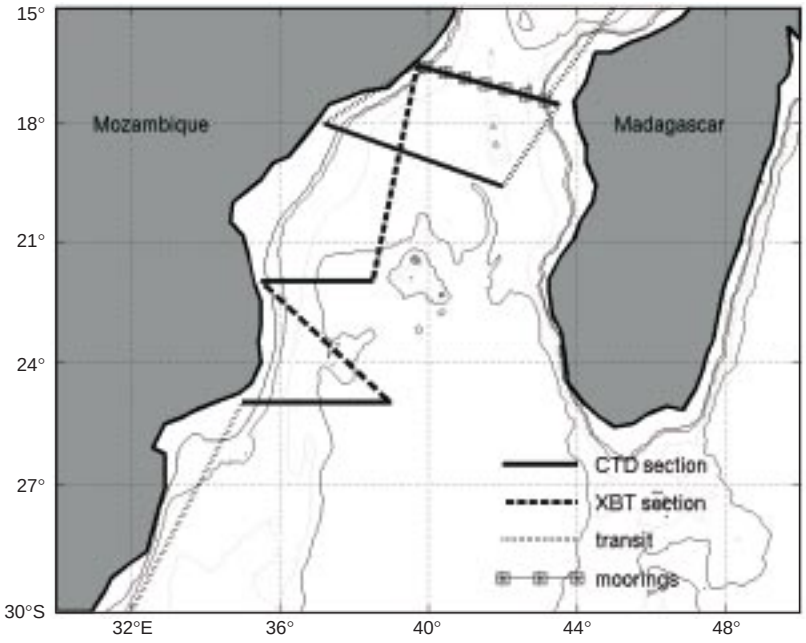


*Figure 1. The ACSEX I cruise plan. The cruise is carried out in March/April 2000 and involves hydrography and mooring deployment. The moorings will be recovered during ACSEX II, in the Austral Summer of 2001.*

## The Mozambique Current

The Mozambique Current, is presently being investigated hydrographically as part of the ACSEX I cruise (Fig. 1), which has departed from Cape Town on Sunday, 19 March 2000. Satellite altimetry (Fig. 2) indicates a complicated flow structure in the Channel. It shows that the flow may well be dominated by southwestward propagating Rossby waves or a train of eddies. The ACSEX I cruise has therefore been designed to establish the existence, nature, hydrographics and trajectory of the Mozambique Current, or its eddy train, in a quasi synoptic way. It is guided by the (near) real time altimetric observations (Fig. 2).

The first cross-shore hydrographic section of the ACSEX I cruise is presently (i.e. while writing this note) being taken at 24.15°S, cutting right through the positive and negative sea surface height anomalies there (Fig. 2).

The hydrographic surveys involve the lowering of a CTD-rosette sampler to determine T, S, nutrients and oxygen. This is combined with a ship mounted ADCP and a Lowered ADCP to determine the absolute current speeds over the full depth and thus the absolute volume, heat and salt fluxes.

The last part of the ACSEX I cruise consists of the deployment of the current meter moorings across the narrow part of the Mozambique Channel. First three moorings will be deployed for a period of one week at the continental slope on the African side of the Channel. Hopefully this will give the necessary information on the strength and spatial variation of the current field in this region where the (slope bound) currents are expected to be largest. Conventional current meters and ADCPs will sample at a high frequency (every 1–2 minutes) in order to obtain additional information on the presence of high frequency internal waves. The moorings will be deployed during neap tide and recovered during spring tide.

First analysis of the data may result in adaptations to the planned set-up of the long-term moorings (Fig. 3). Instruments in these moorings will sample at a lower frequency (every 15–30 minutes). The design for the moored array consists of the deployment of 2 ADCP moorings on the Mozambique side of the Channel and 5 conventional current meter moorings, to be deployed more or less evenly distributed between these ADCP moorings and the Madagascar side of the Channel (Fig. 3).

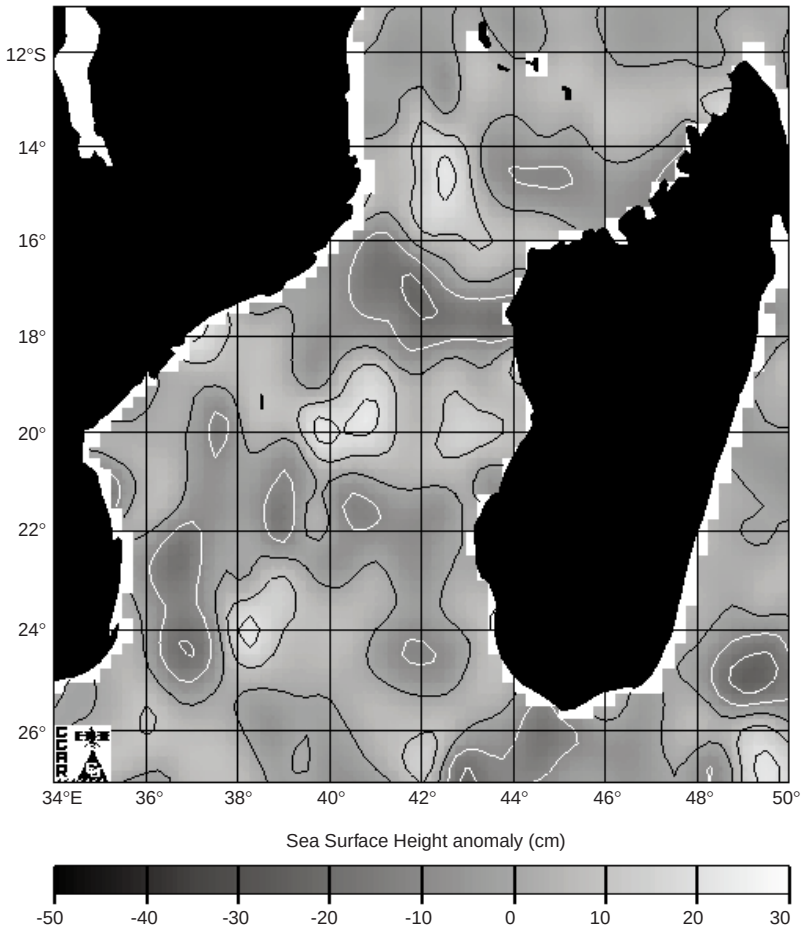


*Figure 2. The sea surface height anomaly field in March 2000 as determined from TOPEX/POSEIDON/ERS-2 satellite altimetry, (processed by the Colorado Center for Astrodynamics Research (CCAR), Web site: www-ccar.colorado.edu/~realtime/global-historical_ssh/).*

## The East Madagascar Current

The southward branch of the South Equatorial Current forms the East Madagascar Current. This current is one of the least known of all currents in the world – especially western boundary currents – notwithstanding its possibly important role in the whole greater Agulhas Current system. A few fortuitous lines of oceanographic stations have crossed it just east of the southern tip of Madagascar (Lutjeharms et al., 1981) and a few drifters have moved through it. These observations have shown that the current is narrow, intense and seemingly locked to the steep slope east of Madagascar. Upwelling inshore of the current has been inferred from satellite information from the SeaWiFs and other satellites. One set of current meter moorings slightly farther upstream (Schott et al., 1988; Swallow et al., 1988) has indicated a strong and very stable current. There has been no evidence from these observations that waters from the East Madagascar Current feed directly into the Agulhas Current, although a number of global circulation models (Maltrud et al., 1998) continue to indicate this.

Satellite observations in the thermal infrared have in fact suggested (Lutjeharms, 1988) that there are periods that the East Madagascar Current retroflects sharply south of Madagascar, subsequently carrying most of its water eastward. This provides an intriguing theoretical and observational problem: the retroflected current flows in a

direction opposite to the large scale circulation. The possibility of loop occlusion and ring shedding has therefore been mooted in the literature (Lutjeharms et al., 1981). Anomalies in the sea height field have been observed to come from east of Madagascar and to eventually interact with the Agulhas Current (Grundlingh, 1995). Whether these specific eddies come from the East Madagascar Current or from the South Equatorial Current remains unclear. Information on the southern termination of this current is virtually non-existent.

The aim of the ACSEX II cruise is therefore to investigate hydrographically as much of this virgin current as time will allow. We want to establish its vertical and lateral dimensions, the fluxes of heat, volume and salt in its different components, the water masses it carries, the nature of its assumed retroflection, the nature of its rings, the upwelling on its inshore side, the manner in which its return current functions and the presence and nature of any other dynamical anomalies. If successful, this cruise will give the first comprehensive portrayal of this important current.

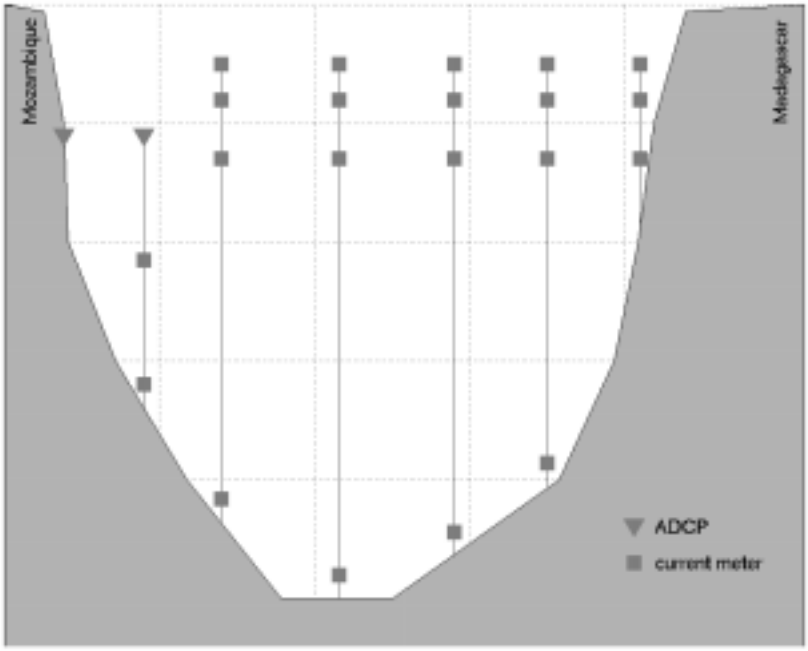


*Figure 3. The ACSEX mooring array to be deployed across the narrow section of the Mozambique Channel (see Fig. 1 for location) for a period of one year (March 2000–March 2001).*

The cruise data, together with the satellite data, will be assimilated in a detailed data assimilation system for the oceans around South Africa that we are presently developing. This system provides us with the means to investigate the processes that influence the inter-ocean exchange in great detail. Moreover, the sensitivity of the exchange to these various processes will be determined.

## Acknowledgements

ACSEX is funded by the Institute for Marine and Atmospheric research of Utrecht University (IMAU), the Netherlands Institute of Sea Research (NIOZ) and the Netherlands Organisation for Scientific Research (NWO). It forms part of the Netherlands contribution to CLIVAR. W. P. M. de Ruijter is supported by the Dutch National Research Programme on Global Change (NRP II) under Grant 013001237.10. J. R. E. Lutjeharms is supported by the University of Cape Town and the South African Foundation for Research Development.

## References

Biastoch, A., and W. Krauss, 1999: The role of mesoscale eddies in the source regions of the Agulhas Current. J. Phys. Oceanogr., 29, 2303-2317.

de Ruijter, W. P. M., A. Biastoch, S. S. Drijfhout, J. R. E. Lutjeharms, R. P. Matano, T. Pichevin, P. J. van Leeuwen, and W. Weijer, 1999: Indian–Atlantic inter-ocean exchange: dynamics, estimation and impact. J. Geophys. Res., 104, 20885–20910.

Gordon, A. L., 1986: Inter-ocean exchange of thermocline water. J. Geophys. Res., 91, 5037–5046.

Grundlingh, M. L., 1995: Tracking eddies in the south east Atlantic and south west Indian Oceans with TOPEX/ POSEIDON. J. Geophys. Res., 100, 24977–24986.

Lutjeharms, J. R. E., 1988: Remote sensing corroboration of the retroflection of the East Madagascar Current. Deep-Sea Res., 35, 2045–2050.

Lutjeharms, J. R. E., N. D. Bang, and C. P. Duncan, 1981: Characteristics of the currents east and south of Madagascar. Deep-Sea Res., 28, 879–899.

Maltrud, M. E., R. D. Smith, A. J. Semtner, and R. C. Malone, 1998: Global eddy-resolving ocean simulations driven by 1985–1995 atmospheric winds. J. Geophys. Res., 103, 30825–30853.

Schott, F., M. Fieux, J. Kindle, J. Swallow, and R. Zantopp, 1988: The boundary currents east and north of Madagascar. 2. Direct measurements and model comparisons. J. Geophys. Res., 93, 4963–4974.

Swallow, J. C., M. Fieux, and F. Schott, 1988: The boundary currents east and north of Madagascar. Part I. Geostrophic currents and transport. J. Geophys. Res., 93, 4951–4962.

# What forces the Southwest Monsoon Current?

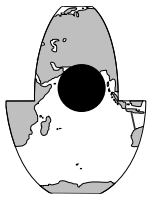

*D. Shankar, National Institute of Oceanography, India.*
*shankar@csnio.ren.nic.in*

The understanding of the circulation and water-mass pathways of the Arabian Sea, was identified at the WOCE Indian Ocean Workshop as an important topic for research (Chapman, 1999). A major component of this circulation is the Southwest Monsoon Current (SMC), which carries the high-salinity waters from the Arabian Sea to the Bay of Bengal during the south-west monsoon. The SMC flows across the middle of the Arabian Sea, from its western boundary to the southern tip of Sri Lanka, and then into the Bay of Bengal (Shenoi et al., 1999). There are not many studies that examine the causes of this striking mid-ocean current, the general idea being that the principal cause is Ekman pumping in the Arabian Sea. In what follows, we use a linear, $1\frac{1}{2}$-layer reduced-gravity model of the Indian Ocean to examine the mechanisms that force the SMC.

## Numerical model and simulations

The numerical model is as described in Shankar and Shetye (1997), except for the inclusion of the Lakshadweep and Maldive islands. The model is forced by the wind-stress climatology of Hellerman and Rosenstein (1983) and the equations are solved on an equatorial β-plane. The linear model reproduces the observed circulation in the north Indian Ocean, with one exception: the Great Whirl does not form off Somalia; instead, it merges with the Socotra high to form a single high in sea level (Fig. 1, page 21).

The structure of the SMC in the eastern Arabian Sea shows that it is intimately connected to the Lakshadweep low, which forms off south-west India during the south-west monsoon (Shankar, 1998; Shankar and Shetye, 1997). Remote forcing by coastal Kelvin waves from the Bay of Bengal contributes significantly to the formation of the low. What is the role of these waves in forcing the SMC in the Arabian Sea?

To isolate the effect of different processes, two sets of boundary conditions are applied along continental boundaries (Shankar, 1998). One set is the usual no-slip condition:

$$u = v = 0. \tag{1}$$

The other set,

$$\tilde{u} = \mathbf{n}\cdot\mathbf{v} = -\mathbf{n}\cdot\mathbf{k}\times\frac{\tau}{f}, \tilde{v} = \mathbf{k}\times\mathbf{n}\cdot\mathbf{v}, \tag{2}$$

is applied to the boundaries of the Bay of Bengal and the west coasts of India and Sri Lanka in the process solutions. In (2), **k** is a unit vector directed out of the β-plane and **n** is a unit vector normal to the boundary; it points into the bay (offshore) along its western and northern margins, out of the bay (inshore) along its north-eastern and eastern margins, and out of the sea (inshore) along the southern boundaries of India and Sri Lanka and along their west coasts; $\mathbf{v} = (\tilde{u}, \tilde{v})$, where $\tilde{u}$ and $\tilde{v}$ are the velocity components normal to and along the boundary; and $\tau$ is the wind stress. This condition allows Ekman flows to pass through the boundaries, filtering circulations driven by coastal Ekman pumping out of the solutions; it was used earlier by McCreary et al. (1996) to study the East India Coastal Current.

The main, or control, run is the linear solution obtained by applying (1) at all continental boundaries. The process solutions are obtained as described below.

1. The effect of alongshore winds adjacent to the east coasts of India and Sri Lanka (process LA): condition (2) is applied along the east coasts of India and Sri Lanka from (87°E, 20°N) to (82°E, 63°N), thereby eliminating the effect of the alongshore winds there; the difference between the main run and this run gives the process solution forced by LA.
2. The effect of alongshore winds adjacent to the eastern and northern boundaries of the Bay of Bengal (process RA): condition (2) is applied along the eastern and northern boundaries of the bay from (97°E, 25°N) to (87°E, 20°N) the difference between the main run and this run gives the process solution forced by RA.
3. The effect of alongshore winds adjacent to the west coasts of India and Sri Lanka (process WLA): condition (2) is applied along the west coasts of India and Sri Lanka from (82°E, 6.5°N) to (67.5°E, 25°N); the difference between the main run and this run gives the process solution forced by WLA.
4. The effect of all other processes (process OP): condition (2) is applied along the coast from (97°E, 2.5°N) to (67.5°E, 25°N), thereby filtering out the response to processes LA, RA, and WLA; this solution describes the response to all other processes, including Ekman pumping in the interior Arabian Sea and forcing by winds in the equatorial Indian Ocean.

## Results and discussion

The solutions for the main run and for processes LA, WLA, and OP are shown for July in Fig. 1. The response to RA (not shown) is negligible in comparison. The winds along the coasts of India and Sri Lanka (LA and WLA) force the complete structure of the SMC in the Arabian Sea, including its connection to the Somali current. The SMC forced by LA, however, is too far north in the central Arabian Sea. The response to OP is the most striking. The Somali Current is forced by OP, but the flow around the sea-level highs associated with it does not continue to the Indian coast; the SMC forced by OP flows westward in the eastern

Arabian Sea! Since the SMC in the Bay of Bengal is forced exclusively by OP, this results in a divergence at the southern tip of Sri Lanka.

Therefore, we can split the SMC into three dynamical parts. In the Bay of Bengal, it is the front of the equatorial Rossby wave (McCreary et al., 1993; Vinayachandran and Yamagata, 1998; Shankar, 1998). In the eastern Arabian Sea, it is associated with the Kelvin waves along the west coasts of India and Sri Lanka; these waves radiate Rossby waves, which propagate westward. In the western Arabian Sea, it is linked to the Somali Current and the circulation around the highs associated with it; to the east of this branch of the SMC, in the central Arabian Sea, there is significant contribution from Ekman flow.

In the eastern and central Arabian Sea, the SMC appears as the front of a propagating Rossby wave, this wave being the resultant of Rossby waves forced by the processes described above. The consequent rapid changes in the current and its susceptibility to changes in winds elsewhere in the Indian Ocean make the SMC difficult to track in observations.


### Acknowledgements

This work was supported by grants from the Department of Ocean Development, Government of India.


### References


Chapman, P., 1999: Indian Ocean Workshop promotes co-operation. Int. WOCE Newsl., 36, 31, unpublished manuscript.

Hellerman, S., and M. Rosenstein, 1983. Normal monthly wind stress over the world ocean with error estimates. J. Phys. Oceanogr., 13, 1093–1104.

McCreary, J. R., W. Han, D. Shankar, and S. R. Shetye, 1996: Dynamics of the East India Coastal Current, 2. Numerical solutions. J. Geophys. Res., 101(C6), 13993–14010.

McCreary, J. P., P. K. Kundu, and R. L. Molinari, 1993: A numerical investigation of the dynamics, thermodynamics and mixed-layer processes in the Indian Ocean. Prog. Oceanogr., 31, 181–244.

Shankar, D., 1998. Low-frequency variability of sea level along the coast of India. PhD thesis, Goa University, India.

Shankar, D., and S. R. Shetye, 1997: On the dynamics of the Lakshadweep high and low in the south-eastern Arabian Sea. J. Geophys. Res., 102(C6), 12551–12562.

Shenoi, S. S. C., P. K. Saji, and A. M. Almeida, 1999: Near-surface circulation and kinetic energy in the tropical Indian Ocean derived from Lagrangian drifters. J. Mar. Res., in press.

Vinayachandran, P. N., and T. Yamagata, 1998: Monsoon response of the sea around Sri Lanka: Generation of thermal domes and anticyclonic vortices. J. Phys. Oceanogr., 28(10), 1946–1960.


## *eWOCE* – An Interactive Electronic Atlas of WOCE Hydrographic, Nutrient and Tracer Data


*Reiner Schlitzer, Alfred-Wegener-Institut für Polar und Meeresforschung, Germany.*
*rschlitzer@AWI-Bremerhaven.DE*


To facilitate the use of the global WOCE data set, all currently available data of the WOCE Hydrographic Programme (WHP; http://whpo.ucsd.edu/whp_data.html) have been compiled in an integrated data set. When used with the Ocean Data View visualisation software for Windows, this data set constitutes an "Electronic Atlas of WOCE Data" (*eWOCE*) that allows graphical display and interactive analysis of the data in many different ways. *eWOCE* is available over the Internet at http://www.awi-bremerhaven.de/GEO/eWOCE.

### The data set

The *eWOCE* data set (WoceBtl) contains bottle data for almost 10,000 stations from publicly available WHP sections (Fig. 1, page 24). In addition to temperature and salinity observations, most stations also contain oxygen, phosphate, nitrate, and silicate data. CFC observations are provided for about 2350 stations (about 25%), and more than 650 stations contain data for carbon system parameters (for example, total inorganic carbon, alkalinity, and/or $CO_2$ partial pressure). About 75% of the stations were occupied during the WOCE period between 1987 and 1998, while the rest of the stations are pre-WOCE and included for reference and for the analysis of temporal changes on decadal timescales.

The WoceBtl data collection will be updated when more WOCE data becomes public, and the Internet address given above will always link to an up-to-date data set. A data collection containing WOCE conductivity-temperature-depth (CTD) observations is available on request from the author. Note that users can extend the WoceBtl data collection and add data from other sources using the Ocean Data View software described below.

### Visualisation software

To exploit the information in the WoceBtl database and to analyse and display the data, use the Ocean Data View (ODV) visualisation software for Microsoft Windows

9x/2000/NT systems, which comes with *eWOCE*. A UNIX version of ODV for SUN Solaris workstations is under development and should be available this year. Before using ODV you must install it on your computer following the instructions given on the Web page. In the following, a general description of the goals and functionality of ODV is given. You can skip this section if you already know ODV and want to run *eWOCE* now. A review of the Ocean Data View software by Murray Brown can be found in Oceanography, 11(2), 19–21, 1998.

## Overview

ODV is a Windows program for the exploration and graphical analysis of oceanographic profile data (bottle, CTD, expendable bathythermograph (XBT)). ODV lets users interactively browse large sets of station data and produce high quality station maps, general property–property plots of one or more stations, scatter plots of selected stations, property sections along arbitrary cruise tracks, and property distributions on general isosurfaces. ODV supports display of original data as coloured dots or actual data values. In addition, two fast gridding algorithms allow colour shading and/or contouring of gridded fields along sections and on isosurfaces (any plot with a Z-variable can be gridded, colour-shaded and/or contoured). A large number of derived quantities can be calculated quickly and can be displayed and analysed in the same way as the basic variables stored on disk.

ODV is designed to be flexible and easy to use. Users are not required to know the details of the internal data storage format nor are they required to have programming experience. ODV always displays a map of available stations on the screen and facilitates navigation through the data by letting the user select stations, sections, and isosurfaces with the mouse. The screen layout and various other configuration features can be modified easily, and favourite settings can be stored in configuration files on disk for later use.

ODV can create and manage very large data collections. It is therefore possible to store the available global historical hydrographic data with newly arriving data on relatively inexpensive and widely available hardware and have these data ready for scientific analysis in the field or back home in the laboratory. In addition to actual research applications, ODV can be useful for data quality evaluation and for teaching and training.

## Data Import and Export

The ODV data format provides dense storage and allows instant access to any station, even in large data collections. The data format is flexible: you can store data for up to 50 variables, where type and number of the variables is arbitrary and may vary from one collection to another. Typically only 1 MB of disk space is required to store about 1600 bottle stations containing data for seven variables.

ODV allows easy import of new data into collections and also allows easy export of some or all data from a collection. Hydrographic data in WOCE WHP format (distributed via Internet at http://whpo.ucsd.edu/whp_data.html), data from the World Ocean Atlas 1994 (distributed on CD-ROM by US National Oceanographic Data Center, NODC), World Ocean Database 1998 (distributed on CD-ROM by NODC), data in NODC SD2 format, and data in a TAB-separated spreadsheet format can directly be incorporated into the ODV system. ODV maintains quality flags associated with each individual data value. These quality flags can be used by ODV as a data quality filter to exclude bad or questionable values from the analysis.

## Derived variables

In addition to the basic oceanographic variables stored in the data files, ODV can calculate and display a large number of derived variables. These derived variables (potential temperature, potential density, dynamic height, and many others) are either coded in the ODV software or defined in user-provided macro files. The macro language is easy and general enough to allow a large number of applications. Use of macro files for new derived quantities broadens the scope of ODV considerably and allows easy experimentation with new quantities not yet established in the scientific community. A separate macro editor that can be invoked from ODV facilitates creation and modification of ODV macros. Any basic or derived variable can be displayed in ODV plots, and they all can be used to define isosurfaces. For example, depth horizons, isopycnals, isothermals, or isohalines; property minimum or maximum layers like, for instance, the intermediate water salinity minimum layer can be defined as isosurfaces by use of the zero-crossing of the vertical derivative (a derived quantity) of these variables.

## Graphics and hardcopies

ODV displays colour property sections and colour distributions on isosurfaces in two ways, either by showing the original data at the data locations (coloured dots of user-defined size or numeric values: method 1) or by projecting the original data on a variable resolution, rectangular grid and then displaying the gridded fields (method 2). While method 1 produces “honest” distributions of the data, instantly revealing regions of poor sampling and highlighting occasional bad data values, method 2 is nicer to look at and avoids the overlapping that occurs in (1) especially if large dot sizes are used. The ODV gridding algorithm is reliable and fast, and fields with thousands of data points are estimated in a matter of seconds on standard hardware. It is important to note that gridded fields are data products and that some small-scale features in the data might be lost due to the gridding procedure. In both display modes, ODV allows the export of section or surface data to ASCII files suitable for dedicated gridding, shading, and contouring software.

Colour or black and white paper hardcopies of the ODV graphics screen or of individual data plots can be

obtained easily via the print command or by producing PostScript files (.eps). eps files can be printed on any PostScript printer or can be included in page description documents. ODV can also write the contents of its graphics screen to GIF and EMF files suitable for inclusion in text documents or for post-processing with standard graphics software.

### Using *eWOCE*

After successful installation, you run ODV on the WoceBtl data set by double-clicking on the WoceBtl.var file (default location: c: \ Program Files \ Ocean Data View 4.0 \ Data \ WoceBtl). ODV will load the most recent configuration and draw a station map and several data plots displaying the data of one WHP line (see Fig. 2, page 24, for an example). There are configuration files for all currently available WOCE sections and you can select any one using the "Configuration>Load Configuration" option from the main menu. Note that configuration files for Atlantic, Pacific, Indian, and Southern Ocean sections are in separate subdirectories.

Also provided are configuration files for producing plots of property distributions on depth horizons for the global WOCE data set (see Fig. 3, page 24, for an example of an isosurface plot). Use these configurations as templates for producing distribution plots on isopycnals or isosurfaces defined by any other variable. Property minimum or maximum layers (for example, the intermediate water salinity minimum layer) can be selected as isosurfaces by using the zero crossing of the vertical derivative (a derived quantity) of the respective variables.

ODV's functionality is invoked through the main menu (just below the ODV title bar) or via pop-up menus that are activated by clicking the right mouse button. Different pop-up menus appear depending on the mouse position at the time of the click. Stations or samples are selected simply by clicking on them with the left mouse button. Information about the currently selected station and sample is listed in a text window just below the main menu. The current station and current sample are marked in the map and data plots by a red circle and red crosses, respectively. Additional information about collection variables, current cruise, selection criteria, and property values is shown in pop-up windows that appear when the mouse rests over various items in the text window or the title bar of the ODV window.

For more information on how to use ODV and to modify existing configuration templates, invoke the ODV help by pressing F1.

## The Deep Basin Experiment: A Meeting Report

*Nelson G. Hogg, Woods Hole Oceanographic Institution, USA. nhogg@whoi.edu*

From 15 to 17 November 1999 a meeting of Deep Basin Experiment (DBE) participants was held at the Carriage House, Woods Hole Oceanographic Institution with 26 scientists from France, Germany, Great Britain and the United States attending. This is a particularly critical time for the DBE: most (but not all) of the field work has been completed. Investigators have been working singly or in small groups on various subsets of the data. The main purposes of this meeting were to make the group aware of what work is going on and what results have been achieved, and to stimulate research toward the overarching questions posed in the original DBE manifesto.

Reports summarising data status and availability, publications completed and in process, and further studies contemplated were presented on the first morning. These were followed by short scientific reports grouped under the water mass themes appropriate to the DBE: Antarctic Intermediate Water (AAIW), North Atlantic Deep Water (NADW) and Antarctic Bottom Water (AABW). The meeting ended with a brief discussion about the future and how we might tackle an overall synthesis. It was agreed that the next meeting would take place in Brest, France, in September 2000.

To supplement what is summarised below the interested reader is referred to a previously published description of the DBE given in Hogg et al. (1996) and a recent summary of circulation in the South Atlantic by Stramma and England (1999).

### Summary of research

Although the meeting was structured around water mass themes it seems more appropriate for this report to repackage this under the headings of the original DBE objectives, namely*

#### To observe and quantify the deep circulation within an abyssal basin

The three water mass levels were instrumented with a large number of neutrally buoyant floats. French and German scientists have used a combination of cycling "MARVOR" floats and one-shot "RAFOS" floats to

*Names in brackets indicate those who spoke on the topic of the preceding sentence(s).

determine the circulation of AAIW. This has proven to be quite successful: the large-scale, subtropical gyre that feeds water westward at the southern boundary of the Brazil Basin (BB) with resulting bifurcation over the Santos Plateau at the western boundary has been well observed (O. Boebel, P. Richardson). The transports across WHP line A17 also exhibit a "Santos" bifurcation and many of the features of the circulation can be explained by a simple ventilated thermocline model (C. Schmid). Further north the interior flow is observed less well and appears to have smaller spatial scales. The complex system of zonal currents in the tropics and equatorial regions that has been described by other investigators is not apparent in the float data although there is some confirmation of the Southern Intermediate Counter Current (SICC). Just one of the floats at this level crossed the equator in the western boundary current but a number accomplished the task by taking interior, nearly zonal, routes near the equator. In the neighbourhood of the Vitoria–Trindade Seamount Chain (VTSC) there is tantalising evidence of a recirculating zonal flow but too few floats were in this feature to make it definitive (M. Ollitrault).

At the NADW level a well defined Deep Western Boundary Current (DWBC) exists, consistent with the classic Stommel–Arons (Stommel, 1958) picture but the interior flow appears to be zonally banded with small meridional length scales (W. B. Owens). A prominent eastward flow extends offshore from the VTSC between 20°S and 25°S. This is the region of the Namib-Col Current but on the basis of various computations combining direct current measures and simple box models from hydrographic data the offshore flow seems to carry 8–20 Sv at least as far east as the Mid-Atlantic Ridge (G. Siedler, M. Vanicek, N. Hogg). What happens at the ridge is a puzzle: does it feed a northward flowing boundary current along the ridge flanks (K. Speer) or continue into the Angola Basin (M. Vanicek)? In addition to the 20–25°S eastward flow, the A17 transports suggest significant escapes from the boundary near 3° on either side of the equator, at 10°S, and at 30–34°S (M. Arhan).

Just north of the VTSC a moored array reveals a boundary current that carries a surprising 39±20 Sv within the NADW toward the south-east and extends downward through the AABW layer. There is no evidence for a return recirculation to the north (G. Weatherly).

There were fewer floats put in the bottom water layer than in those above but the flow there seems to share the same zonal structure away from the western boundary. In addition, although the AABW does enter the basin from the south the flow north of the VTSC is generally southward closely resembling that within the NADW above (W. B. Owens, G. Weatherly, M. Arhan).

A large population of small vortices has been observed in the float trajectories, at all levels. They are of both signs of rotation with the direction of propagation generally consistent with theoretical arguments (P. Kassis). Several have also been found in the WOCE hydrographic surveys of the BB (G. Weatherly). Those within the NADW have property anomalies consistent with a source at the western boundary but they have been observed throughout the basin and generally travel westward (P. Kassis).

The WOCE hydrographic sections from the BB have been analysed for regional aspects of the circulation with little, at this point, attempt to determine basin-wide circulation patterns. Given the dominance of zonal flows in the interior the meridional sections have been especially useful for giving support to the existence of flow away from the western boundary (M. Arhan) and extending eastward with CFCs playing an important role, especially near the equator (C. Andrièe, M. Vanicek, W. Smethie).

### To distinguish between boundary and internal mixing processes.

There are 4 major passages connecting the Brazil Basin to neighbouring basins and all were instrumented with current meter arrays during the DBE so as to better constrain the mass and heat budgets for the bottom water relative to that done previously (Hogg et al., 1982). At the exits for bottom water in the north the Romanche–Chain Fracture Zones allow 1.22 Sv (H. Mercier) and the equatorial passage near 35°W about 2.0 Sv (M. Hall) to leave. At the south the Vema Channel and the Hunter Channel both contribute significant amounts of bottom water to the Brazil Basin with the former estimated at 4.0 Sv and the latter at 2.9 Sv (W. Zenk) with little net transport of AABW coming over the Santos Plateau to the west. The Hunter array was the least well equipped to determine the transport with any accuracy.

These refined passage transports have been used to recompute the basin averaged diapycnal diffusivity of between 3 and $5\,cm^2/s$, not significantly different from the earlier values (M. Hall). The real question for the DBE is how uniform this mixing process actually is. The original concept was to coarsely subdivide the basin with hydrographic surveys and make use of direct velocity measurements to constrain box inversion so as to be able to distinguish between regions that were over smooth (i.e. central basin) and rough (i.e. western boundary, Mid-Atlantic Ridge) areas. The work based on inverse techniques is still in its infancy but the Brazil Basin Tracer Release Experiment (BBTRE) has somewhat finessed the outcome. The release of a small quantity of sulphur hexafluoride close to the 1.6°C (potential temperature) surface and subsequent sampling at periods of 12 and 22 months has permitted the direct estimation of diapycnal diffusivity. Rates are between 2 and $10\,cm^2/s$ depending on how close to the (rough) bottom one is (J. Ledwell). A reasonable candidate for the source of the mixing is the conversion of barotropic

tidal energy into internal tides by interaction with small scale bathymetry and subsequent breaking through intensified shears (K. Polzin). Horizontal spreading is consistent with a lateral diffusivity of order $100\,cm^2/s$ (J. Ledwell). The combination of direct estimates of mixing from microstructure observations with regional distribution of water properties has permitted estimation of the local 3-dimensional flow regime (L. St. Laurent). This inverse model predicts upwelling where density surfaces intersect the western flanks of the ridge (within canyons formed by the fracture zones) whose strength is sufficient to account for virtually all that demanded by the basin averaged budgets (if extrapolated along the length of the ridge). Such mixing will drive flow away from the ridge that is very different from that of the old Stommel-Arons scheme (M. Spall).

### To understand how passages affect the water flowing through them

As well as being important tactical locations to measure the mass and heat flux of bottom water passages are likely places for water modification through mixing in the accelerated flows. Two modelling studies are underway, one centred on the Romanche Fracture Zone at the equator (B. Ferron) and the other on the Vema Channel (T. Müller). By way of contrast a density current flows downhill some hundreds of meters at the exit of the Romanche and results in intense mixing ($> 300\,cm^2/s$) while the Vema Channel and its northward extension has a much gentler exit which, along with the geostrophic tendency to force flow to follow depth contours, results in little mixing. A concentration of hydrographic sections near the Vema Channel has permitted a special focus on this region (E. McDonagh). Its outflow has been traced to about 13°S with little change but thereafter seems to split into 2 cores, one goes to deeper depth contours toward the Romanche and the other to the 35°W equatorial exit to the western North Atlantic (G. Weatherly).

### To study the means by which deep water flows across the equator

This topic has been mostly dealt with by other groups outside the DBE and was, by no means, fully covered at the meeting although some examples of floats within the AAIW traversing the equator were given (M. Ollitrault) and the zonally banded structure implied by the CFCs was presented (C. Andriè). Once again the reader is referred to the recent summary of Stramma and England (1999).

## The future

Much of the research effort is now turning toward analysis of the collected data and synthesis of the various data sets so that the regional circulation will be better defined and the above objectives more completely addressed. Overlapping groups of investigators will pursue a variety of subjects during this WOCE AIMS phase. Virtually all of the DBE data sets will be made public by the end of this year. Exceptions are the A14 meridional line in the Angola Basin, promised for summer of 2000, and the last half of the MARVOR float data from the AAIW layer for which tracking has not been completed. The preliminary results have already provoked new measurement programmes aimed at quantifying the long period changes in the Vema Channel (T. Müller) and the 35°W equatorial passage (R. Limburner) and following up on questions related to enhanced mixing over rough topography (J. Toole). The possibility of a zonal connection between the NADW DWBC near the Vitoria–Trindade Seamounts and the Angola Basin stimulated the interest of a number of participants and seems likely to lead to future field programmes.

### References


Hogg, N., P. Biscaye, W. Gardner, and W. J. Schmitz, Jr., 1982: On the transport and modification of Antarctic Bottom Water in the Vema Channel. J. Mar. Res., 40(Suppl.), 231–263.

Hogg, N. G., W. B. Owens, G. Siedler, and W. Zenk., 1996: Circulation in the deep Brazil Basin. In: The South Atlantic: Present and past circulation, G. Wefer, W. H. Berger, G. Siedler, and D. Webb (eds.), pp. 249–260, Springer-Verlag, Berlin, Heidelberg.

Stommel, H., 1958: The abyssal circulation. Letter to the editors. Deep-Sea Res., 5, 80–82.

Stramma, L., and M. England, 1999: On the water masses and mean circulation of the South Atlantic Ocean. J. Geophys. Res, 104(C9), 20863–20883.

# Second Announcement:
# The WOCE/CLIVAR Representativeness and Variability Workshop
# 17–20 October 2000, Fukuoka, Japan

## The organising committee

T. Joyce, Co-chairman; S. Imawaki, Co-chairman; D. Roemmich; N. Bindoff; W. Large; P.-Y. Le Traon; D. Webb; K. Hanawa; P. Koltermann

## The objectives

- To review information gained on seasonal to interannual variability during WOCE
- To assess information gained on decadal variability from comparison of WOCE and pre-WOCE data
- To estimate the impact of this variability on the representativeness of the WOCE (particularly WHP) data sets and derived quantities (e.g. heat and fresh-water fluxes)
- To review the ability of models to represent seasonal and longer-term ocean variability and the variation in water mass properties, volumes and formation rates
- To identify, and take steps to initiate, data analysis and modelling research needed to better assess the representativeness of WOCE data sets and derived quantities
- To identify the principal mechanisms (e.g. local or remote air-sea exchange, advection, propagation, coupled air-sea processes) behind the oceanic signals of climate variability as measured in WOCE
- To make recommendations based on the workshop conclusions for the design of future research (CLIVAR) and operational (GOOS) observing systems.

## The provisional timetable

**Tuesday, 17 October**
Introductory remarks [Joyce and Imawaki]
Plenary session 1: global views of WOCE variability: data and models
Introduction of posters and poster session
Plenary session 2: principal mechanisms for variability
Introduction of posters and poster session
Icebreaker at hotel

**Wednesday, 18 October**
Plenary session 3: model/data comparisons, where are we?
Introduction of posters and poster session
Plenary session 4: Pacific/Indian variability
Introduction of posters and poster session
Workshop Dinner

**Thursday, 19 October**
Plenary session 5: Atlantic variability
Introduction of posters and poster session
Focus groups discussions

**Friday, 20 October**
Plenary session 6: Southern Ocean and Arctic variability
Introduction of posters and poster session
Focus groups discussions
Plenary session 7: focus groups presentations, workshop summaries

## Posters

Abstracts of posters should be sent to the WOCE IPO (woceipo@soc.soton.ac.uk) by 31 July 2000. The decisions on which posters to accept will be made before 31 August when lead authors will be informed of the decision by e-mail. At the same time copies of the accepted abstracts will be linked to the workshop web page: www.soc.soton.ac.uk/OTHERS/woceipo/varbwk

Printed and bound copies of the abstracts will be available at the workshop.

## Registration

Pre-registration for the workshop, accommodation and payment for the workshop dinner are being handled by a travel agency in Fukuoka. Once details are agreed the workshop web page (www.soc.soton.ac.uk/OTHERS/woceipo/varbwk) will link to a workshop web page maintained by the travel agency. The registration fee for the workshop will be $US100 or 10,000 Japanese Yen. For students the fee will be $US50 or 5,000 Yen. The deadline for pre-registration will be 31 August.

## Local information

Fukuoka City is situated on the northern coast of Kyushu, the third largest and south-western most of the four main islands of Japan. The climate is rather mild with the annual mean temperature of about 17°C and is similar to that of the south-eastern coast of the US.

Fukuoka Airport is located fifteen to twenty-five minute by car from Hakata Station and the Tenjin downtown area. If you travel by subway the trip takes less than ten minutes.

Fukuoka train station, Hakata, is well connected with Hiroshima, Osaka, Kyoto, Nagoya and Tokyo by the Shinkansen bullet train. The train to Tokyo takes about 6 hours, connections to Narita Airport taking a further 1 to 2 hours.

The workshop will be held at the Takakura Hotel, Fukuoka. A special rate will be available for attendees.

# "Ocean Circulation and Climate"
## *Gerold Siedler, John Church and John Gould (Editors)*

The book that builds on the plenary papers from the 1998 WOCE Conference in Halifax will be published at the end of the year by Academic Press. This will be an important record of the present status of the science that is at the centre of WOCE objectives and a book that all oceanographic libraries and many individuals will want to own.

Until the final page count and number of colour illustrations is known the price cannot be announced but it will be available at a discount to those who attended the 1998 Conference.

Further publicity will be arranged by Academic Press.

The contents will be:

## MEETING TIMETABLE

### 2000

| | | |
|---|---|---|
| 15–18 May | GODAE SG 4th Session | Southampton, UK |
| 30 May–3 June | AGU Spring Meeting | Washington, USA |
| 19–22 June | Ocean Winds Workshop | Brest, France |
| 27–30 June | 2000 Western Pacific Geophysics Meeting | Tokyo, Japan |
| 17-28 July | Dynamics of Decadal to Centennial Climate Variability | Boulder, USA |
| TBD September | Jason/Topex Science Working Team | Santa Barbara, USA |
| 4-6 October | CLIVAR-WGCM Workshop on Decadal Climate Variability | La Jolla, USA |
| 9-13 October | Workshop on Shallow Tropical–Subtropical THC | Venice, Italy |
| 17–20 October | WOCE/CLIVAR Representativeness and Variability Workshop | Fukuoka, Japan |
| 20–28 October | PICES 9th Annual Meeting | Hakodate, Japan |
| 21–22 October | WOCE SSG-27 | Fukuoka, Japan |
| 25–27 October | Ocean 2000: 2nd International Conference on Oceanic Engineering | Valdivia, Chile |
| 16–17 November | TAO Implementation Panel 9th Session | Perth, Australia |
| 27-30 November | AGU Chapman Conference: The NAO | Orense, Spain |
| 15–19 December | AGU Fall Meeting | San Francisco, USA |

### 2001

| | | |
|---|---|---|
| 8-12 January | Workshop on Decadal Climate Variability | Hawaii, USA |
| 14-19 January | Climate Variability, The Oceans, and Social Impact (AMS) | Albuquerque, USA |
| 2-6 April | European Geophysical Society XXVI | Vienna, Austria |
| 29 May-2 June | AGU 2001 Spring Meeting | Boston, USA |
| 21-28 October | IAPSO-IABO 2001: An Ocean Odyssey | Mar del Plata, Argentina |
| 10-14 December | AGU 2001 Fall Meeting | San Francisco, USA |

The WOCE International Newsletter is published by the WOCE International Project Office.

Editor:
*Roberta Boscolo*

Compilation and layout:
*Sheelagh Collyer*

The International WOCE Newsletter is distributed free-of-charge upon request thanks to the funding contributions from France, Japan, UK, and WCRP.

This Newsletter provides a means of rapid reporting of work in progress related to the Goals of WOCE as described in the WOCE Scientific and Implementation Plan.



Requests to be added to the mailing list and changes of address should be sent to:
WOCE IPO
Southampton Oceanography Centre
Empress Dock
Southampton SO14 3ZH
United Kingdom
Tel. +44 23 8059 6205
Fax. +44 23 8059 6204
e-mail: woceipo@soc.soton.ac.uk

Contents of past issues together with the electronic PDF version can be found at:
http://www.soc.soton.ac.uk/OTHERS/woceipo/acrobat.html

Articles, letters, announcements and reviews are welcome and should be addressed to the editor.

Printed by Technart Ltd.
Southern Road
Southampton SO15 1HG
United Kingdom.

If undelivered please return to:

WOCE IPO
Southampton Oceanography Centre
Empress Dock
Southampton SO14 3ZH
United Kingdom.

## CONTENTS OF THIS ISSUE